Spectrodirectional Reflectance Analysis and Definition for the Estimation of Vegetation Variables

Dissertation

zur

Erlangung der naturwissenschaftlichen Doktorwürde
(Dr. sc. nat.)

vorgelegt der

Mathematisch-naturwissenschaftlichen Fakultät
der
Universität Zürich

von

Gabriela Schaepman-Strub
von
Läufelfingen BL und Zürich ZH

Begutachtet von

Prof. Dr. Klaus I. Itten
Prof. Dr. John Miller

Zürich, 2004

Author:
Gabriela Schaepman
Remote Sensing Laboratories
Department of Geography
University of Zurich
Winterthurerstrasse 190
CH-8057 Zurich
Switzerland
gschaep@geo.unizh.ch
http://www.geo.unizh.ch

Printed on acid-free paper which falls within the ANSI guidelines to ensure permanence and durability.

Schaepman-Strub, Gabriela:
Spectrodirectional Reflectance Analysis and Definition for the Estimation of Vegetation Variables

Remote Sensing Series 43 – Zürich: Remote Sensing Laboratories, University of Zurich, 2004

ISBN 3-03703-008-9

Printed by the Druckerei der Zentralstelle der Studentenschaft der Universität Zürich.

Front cover:

Die vorliegende Arbeit wurde von der Mathematisch-naturwissenschaftlichen Fakultät der Universität Zürich auf Antrag von Prof. Dr. Klaus I. Itten (Geographisches Institut, Universität Zürich) und Prof. Dr. J. Miller (York University, Toronto, Canada) als Dissertation angenommen.

Abstract

The study of climatological, ecological, environmental and agricultural processes with spatial extent is most often based on spatially continuous and georeferenced information of the biosphere. Remote sensing has proven its unique contribution to the investigation, mapping and monitoring of these processes. The combination of spectroscopy with multiangular remote sensing, i.e., spectrodirectional data research, is a recent development promising a more accurate estimation of vegetation variables. Continuous narrowband reflectance data allow for the analysis of specific absorption features of biochemicals. Multiangular remote sensing emphasizes the influence of the direction of illumination and observation on reflectance data, for the estimation of the canopy structure, through biophysical variables. The combination of both can be used for a more adequate description of energy fluxes between the bio- and the atmosphere.

While estimating vegetation variables, uncertainties of the spectrodirectional data are propagated into the products. This thesis quantifies and discusses two majour sources of uncertainties at the reflectance level: (1) spectral effects in directional reflectance data throughout the day, and their representation in a radiative transfer model, and (2) equating different reflectance quantities in applications.

The first part of the thesis concentrates on the setup of the field experiment, followed by the analysis of measured hemispherical-directional reflectance data of an Alfalfa canopy. It is shown, that neglecting sun and view angle effects in measured vegetation reflectance data will introduce wavelength dependent uncertainties. Their quantification on diurnal nadir data indicates the effect on field measurements for validation purposes of airborne and satellite sensor data. Further it is exemplified, that neglecting the wavelength dependence of directional effects highly affects empirical approaches (e.g., vegetation indices). Eventhough the processes causing spectral effects in directional data are nowadays represented in reflectance models, simulated data exhibit smaller variations than measurements of the field experiment. Quantitative results indicate large uncertainties at the reflectance level, which are propagated into the estimation of vegetation variables using empirical approaches, as well as the inversion of radiative transfer models.

The second part of the thesis emphasizes the proper usage of reflectance nomenclature for any application in remote sensing, including approximations of the bidirectional reflectance distribution function (BRDF). It derives a baseline for the selection of the appropriate quantity out of different reflectance products delivered from recent satellite sensors. Existing concepts of nomenclature are reviewed and modelling studies show reflectance quantities and their differences for a vegetation canopy, snow, and an artificial surface. For the first time, the differences

of hemispherical-directional and bidirectional reflectance products of the MISR sensor are quantified and extensively analysed for different biomes. Results show numerically small but wavelength dependent differences, which reach assigned data uncertainties.

With its quantitative approach, the thesis shows the importance of spectrodirectional effects in remote sensing data, reviews the existing nomenclature of reflectance quantities, and emphazises its importance by case studies addressing different remote sensing communities.

The thesis concludes by summarizing the above findings. It recommends to reduce and include reflectance data uncertainties in future applications by following the proposed reflectance nomenclature. The representation of spectral effects in spectrodirectional measurements and modelling results shall be further investigated, with respect to the single scattering components of the coupled soil-vegetation-atmosphere radiative transfer.

Zusammenfassung

Die Untersuchung klimatologischer, oekologischer, umweltrelevanter und agronomischer Prozesse mit Raumbezug basiert meist auf räumlich kontinuierlicher und georeferenzierter Information der Biosphäre. Die Fernerkundung leistet einen einmaligen Beitrag zur Erforschung, Kartierung und Überwachung dieser Prozesse. Die Kombination von Spektroskopie und Fernerkundung mit variablem Aufnahmewinkel , i.e. die Forschung mit spektrodirektionalen Daten, ist eine neuere Entwicklung, die eine genauere Schätzung von Vegetationsvariablen verspricht. Kontinuierliche, schmalbandige Reflektanzdaten erlauben die Analyse von spezifischen Absorptionseigenschaften von biochemischen Stoffen. Die direktionale Fernerkundung betont den Einfluss der Beleuchtungs- und Aufnahmewinkel auf Reflektanzdaten, für die Schätzung der Pflanzendeckenstruktur mittels biophysikalischer Variablen. Die Kombination der beiden kann für eine angemessenere Beschreibung von Energieflüssen zwischen der Bio- und der Atmosphäre verwendet werden.

Während der Schätzung von Vegetationsvariablen pflanzen sich die Unsicherheiten der spektrodirektionalen Daten in den Produkten fort. Diese Dissertation quantifiziert und diskutiert zwei wesentliche Unsicherheitsquellen auf Reflektanzebene: (1) spektrale Effekte in direktionalen Reflektanzdaten während des Tages und ihre Repräsentation in einem Strahlungstransfermodell, sowie (2) das Gleichsetzen von verschiedenen Reflektanzgrössen in Anwendungen.

Der erste Teil der Arbeit konzentriert sich auf den Aufbau des Feldexperimentes, gefolgt von der Analyse der gemessenen hemisphärisch-direktionalen Reflektanzdaten einer Alfalfa Pflanzendecke. Es wird gezeigt, dass die Vernachlässigung des Sonnen- und Blickwinkeleffektes in gemessenen Reflektanzdaten zu wellenlängenabhängigen Unsicherheiten führt. Deren Quantifizierung an Nadirdaten während eines Tages weist auf die Auswirkungen auf Feldmessungen zu Validierungszwecken von flugzeug- oder satellitengestützten Daten hin. Weiter wird beispielhaft dargestellt, dass die wellenlängenabhängigen direktionalen Effekte empirische Ansätze (z.B. Vegetationsindices) stark beeinträchtigen. Obwohl die Prozesse, die die spektralen Effekte in direktionalen Daten hervorrufen, in Reflektanzmodellen eingebunden sind, zeigen simulierte Daten kleinere Variationen als die Messungen des Feldexperimentes. Die quantitativen Resultate deuten auf hohe Unsicherheiten auf dem Reflektanzlevel hin, die sich in der Schätzung von Vegetationsvariablen durch empirische Ansätze, wie auch bei der Inversion von Strahlungstransfermodellen, fortsetzen.

Im zweiten Teil der Dissertation wird der Schwerpunkt auf die angemessene Verwendung der Reflektanznomenklatur für jede beliebige Anwendung in der Fernerkundung gelegt, einschliesslich Annäherungen an die bidirektionalen Re-

flektanzverteilungsfunktion (BRDF). Dieser Teil gibt eine Basis für die Auswahl der geeignetsten Grösse aus verschiedenen Reflektanzprodukten, wie sie von neueren Satellitensensoren erhältlich sind. Bestehende Nomenklaturkonzepte werden besprochen und Modellierstudien zeigen Reflektanzgrössen und ihre Unterschiede für eine Pflanzendecke, Schnee und eine künstliche Oberfläche. Zum ersten Mal werden die Differenzen von hemisphärisch-direktionalen und bidirektionalen Reflektanzprodukten des MISR Sensors für verschiedene Biome quantifiziert und umfassend analysiert. Die Resultate zeigen numerisch kleine, aber wellenlängenabhängige Differenzen, die die zugewiesenen Datenunsicherheiten erreichen.

Mit ihrem quantitativen Ansatz weist diese Dissertation auf die Bedeutung der spektrodirektionalen Effekte in Fernerkundungsdaten hin, bespricht existierende Nomenklaturen von Reflektanzgrössen und zeigt deren Wichtigkeit an Fallstudien auf, die verschiedene Fernerkundungsgemeinschaften ansprechen.

Diese Dissertation schliesst mit der Zusammenfassung der oben genannten Feststellungen ab. Sie empfiehlt, Datenunsicherheiten zu reduzieren und in zukünftige Anwendungen miteinzubeziehen, unter Berücksichtigung der vorgeschlagenen Reflektanznomenklatur. Die Repräsentation der spektralen Effekte in spektrodirektionalen Messungen und modellierten Resultaten soll weiter erforscht werden, unter besonderer Berücksichtigung der Einfachstreukomoponenten des gekoppelten Strahlungstransfersystems Boden-Vegetation-Atmosphäre.

Table of Content

Chapter 5

Chapter 6

List of Figures

List of Tables

List of Abbreviations

AATSR	Advanced Along-Track Scanning Radiometer
ADEOS	Advanced Earth Observing Satellite
AgRISTARS	Agriculture and Resources Inventory Surveys Through Aerospace Remote Sensing
AIRMISR	Airborne Multi-angle Imaging SpectroRadiometer
AIRSAR	Airborne Synthetic Aperture Radar (JPL)
AMBRALS	Algorithm for MODIS Bidirectional Reflectance Anisotropy of the Land Surface
ANIF	ANIsotropy Factor
AOD	Aerosol Optical Depth
APEX	Airborne Prism EXperiment
ARAT	Atmospheric Research and Remote Sensing Aircraft
ASAS	Advanced Solid-state Array Spectroradiometer
ASD	Analytical Spectral Devices
ASG	Automated Spectro-Goniometer
ATCOR	ATmospheric CORrection model
ATSR	Along-Track Scanning Radiometer
AVIRIS	Airborne Visible and InfraRed Imaging Spectrometer
BHR	BiHemispherical Reflectance
BOREAS	Boreal Ecosystem-Atmosphere Study
BRDF	Bidirectional Reflectance Distribution Function
BRF	Bidirectional Reflectance Factor
CAR	Cloud Absorption Radiometer
CCD	Charge-Coupled Device (imaging system)
CCRF	Conical-Conical Reflectance Factor
CHRIS	Compact High Resolution Imaging Spectrometer
DAEDALUS	Airborne Scanner
DAIS	Digital Airborne Imaging Spectrometer
DAISEX	Digital Airborne Imaging Spectrometer EXperiment
DART	Discrete Anisotropic Radiative Transfer
DGPS	Differential Global Positioning System
DHR	Directional-Hemispherical Reflectance
DISORT	DIScrete Ordinate radiative Transfer model
DLR	Deutsches Zentrum für Luft- und Raumfahrt (German Aerospace Center)
DM	Dry Matter
EC	European Community
EFEDA	European Field Experiment in a Desertification threatened Area

EGO	European Goniometric Facility
EOEP	Earth Observation Envelope Programme (ESA)
EOPP	Earth Observation Preparatory Programme (ESA)
ERS	European Remote Sensing Satellite
ESA	European Space Agency
FAPAR	Fraction of Absorbed Photosynthetically Active Radiation
FIFE	First International Satellite Land Surface Climatology Project (ISLSCP) Field Experiment
FIGOS	FIeld GOniometer System
FIR	FarInfrared
FLIGHT	Forest LIGHT interaction model
FOV	Field Of View
FPAR	Fraction of absorbed Photosynthetically Active Radiation
GER	Geophysical and Environmental Research Corporation, Millbrook (NY), USA
GER3700	Geophysical and Environmental Research Corp. 704 channel spectroradiometer
GIFOV	Ground Instantaneous Field Of View
GIS	Geographical Information System
GPS	Global Positioning System
HCRF	Hemispherical-Conical Reflectance Factor
HDRF	Hemispherical-Directional Reflectance Factor
HyMap	HYperspectral MAPping
IEEE	Institute of Electrical and Electronics Engineers
IFOV	Instantaneous Field Of View
IGBP	International Geosphere-Biosphere Programme
INRA	Institute National de Recherches Agronomiques (France)
ISLSCP	International Satellite Land Surface Climatology Project
ISPRS	International Society for Photogrammetry and Remote Sensing
JPL	Jet Propulsion Laboratory, Pasadena, California, USA
JRC	Joint Research Centre of the European Community, Ispra, Italy
LACIE	Large Area Crop Inventory Experiment
LAGOS	LAboratory GOniometer System
LAI	Leaf Area Index
LEANDRE	Airborne LIDAR instrument
LIBERTY	Leaf Incorporating Biochemistry Exhibiting Reflectance and Transmittance Yields
LIDAR	LIght Detection And Ranging
LIDF	Leaf Inclination Distribution Function
LSPIM	Land-Surface Processes and Interaction Mission (ESA)
MERIS	MEdium Resolution Imaging Specrometer (ESA)
MGVI	MERIS Global Vegetation Index
MIR	Middle InfraRed
MISR	Multi-angle Imaging SpectroRadiometer (NASA)

MODIS	Moderate Resolution Imaging Spectroradiometer (NASA)
MODTRAN	MODerate resolution TRANsmittance
MRPV	Modified Rahman-Pinty -Verstraete model
NASA	National Aeronautics and Space Administration, USA
NDVI	Normalized Difference Vegetation Index
NIR	Near-InfraRed
NIST	National Institute of Standards and Technology, USA
NOAA-AVHRR	National Oceanic and Atmospheric Administration - Advanced Very High Resolution Radiometers
ONERA	Office National d'Études et de Recherches Aérospatiales, France
ONVI	Optimized Vegetation Normalized Index
PARABOLA	Portable Apparatus for Rapid Acquisition of Bi-directional Observation of the Land and Atmosphere
PCM	Precision Crop Management
POLDER	POLarization and Directionality of the Earth's Reflectances
PROBA	PRoject for On Board Autonomy (space platform)
PROSPECT	leaf optical PROperties SPECTra model
RAMI	RAdiation transfer Model Intercomparison exercise
RAYTRAN	Ray tracing model to compute light scattering in three-dimensional heterogeneous media
REKLIP	REgio KLIma Project
RESMEDES	REmote Sensing of MEditerranean Desertification and Environmental Stability (European Community Project)
RESRAPS	REmote Sensing and RAdiometric Properties of the Surface: Assessment of Desertification from Space
RESYSMED	Synthesis of Change Detection Parameters into a Land-Surface Change Indicator for Long-term Desertification Studies (European Community Project)
RGB	Red Green Blue
RISMOP	Radiometric Impact of Surface MOisture after Precipitation (experimental campaign)
ROSIS	Reflective Optics System Imaging Spectrometer
RSL	Remote Sensing Laboratories, Department of Geography, University of Zurich, Switzerland
RPV	Rahman-Pinty-Verstraete model
SA	Sun Azimuth
SAFARI	Southern African Fire Atmosphere Research Initiative (starting in 1992, last major initiative in 2000)
SAIL	Scattering by Arbitrarily Inclined Leaves
SAILHS	Scattering by Arbitrarily Inclined Leaves, with implemented Hot spot
SAM	Spectral Angle Mapper
SAR	Synthetic Aperture Radar

SAVI	Soil Adjusted Vegetation Index
SIR-C/X-SAR	Spaceborne Imaging Radar- C/X-Band Synthetic Aperture Radar
SLM	Specific Leaf Mass
SPECTRA	Surface Processes and Ecosystem Changes Through Response Analysis
SPOT-HRV	SPOT - High Resolution Visible sensors
SPRINT	Spreading of Photons for Radiation INTerception
STAAARTE	Scientific Training and Access to Aircraft for Atmospheric Research Throughout Europe
SWIR	ShortWave InfraRed
SZ	Solar Zenith
TERRA	NASA EOS platform carrying five satellite sensors, launched in April 1999
TIR	Thermal InfraRed
TM	Thematic Mapper
TMS	Thematic Mapper Simulator
TOA	Top Of the Atmosphere
TOPORAD	TOPOgraphic distribution of solar RADiation model
URSS	Upper Rhine Super Site (Test site of DAISEX'99 campaign)
UV	UltraViolet part of the electromagnetic spectrum
VI	Vegetation Index
VIS	VISible part of the electromagnetic spectrum
VNIR	Visible and NearInfraRed
WAAC	Wide Angle Airborne Camera
WDVI	Weighted Difference Vegetation Index
WS	White-Sky

List of Symbols

λ	Wavelength	[µm], [nm]
A	Surface area	[m^2]
A_{BHR}	BHR, bihemispherical reflectance, albedo	
$ANIF$	Anisotropy factor, reflectance in a specific view direction in relation to the nadir reflectance	
$ANIF_{BHR}$	Anisotropy index, reflectance in a specific view direction in relation to the bihemispherical reflectance	
d	Relative amount of direct irradiance ($d \in [0, 1]$)	
E	Irradiance, incident flux density	[Wm^{-2}]
f	Function	
θ_i, φ_i	Zenith and azimuth angle of the direction of illumination	
θ_r, φ_r	Zenith and azimuth angle of the direction of reflection	
$\vec{r}$	Location	
p	Polarization	
Φ	Radiant flux	[W]
ϑ	View direction	
t	Time	
ρ	Reflectance	[dimensionless]
L	Radiance	[$Wm^{-2}sr^{-1}$]
L_r	Reflected radiance of the target	[$Wm^{-2}sr^{-1}$]
L_r^{ref}	Reflected radiance of the reference panel	[$Wm^{-2}sr^{-1}$]
ω	Solid angle	[sr]
Ω	Projected solid angle	[sr]
R	Reflectance factor	[dimensionless]
R^{hem}	HDRF, hemispherical-directional reflectance factor	
R^{ref}	BRF, bidirectional reflectance factor of the reference panel	
S	Distribution of direction of radiation	

Sub- and superscripts

diff	Diffuse
dir	Direct
i	Incident
r	Reflected
id	Ideal (lossless) and diffuse (isotropic or Lambertian)

Chapter 1

Introduction and Problem Description

1.1 Importance of spatial characterization of vegetation and the role of spectrodirectional remote sensing

Detailed information about the extent and status of the biosphere is important for the prediction of the Earth's climate and the human impact in the framework of the Kyoto Protocol (UNFCCC, 1999) and carbon cycle research (ESA, 2004; CarboEurope-IP, 2003). More generally, the description and study of most ecological, environmental and agricultural processes with spatial extent do need spatially continuous and georeferenced information about the biosphere.

Remote sensing has proven to be a unique tool to contribute to the investigation, mapping and monitoring of these processes. There is a wide range of applications, which can be categorized by (1) the temporal and spatial scale (from studies using unique data at a local scale to analysis of global data sets throughout 20 years), (2) the applied remote sensing technique in terms of the platform (ranging from field spectrometers to satellite sensors), number of spectral bands, view angles, and polarisation, (3) the derived information about the vegetation (in terms of biochemical contents, canopy structure or biome and species identification), and finally by (4) the utilized methodology for the estimation of the desired vegetation variable (e.g., correlating vegetation indices, inverting radiative transfer models or assimilating remote sensing data into ecological or climate models).

All available radiometric descriptions of the vegetation canopy are an element of the above mentioned data space. For the real case, only a selected combination of these dimensions may be relevant or available. This thesis is concentrating on the combination of spectroscopy and multiangular remote sensing, i.e., on spectrodirectional data research. The transition from multispectral, broadband to continuous, narrowband spectrometers results in a more detailed description of the spectral space. The latter thus allows for an in-depth analysis of specific absorption features of vegetation canopy components. Broadband sensor data can be considered as a special case of spectrometer data, with integrated reflectance signals over a specified wavelength range. On the other hand, multiangular remote sensing is expanding the most common observation geometry in remote sensing, the combination of nadir view and a single sun illumination, to a more extensive description of the vegetation reflectance with regard to the geometrical space of view and illumination angles. This gives a more complete view on the energy fluxes between vegetation canopies and the atmosphere. The following examples highlight areas of applications for multiangular remote sensing and spectroscopy of the biosphere.

Remote sensing enables to monitor regional to global scale vegetation dynamics to improve the understanding and modelling of inter-annual variability in terrestrial ecosystem carbon exchange and climate-biosphere interactions (e.g., Buermann, 2001; Nemani, 2003; Zhang, 2003). Advancement in ecosystem modelling for the mapping of the net primary production is giving ways from simpler big-leaf photosynthesis models to more complex sunlit/shaded leaf sepa-

ration models and thus increases the demand for advanced description of canopy architecture (dePury, 1997). Multiangular optical remote sensing data can be used to map the required key structural variables serving as an input to advanced photosynthesis models for estimating the net primary production (Chen, 2003). The description of the vegetation structure includes different biophysical variables at the canopy level, such as the leaf area index (LAI), leaf angle distribution (LAD), fractional cover (fcover), gap size distribution, and biomass.

Jointly with improvements of the quality of available spectrometer data, advances in the estimation of biochemical components (such as the water, nitrogen, and chlorophyll content) and species discrimination have been achieved. Recent applications include investigations in arid and semiarid ecosystem functioning (Asner, 1998b; Serrano, 2002; Asner, 2003; Huete, 2003), land degradation (Haboudane, 2002a), invasion by non-native species (e.g., Ustin, 2001; Underwood, 2003), forest ecosystems (Martin, 1997), pasture quality explaining wildlife and livestock feeding patterns (Mutanga, 2004), the phenological cycle of crops (e.g., Kneubühler, 2002), and precision crop management (Strachan, 2002; Datt, 2003; Haboudane, 2002b; Inoue, 2003), to mention only a few.

For an improved understanding of the vegetation signal in the optical domain, the next section gives an overview of the contributing factors. Further, common approaches in remote sensing for the estimation of vegetation variables are presented. This forms the background for the detailed motivation of this thesis, with its main focus on the analysis of combined multiangular remote sensing and spectroscopy of vegetation canopies.

1.2 Estimation of vegetation characteristics by remote sensing

1.2.1 Description of the vegetation canopy reflectance

Various models do exist to simulate vegetation canopy reflectance, including two main components (e.g., Pinty, 2001; Pinty, 2004). First, leaf or needle optical properties (i.e., reflectance, transmittance and absorptance) are computed, based on leaf or needle structure, water content and biochemicals. In a second step, these leaf optical properties are used as an input to canopy models, which further account for e.g., the plant and canopy architecture, soil and understory reflectance, illumination composition and geometry, as well as the observation angle.

In the following, the major factors affecting the spectral and directional reflectance characteristics of vegetation canopies are explained in more detail. For the relative importance of these single factors on the canopy reflectance see also Baret, 1994; Asner, 1998a; and Bacour, 2002a.

a) Incoming radiation

In an outdoor environment, the illumination on a target is composed of a direct and diffuse radiance part. The direct part is the uncollided sunlight and thus is illuminating the observed target from the sun direction, within a small angular extent. The diffuse illumination is the radiance component colliding with atmospheric particles, the soil, vegetation or other objects and arriving at the target in a secondary or higher scattering order, from the entire sky sphere. Further, the diffuse component is influenced by the terrain surrounding the observed surface. This effect can be described using a topographic radiation model such as TOPORAD (Dozier, 1980).

Thus, depending on the scattering characteristics of the atmosphere and the target's environment, the amount and spectral character of the incident diffuse radiance is not homogeneously distributed over the sky sphere, but varies with the direction.

The total amount and spectral characteristics of incoming radiance can be estimated using radiometric observations of a near-Lambertian reference panel. Additionally, some devices designed for multiangular observations are scanning the sky and ground sphere, and thus assess the angular characteristics of the irradiance (Deering, 1986). For a more precise description of the incoming radiation, the direct and diffuse components can be assessed by employing sun photometers (Ehsani, 1998; Yankee Environmental Systems, 2002).

Not only the amount and spectral characteristics of the irradiance, but also the direction of the illumination source with respect to the vegetation structure and the viewing angle of the sensor are highly influencing the vegetation reflectance (e.g., Kimes, 1983).

b) Soil reflectance and understory

Incoming radiation is partly interacting with the vegetation canopy (being reflected, absorbed or transmitted) or can reach the soil or understory of the vegetation canopy uncollided. Be it in the first or higher scattering order, the radiance reflected by the understory and soil contributes to the vegetation canopy reflectance. The canopy transmittance (being a function of the leaf optical properties, the canopy structure, the illumination and view angle) as well as the soil brightness itself determine the contribution of the soil reflectance in the observed canopy signal (Tucker, 1977; Ottermann, 1995; Bacour, 2002a).

Spectral characteristics of the soil (Palacios-Orueta, 1996), litter and understory (Nagler, 2000), the soil brightness (Richardson, 1975; Galvao, 1998), as well as the soil directional characteristics (Pinty, 1989; Irons, 1992; Jacquemoud, 1992; Liu, 1994; Valeriano, 1995; Hapke, 1996; Cierniewski, 2002) have been investigated within various experimental and modelling studies.

Even though the anisotropic reflectance characteristics of the soil surface have been proven and successfully simulated, many canopy reflectance models assume the soil or understory to be Lambertian.

c) Leaf optical properties

Leaves and needles do represent the main scattering elements of vegetation canopies. Thus, the size, distribution and optical properties of leaves (i.e., reflectance, absorptance and transmittance), are of major importance for the description of the radiative transfer in vegetation canopies (Ottermann, 1995; Asner, 1998a; Panferov, 2001; Knyazikhin, 2004).

Models, such as PROSPECT (Jacquemoud, 1990) and LIBERTY (Dawson, 1998) do simulate leaf optical properties, based on the leaf structure(e.g., leaf mesophyll description) and it's biochemical composition, such as water content, dry matter, chlorophyll and carotinoid content. Some biochemicals are masked by the leaf water and are not represented in leaf models. Nevertheless their quantitative representation in the leaf reflectance spectrum has successfully been demonstrated using correlation analysis with fresh and dried leaf samples (Wessman, 1988; Curran, 1989; Fourty, 1998). Thus, nitrogen is an important quantity for ecological applications, but is not an input variable of the leaf model PROSPECT. Therefore it cannot be directly estimated by the inversion of the leaf model, but rather has to be derived through an empirical relationship with the chlorophyll content.

Several studies demonstrated the existence of directional leaf transmittance and reflectance properties of selected species (Sandmeier, 2000b; Jacquemoud, 2003). Nevertheless, most canopy reflectance models assume leaves to be Lambertian.

Scattering elements of vegetation canopies do not only include leaves, but standing litter, stem and branches as well. Their optical properties are of major importance for the analysis of reflectance data of certain ecosystems, such as grasslands (e.g., Asner, 1998a).

d) Canopy structure

The amount, size, orientation and distribution of the main scattering elements, i.e., the leaves and needles, are of major importance for the radiation regime of vegetation canopies. While the potential spectral space of the radiation at the canopy level is given by the leaf, stem, litter, understory and soil optical properties, the plant architecture and canopy structure determine their relative contribution to the canopy reflectance. In radiative transfer models, the plant architecture is described by quantities such as the one-sided green leaf area, the shape and size of the scattering elements, leaf angle distribution, the leaf clumping, and the plant geometry.

Depending on the ecosystem type and the phenology of an observed canopy, there exists a big difference in the amount and distribution of the single plants, trees and bushes in a landscape. Further, terrain effects do influence the reflectance of canopies by the magnitude and orientation of the slope (Combal, 2002). Regarding the scene composition, two major types of models describing the radiative transfer in vegetation canopies do exist: a) 1-D models (e.g., SAIL (Verhoef, 1984), Markov chain model of Kuusk (1995)) adapted to the simulation of ho-

mogeneous canopies (such as agricultural crops without a specific row structure), and b) 3-D models, capable of calculating the radiative transfer of heterogeneous scenes, such as forest areas (e.g., DART (Gastellu-Etchegorry, 1996), FLIGHT (North, 1996), RAYTRAN (Govaerts, 1998), SPRINT (Thompson, 1998)). The radiation transfer model intercomparison (RAMI) exercise systematically and quantitatively assesses model discrepancies with respect to several applications (Pinty, 2001; Pinty, 2004).

e) Viewing geometry

The viewing geometry is defined by the zenith and azimuth angle of the sensor, with respect to the sun and the observed surface.

One of the most known effects of the viewing direction is the sun glint over water. A blinding effect over water occurs for a certain angular configuration of the sun and the position of the observer, whereas this effect disappears when looking from a different location. For vegetation areas, the brightest reflectance signal of the canopy can be observed in the backscattering direction where shadows are covered, i.e., from the position where the view angle corresponds to the illumination angle. The corresponding increased reflectance feature is called hot spot.

In addition to the above mentioned geometrical-optical effect (i.e., the shadow-casting), the anisotropy of the reflectance of vegetation canopies is mainly driven by their volume-scattering, and by specular reflection (Lucht, 2000).

Whereas the nadir observation is the most common view direction in remote sensing, multiangular experiments and sensor systems for vegetation studies have been designed and used since a long time (see Chapter 1.2.2). They demonstrate the benefit of such observations for the estimation of structural characteristics and are essential for the development of methods to correct side effects introduced by the viewing and illumination geometry.

1.2.2 Multiangular remote sensing of vegetation canopies

The acquisition of multiangular data using field devices has started many years ago. Overcoming the merely descriptive approach of plant's directional reflection properties, model inversion studies demonstrated the structure-related information content of directional vegetation data. In the preparation and the product validation phases of multiangular satellite sensors, many campaigns employing field devices and prototyping airborne instruments were performed. To state only a few outstanding examples: AgRISTARS (Bauer, 1986), FIFE (1987, Deering, 1992), BOREAS (1993-1996, *http://www.daac.ornl.gov/BOREAS/boreas_home_page.html*), DAISEX (1998-2000, *http://io.uv.es/projects/daisex/*), and SAFARI 2000 (1999-2001, *http://www.daac.ornl.gov/S2K/safari.html*).

A variety of remote sensing field, airborne, as well as on-orbit instruments are used to approach the bidirectional reflectance distribution function (BRDF) and derive the albedo of natural targets. Spaceborne sensors provide data at a global

scale and thus contribute to the understanding of the Earth's ecosystem and atmospheric processes. Airborne and field measurements extend the spectral, directional, spatial, and temporal sampling of the on-orbit counterparts. Additionally they allow for the validation of data derived from the spaceborne instruments. Some of the most known devices designed for multiangular data acquisition are listed in Table 1.1 and Table 1.2. The first table clearly highlights, that the availability of satellite data with a combination of continuous spectral and multiangular coverage is very limited as of today. This gap is potentially to be filled by the European Space Agency's Earth Explorer Core mission SPECTRA (ESA, 2004).

Sensor	Platform	Reference	Angular Sampling	Spectral Coverage
ATSR	ERS-1	Stricker, 1995	0°, 47° forward	1.6, 3.7, 11, 12 µm
ATSR-2	ERS-2	Stricker, 1995	0°, 47° forward	550, 659, 865 nm, 1.6, 3.7, 11, 12 µm
AATSR	ENVISAT	envisat.esa.int /dataproducts	0°, 47° forward	550, 670, 870 nm, 1.6, 3.7, 10.7, 12 µm
CHRIS	PROBA	www.chris-proba.org.uk	0°, ±36°, ±55°	0.41-1.05 µm 81 bands
MISR	TERRA	Diner, 1998b	0°, ±26.1°, ±45.6°, ±60.0°, ±70.5°	446, 558, 672, 866 nm
POLDER 1	ADEOS 1	Deschamps, 1994	wide FOV (2400 km swath), multiple-day composites (41 day cycle)	443, 490, 565, 763, 765, 910 nm; polarized radiance: 443, 565, 865 nm
POLDER 2	ADEOS 2	smsc.cnes.fr/ POLDER/	wide FOV (2400 km swath), multiple-day composites (4 day cycle)	443, 490, 565, 763, 765, 910 nm; polarized radiance: 443, 565, 865 nm
AirMISR	Aircraft	Diner, 1998a	±70.5°, ±60°, ±45.6°, ±26.1°, 0°	0.446, 0.557, 0.672, 0.866 µm
Airborne Polder	Balloon, aircraft	www-loa.univ-lille1.fr/ AirPOLDER/	circular flight pattern, FOV along-track ±51°, cross-track ±43°	443, 500, 550, 590, 670, 700, 720, 800, 864 nm
ASAS	Aircraft	Irons, 1991	along-track +70° to -55°	0.404-1.02 µm, 62 bands
CAR	Aircraft	Tsay, 1998		0.34-2.3 µm,14 bands

Table 1.1: Overview of spaceborne and airborne instruments with multi-angular data acquisition capabilities (FOV = Field of view).

Sensor	Platform	Reference	Angular Sampling	Spectral Coverage
ASG	Field device	Painter, 2003	ground sphere coverage	0.35-2.5 µm
FIGOS	Field device	Sandmeier, 1999	full ground sphere coverage	0.3-2.5 µm, 704 bands
PARA-BOLA	Field device	Deering, 1986	sky, ground sphere coverage, FOV 15°	0.63-0.69, 0.76-0.9, 1.55-1.75 µm
PARA-BOLA III	Field device	Bruegge, 2000	sky, ground sphere coverage, FOV 5°	444, 551, 581, 650, 860, 944, 1028, 1650 nm
WAAC	Field device	Demircan, 2000	ground sphere coverage	350-900 nm, spectral filters (optional)
EGO	Lab. device	Koechler, 1994	ground sphere coverage	depending on radiometer
LAGOS	Lab. device	Dangel, 2003	ground sphere coverage	0.3-2.5 µm, 704 bands
Leaf Goniom.	Lab. device	Despan, 2004	sphere cov. of leaf refl., transm.	0.45-0.9 µm
ONERA Goniom.	Lab., field device	Serrot, 1998	ground sphere coverage	0.3-1.2 µm

Table 1.2: Overview of field and laboratory instruments with multi-angular data acquisition capabilities (FOV = Field of view, Goniom. = Goniometer,Lab. = Laboratory, refl. = reflectance, transm. = transmittance). For an extensive list of laboratory devices see Sandmeier, 2000b.

1.2.3 Methods of leaf and canopy variable estimation

Adapted to the problem formulation, the approach selected to estimate leaf and canopy variables may range from empirically established correlations up to the inversion of physically based radiative transfer models.

For a long time, remote sensing studies estimating vegetation characteristics fully relied on broadband sensor data. They mainly established empirical or semi-empirical relationships of band ratios with ground truth data. The most common quantity derived from remote sensing data and correlated to vegetation variables is the Normalized Difference Vegetation Index (NDVI (Rouse, 1973)). Many other vegetation indices (VIs) were derived to minimise unwanted side effects in NDVI data (Epiphanio, 1995) originating from the temporal and spatial variation in the geometry of illumination and observation, the soil colour and brightness, atmospheric scattering and absorption properties (e.g., MERIS Global Vegetation Index (MGVI (Gobron, 1999)), Optimized Vegetation Normalized Index (OVNI (Vogt, 1997)), Soil Adjusted Vegetation Index (SAVI (Huete, 1988))).

Narrowband vegetation indices calculated from spectrometer data have become a common methodology for the estimation of biochemical contents of vegetation canopies, especially chlorophyll and water content (Serrano, 2000; Zarco-Tejada, 2001; Haboudane, 2002b; Sims, 2002, 2003; le Maire, 2004). Only a few studies inverted radiative transfer models to derive the chlorophyll content (e.g., Fourty, 1996; Bacour, 2002a; Zarco-Tejada, 2004). The estimation of foliar or canopy biochemicals other than water and chlorophyll mostly relies on regression analysis. Spectroscopy in laboratories on leaf samples has a long tradition in chemistry and biology. A step forward was the estimation of canopy biochemicals using field and airborne spectrometers, based on correlations with dried plant material analysis (Wessman, 1988). Applying such relations to independent data sets and different leaf types led to very poor performances (Fourty, 1998). Due to the weakness and lack of specific absorption features of biochemicals, the inversion of radiative transfer models using fresh leaf and canopy reflectance data only allows a robust estimation of water and dry matter content as a whole (i.e., integrated content of cellulose, hemicellulose, protein, sugar, lignin, and starch). Main problems are identified in masking of absorption features of biochemicals by radiometric noise, by chlorophyll pigments in the visible domain, and by water in the middle infrared (Baret, 1997). Thus, recent studies on grassland and forest ecosystems still concentrate on establishing and applying site- and species-specific relations between canopy reflectance and biochemicals (Serrano, 2002; Mutanga, 2004).

The estimation of biophysical variables using multiangular data mostly relies on the inversion of radiative transfer models. Many model inversion studies showed the feasibility of estimating canopy structural variables, but remain experimental, by using simulated or airborne sensor data (e.g., Gao, 1997, 2003; Abuelgasim, 1998; Dawson, 1998, 1999; Bicheron, 1999; Weiss, 2000, 2002; Bacour, 2002a, 2002b; Kimes, 2002; Combal, 2003). As measurement and model uncertainties make the inverse problem ill posed, recent studies emphasize the need of prior knowledge for successfully applying the modelling approach (Tian, 2003; Combal, 2003). The first operational biophysical variables derived from satellite sensor data by radiative transfer based algorithms are the LAI products of MODIS and MISR (Knyazikhin, 1998a, 1998b; Myneni, 2002; Hu, 2003). The algorithm for the estimation of the LAI from MISR data is based on the reflectance data of all nine view angles and the albedo, but relies only on the red and NIR spectral band, due to increased uncertainties introduced by the blue and green band reflectance quantities.

1.3 Rationale of dissertation

1.3.1 Motivation

The estimation of vegetation variables using spectrodirectional remote sensing data reduces the uncertainties of the resulting products (ESA, 2004). Thus, most recent and future satellites are designed to record remote sensing data in higher spectral and directional resolution than conventional systems. Accounting for the entire spectrodirectional data in the analysis process leads to an increased information content for the generation of vegetation products, joined by increased uncertainties due to the sensor's noise and the atmospheric contribution to the measured reflectance signal. To quantify and minimize data uncertainties, ground based experiments are designed, supporting the calibration and validation of spectrodirectional data acquisition by air- and spaceborne imaging sensors. Recent studies have shown good agreement between multiangular ground based and airborne spectrometer reflectance and radiance data (Abdou, 2001; Beisl, 2001). Existing multiangular satellite sensors are limited in various dimensions: They cover only a limited range of view angles, mainly cover the spectrum with a few broad bands only, and the fixed overpass time of the sensor restricts the data acquisition to a fixed set of illumination/obervation geometries for a single spot. The experimental imaging spectrometer CHRIS on PROBA (see Table 1.1) partly fills this gap for a highly-specialized research community, but data availability is limited to a few selected test sites. Therefore, airborne and ground based spectrometers with multiangular capabilities and the possibility of diurnal observations are currently the main suppliers for basic research in spectrodirectional reflectance data. This is of major importance for the validation of radiative transfer modelling approaches, for forward simulations as well as the inversion of the models to estimate vegetation variables. Further, the availability and uncertainty assessment of directional data has to be enhanced to generate reliable databases of BRDF a priori knowledge. This information is used to improve the retrieval of surface bidirectional reflectance and spectral albedo from satellite data (Li, 2001). Many directional observations resulting from field campaigns do exist, but are not comparable so far within each other, due to different acquisition and processing schemes, as well as inconsistent usage of the reflectance nomenclature.

The above summary on the state of the art of applications and methodologies, using spectrodirectional remote sensing data for the estimation of vegetation variables, leads to the following conclusions: (1) all remote sensing data are a function of the corresponding illumination and view angle, including spectrometer data, but (2) many applications using various sources of remotly sensed data, including spectrometer data, do not explicitly take into account specific sun and view angle effects, and (3) mostly are not aware of existing reflectance definitions, whereas

(4) most multiangular data analysis are based on a small number of spectral bands.

By synthetizing the abouve identified shortcomings, the following research questions have been derived for this thesis:

- What is the range of uncertainty in the analysis of measured and modelled spectrodirectional reflectance data introduced by neglecting sun and view angle effects, at the reflectance level?
- What spectral effects are present in measured and simulated spectrodirectional reflectance data?
- What is the range of uncertainty in the analysis of reflectance data introduced by improper usage of existing reflectance nomenclature, at the reflectance level?
- Can a common terminology of reflectance be derived to minimize these uncertainties in the future?

1.3.2 Structure of the thesis

Based on the above research questions, the following structure has been derived for this thesis. The introduction and problem description are given in Chapter 1. Chapter 2 consists of the European Space Agency bulletin contribution 'The DAISEX campaigns in support of a future land-surface-processes mission' (Berger, 2001). It contains an overall description of ESA's Digital Airborne Imaging Spectrometer EXperiment (DAISEX), where most of the fieldwork for this thesis has been carried out.

Chapter 3 and 4 contain two papers describing the analysis of spectrodirectional reflectance data of a dense Alfalfa (*Medicago sativa*) canopy and a soil. The applied FIGOS equipment allows for the investigation of view angle effects, whereas the data acquisition throughout the day enables to assess the influence of the sun geometry. The contribution published in the Journal of Photogrammetry and Remote Sensing (Strub, 2002), 'Evaluation of diurnal hyperspectral HDRF data acquired with the RSL field goniometer during the DAISEX'99 campaign' demonstrates spectral effects in directional reflectance data of soil and vegetation. The vegetation data are further applied to show the influence of directional effects in the derivation of vegetation variables, such as the LAI by means of the Weighted Difference Vegetation Index (Chapter 3). The paper 'Evaluation of spectrodirectional Alfalfa canopy data acquired during DAISEX'99', published in Institute of Electrical and Electronics Engineers (Ieee) Transactions on Geoscience and Remote Sensing (Strub, 2003), focuses on the analysis of spectrodirectional reflectance data acquired over the Alfalfa canopy. First, a possible standard procedure for the preprocessing of field goniometer data is presented. The main part of the contribution compares measured spectrodirectional reflectances and the derived spectral albedo with corresponding modelled data. The comparison is used as a tool to highlight spectral effects in spectrodirectional observations and modelled

data from radiative transfer codes, such as the applied modified version of Scattering by Arbitrarily Inclined Leaves, with implemented Hot spot (SAILH) (Chapter 4).

Whereas the second and third contribution mainly concentrate on observed and simulated spectrodirectional reflectance characteristics at the local scale, the third paper, 'Review of Reflectance Nomenclature used in Optical Remote Sensing with Quantitative Comparisons' (Schaepman-Strub, in preparation), shall clarify the conceptual basis for further analysis in this domain (Chapter 5). The contribution contains a review of the spectrodirectional reflectance nomenclature and exemplifies differences of named quantities using MISR and simulated data. Even though definitions and descriptions of measured reflectance quantities do exist (Nicodemus, 1977; Martonchik, 2000), they are neglected by many remote sensing studies. This contribution shall enhance the awareness of reflectance nomenclature and its adequate use. The importance of this process is highlighted by a modelling and data analysis part quantifying the differences between often equated quantities. Chapter 6 contains the conclusion drawn from this thesis with respect to the research questions posed, and results in an outlook recommending future activities in this particular field.

1.4 References

Abdou, W.A., J.E. Conel, S.H. Pilorz, M.C. Helmlinger, C.J. Bruegge, B.J. Gaitley, W.C. Ledeboer, and J.V. Martonchik, Vicarious calibration - A reflectance-based experiment with Air-MISR, Remote Sensing of Environment, 77 (3), 338-353, 2001.

Abuelgasim, A.A., S. Gopal, and A.H. Strahler, Forward and inverse modelling of canopy directional reflectance using a neural network, International Journal of Remote Sensing, 19 (3), 453-471, 1998.

Asner, G.P., Biophysical and biochemical sources of variability in canopy reflectance, Remote Sensing of Environment, 64 (3), 234-253, 1998a.

Asner, G.P., and K.B. Heidebrecht, Imaging spectroscopy for desertification studies: Comparing AVIRIS and EO-1 Hyperion in Argentina drylands, Ieee Transactions on Geoscience and Remote Sensing, 41 (6), 1283-1296, 2003.

Asner, G.P., C.A. Wessman, and D.S. Schimel, Heterogeneity of savanna canopy structure and function from imaging spectrometry and inverse modeling, Ecological Applications, 8 (4), 1022-1036, 1998b.

Bacour, C., S. Jacquemoud, M. Leroy, O. Hautecoeur, M. Weiss, L. Prevot, N. Bruguier, and H. Chauki, Reliability of the estimation of vegetation characteristics by inversion of three canopy reflectance models on airborne POLDER data, Agronomie, 22 (6), 555-565, 2002a.

Bacour, C., S. Jacquemoud, Y. Tourbier, M. Dechambre, and J.P. Frangi, Design and analysis of numerical experiments to compare four canopy reflectance models, Remote Sensing of Environment, 79 (1), 72-83, 2002b.

Baret, F., and T. Fourty, Estimation of leaf water content and specific leaf weight from reflectance and transmittance measurements, Agronomie, 17 (9-10), 455-464, 1997.

Baret, F., V.C. Vanderbilt, M.D. Steven, and S. Jacquemoud, Use of Spectral Analogy to Evaluate

Canopy Reflectance Sensitivity to Leaf Optical-Properties, Remote Sensing of Environment, 48 (2), 253-260, 1994.

Bauer, M.E., C. Daughtry, L. Biehl, E. Kanemasu, and F. Hall, Field spectroscopy of agricultural crops, Ieee Transactions on Geoscience and Remote Sensing, 24 (1), 65-75, 1986.

Beisl, U., Correction of Bidirectional Effects in Imaging Spectrometer Data, in Remote Sensing Series, edited by K. Itten, D. Nuesch, U. Frei, T. Kellenberger, E. Meier, and M. Schaepman, pp. 189, Remote Sensing Laboratories, Zurich, 2001.

Berger, M., M. Rast, P. Wursteisen, E. Attema, J. Moreno, A. Muller, U. Beisl, R. Richter, M. Schaepman, G. Strub, M.P. Stoll, F. Nerry, and M. Leroy, The DAISEX campaigns in support of a future land-surface-processes mission, Esa Bulletin-European Space Agency (105), 101-111, 2001.

Bicheron, P., and M. Leroy, A method of biophysical parameter retrieval at global scale by inversion of a vegetation reflectance model, Remote Sensing of Environment, 67 (3), 251-266, 1999.

Bruegge, C.J., M.C. Helmlinger, J.E. Conel, B.J. Gaitley, and W.A. Abdou, PARABOLA III: A Sphere-scanning Radiometer for Field Determination of Surface Anisotropic Reflectance Functions, Remote Sensing Reviews, 19 (1-4), 75-94, 2000.

Buermann, W., J.R. Dong, X.B. Zeng, R.B. Myneni, and R.E. Dickinson, Evaluation of the utility of satellite-based vegetation leaf area index data for climate simulations, Journal of Climate, 14 (17), 3536-3550, 2001.

CarboEurope – Integrated Project "Assessment of the European Terrestrial Carbon Balance", Annex I – "Description of work", Contract No. 505572, supported by European Commission, DG Research, Global Change and Ecosystems, 13 November, 2003.

Chen, J.M., J. Liu, S.G. Leblanc, R. Lacaze, and J.L. Roujean, Multi-angular optical remote sensing for assessing vegetation structure and carbon absorption, Remote Sensing of Environment, 84 (4), 516-525, 2003.

Cierniewski, J., M. Verbrugghe, and A. Marlewski, Effects of farming works on soil surface bidirectional reflectance measurements and modelling, International Journal of Remote Sensing, 23 (6), 1075-1094, 2002.

Combal, B., F. Baret, M. Weiss, A. Trubuil, D. Mace, A. Pragnere, R. Myneni, Y. Knyazikhin, and L. Wang, Retrieval of canopy biophysical variables from bidirectional reflectance - Using prior information to solve the ill-posed inverse problem, Remote Sensing of Environment, 84 (1), 1-15, 2003.

Curran, P.J., Remote-Sensing of Foliar Chemistry, Remote Sensing of Environment, 30 (3), 271-278, 1989.

Dangel, S., M. Kneubühler, R. Kohler, M. Schaepman, J. Schopfer, G. Schaepman-Strub, and K. Itten, Combined Field and Laboratory Goniometer System – FIGOS and LAGOS, in IGARSS, Toulouse, France, 2003.

Datt, B., T.R. McVicar, T.G. Van Niel, D.L.B. Jupp, and J.S. Pearlman, Preprocessing EO-1 Hyperion hyperspectral data to support the application of agricultural indexes, Ieee Transactions on Geoscience and Remote Sensing, 41 (6), 1246-1259, 2003.

Dawson, T.P., P.J. Curran, P.R.J. North, and S.E. Plummer, The propagation of foliar biochemical absorption features in forest canopy reflectance: A theoretical analysis, Remote Sensing of Environment, 67 (2), 147-159, 1999.

Dawson, T.P., P.J. Curran, and S.E. Plummer, LIBERTY - Modeling the effects of leaf biochemical concentration on reflectance spectra, Remote Sensing of Environment, 65 (1), 50-60, 1998.

de Pury, D.G.G., and G.D. Farquhar, Simple scaling of photosynthesis from leaves to canopies without the errors of big-leaf models, Plant Cell and Environment, 20 (5), 537-557, 1997.

Deering, D.W., and P. Leone, A Sphere-Scanning Radiometer for Rapid Directional Measurements of Sky and Ground Radiance, Remote Sensing of Environment, 19 (1), 1-24,

1986.

Deering, D.W., E.M. Middleton, J.R. Irons, B.L. Blad, E.A. Waltershea, C.J. Hays, C. Walthall, T.F. Eck, S.P. Ahmad, and B.P. Banerjee, Prairie Grassland Bidirectional Reflectances Measured by Different Instruments at the Fife Site, Journal of Geophysical Research-Atmospheres, 97 (D17), 18887-18903, 1992.

Demircan, A., R. Schuster, M. Radke, M. Schonermark, and H.P. Roser, Use of a wide angle CCD line camera for BRDF measurements, Infrared Physics & Technology, 41 (1), 11-19, 2000.

Deschamps, P.Y., F.M. Breon, M. Leroy, A. Podaire, A. Bricaud, J.C. Buriez, and G. Seze, The Polder Mission - Instrument Characteristics and Scientific Objectives, Ieee Transactions on Geoscience and Remote Sensing, 32 (3), 598-615, 1994.

Despan, D., and S. Jacquemoud, Optical Properties of Soil and Leaf: Necessity and Problems of Modeling, in Reflection Properties of Vegetation and Soil - with a BRDF Data Base, edited by M. VonSchönermark, B. Geiger, and H.P. Röser, pp. 39-70, Wissenschaft und Technik Verlag, Berlin, 2004.

Diner, D.J., L.M. Barge, C.J. Bruegge, T.G. Chrien, J.E. Conel, M.L. Eastwood, J.D. Garcia, M.A. Hernandez, C.G. Kurzweil, W.C. Ledeboer, N.D. Pignatano, C.M. Sarture, and B.G. Smith, The Airborne Multi-angle Imaging SpectroRadiometer (AirMISR): Instrument description and first results, Ieee Transactions on Geoscience and Remote Sensing, 36 (4), 1339-1349, 1998a.

Diner, D.J., J.C. Beckert, T.H. Reilly, C.J. Bruegge, J.E. Conel, R.A. Kahn, J.V. Martonchik, T.P. Ackerman, R. Davies, S.A.W. Gerstl, H.R. Gordon, J.P. Muller, R.B. Myneni, P.J. Sellers, B. Pinty, and M.M. Verstraete, Multi-angle Imaging SpectroRadiometer (MISR) - Instrument description and experiment overview, Ieee Transactions on Geoscience and Remote Sensing, 36 (4), 1072-1087, 1998b.

Ehsani, A.R., J.A. Reagan, and W.H. Erxleben, Design and performance analysis of an automated 10-channel solar radiometer instrument, Journal of Atmospheric and Oceanic Technology, 15 (3), 697-707, 1998.

Epiphanio, J.C.N., and A.R. Huete, Dependence of Ndvi and Savi on Sun Sensor Geometry and Its Effect on Fapar Relationships in Alfalfa, Remote Sensing of Environment, 51 (3), 351-360, 1995.

ESA, SPECTRA - Surface Processes and Ecosystem Changes Through Response Analysis, Reports for Mission Selection, The Six Candidate Earth Explorer Missions, ESA SP-1279(2), pp. 74, European Space Agency, Mission Experts Division, Noordwijk, The Netherlands, 2004.

Fourty, T., and F. Baret, On spectral estimates of fresh leaf biochemistry, International Journal of Remote Sensing, 19 (7), 1283-1297, 1998.

Fourty, T., F. Baret, S. Jacquemoud, G. Schmuck, and J. Verdebout, Leaf optical properties with explicit description of its biochemical composition: Direct and inverse problems, Remote Sensing of Environment, 56 (2), 104-117, 1996.

Galvao, L.S., and I. Vitorello, Variability of laboratory measured soil lines of soils from southeastern Brazil, Remote Sensing of Environment, 63 (2), 166-181, 1998.

Gao, F., C.B. Schaaf, A. Strahler, Y. Jin, and X. Li, Detecting vegetation structure using a kernel-based BRDF model, Remote Sensing of Environment, 86, 198-205, 2003.

Gao, W., and B.M. Lesht, Model inversion of satellite-measured reflectances for obtaining surface biophysical and bidirectional reflectance characteristics of grassland, Remote Sensing of Environment, 59 (3), 461-471, 1997.

Gastellu Etchegorry, J.P., V. Demarez, V. Pinel, and F. Zagolski, Modeling radiative transfer in heterogeneous 3-D vegetation canopies, Remote Sensing of Environment, 58 (2), 131-156, 1996.

Gobron, N., B. Pinty, M. Verstraete, and Y. Govaerts, The MERIS Global Vegetation Index (MGVI): description and preliminary application, International Journal of Remote Sens-

ing, 20 (9), 1917-1927, 1999.
Govaerts, Y.M., and M.M. Verstraete, Raytran: A Monte Carlo ray-tracing model to compute light scattering in three-dimensional heterogeneous media, Ieee Transactions on Geoscience and Remote Sensing, 36 (2), 493-505, 1998.
Haboudane, D., F. Bonn, A. Royer, S. Sommer, and W. Mehl, Land degradation and erosion risk mapping by fusion of spectrally-based information and digital geomorphometric attributes, International Journal of Remote Sensing, 23 (18), 3795-3820, 2002a.
Haboudane, D., J.R. Miller, N. Tremblay, P.J. Zarco-Tejada, and L. Dextraze, Integrated narrow-band vegetation indices for prediction of crop chlorophyll content for application to precision agriculture, Remote Sensing of Environment, 81 (2-3), 416-426, 2002b.
Hapke, B., D. DiMucci, R. Nelson, and W. Smythe, The cause of the hot spot in vegetation canopies and soils: Shadow-hiding versus coherent backscatter, Remote Sensing of Environment, 58 (1), 63-68, 1996.
Hu, J., B. Tan, N. Shabanov, K.A. Crean, J.V. Martonchik, D.J. Diner, Y. Knyazikhin, and R. Myneni, Performance of the MISR LAI and FPAR algorithm: a case study in Africa, Remote Sensing of Environment, 2003.
Huete, A.R., A Soil-Adjusted Vegetation Index (Savi), Remote Sensing of Environment, 25 (3), 295-309, 1988.
Huete, A.R., T. Miura, and X. Gao, Land cover conversion and degradation analyses through coupled soil-plant biophysical parameters derived from hyperspectral EO-1 Hyperion, Ieee Transactions on Geoscience and Remote Sensing, 41 (6), 1268-1276, 2003.
Inoue, Y., Synergy of remote sensing and modeling for estimating ecophysiological processes in plant production, Plant Production Science, 6 (1), 3-16, 2003.
Irons, J.R., G.S. Campbell, J.M. Norman, D.W. Graham, and W.M. Kovalick, Prediction and Measurement of Soil Bidirectional Reflectance, Ieee Transactions on Geoscience and Remote Sensing, 30 (2), 249-260, 1992.
Irons, J.R., K.J. Ranson, D.L. Williams, R.R. Irish, and F.G. Huegel, An Off-Nadir-Pointing Imaging Spectroradiometer for Terrestrial Ecosystem Studies, Ieee Transactions on Geoscience and Remote Sensing, 29 (1), 66-74, 1991.
Jacquemoud, S., and F. Baret, Prospect - a Model of Leaf Optical-Properties Spectra, Remote Sensing of Environment, 34 (2), 75-91, 1990.
Jacquemoud, S., F. Baret, and J.F. Hanocq, Modeling Spectral and Bidirectional Soil Reflectance, Remote Sensing of Environment, 41 (2-3), 123-132, 1992.
Kimes, D., J. Gastellu-Etchegorry, and P. Esteve, Recovery of forest canopy characteristics through inversion of a complex 3D model, Remote Sensing of Environment, 79 (2-3), 320-328, 2002.
Kimes, D.S., Dynamics of Directional Reflectance Factor Distributions for Vegetation Canopies, Applied Optics, 22 (9), 1364-1372, 1983.
Kneubühler, M., Spectral Assessment of Crop Phenology Based on Spring Wheat and Winter Barley, in Remote Sensing Series, edited by K. Itten, D. Nuesch, U. Frei, T. Kellenberger, E. Meier, and M. Schaepman, pp. 194, Remote Sensing Laboratories, Zurich, 2002.
Knyazikhin, Y., A. Marshak, and R. Myneni, Three-Dimensional Radiative Transfer in Vegetation Canopies, in Three-Dimensional Radiative Transfer in the Cloudy Atmosphere, edited by A. Davis, and A. Marshak, pp. 337-368, Springer-Verlag, 2004, in print.
Knyazikhin, Y., J.V. Martonchik, D.J. Diner, R.B. Myneni, M. Verstraete, B. Pinty, and N. Gobron, Estimation of vegetation canopy leaf area index and fraction of absorbed photosynthetically active radiation from atmosphere-corrected MISR data, Journal of Geophysical Research-Atmospheres, 103 (D24), 32239-32256, 1998a.
Knyazikhin, Y., J.V. Martonchik, R.B. Myneni, D.J. Diner, and S.W. Running, Synergistic algorithm for estimating vegetation canopy leaf area index and fraction of absorbed photosynthetically active radiation from MODIS and MISR data, Journal of Geophysical Research-Atmospheres, 103 (D24), 32257-32275, 1998b.

Koechler, C., B. Hosgood, G. Andreoli, G. Schmuck, J. Verdebout, A. Pegoraro, J. Hill, W. Mehl, D. Roberts, and M. Smith, The European optical goniometeric facility: technical description and first experiments on spectral unmixing, in IGARRSS'94, pp. 2375-2377, Pasadena, USA, 1994.

Kuusk, A., A Markov-Chain Model of Canopy Reflectance, Agricultural and Forest Meteorology, 76 (3-4), 221-236, 1995.

le Maire, G., C. Francois, and E. Dufrene, Towards universal broad leaf chlorophyll indices using PROSPECT simulated database and hyperspectral reflectance measurements, Remote Sensing of Environment, 89 (1), 1-28, 2004.

Li, X.W., F. Gao, J.D. Wang, and A. Strahler, A priori knowledge accumulation and its application to linear BRDF model inversion, Journal of Geophysical Research-Atmospheres, 106 (D11), 11925-11935, 2001.

Liu, C.H., A.J. Chen, and G.R. Liu, Variability of the Bare Soil Albedo Due to Different Solar Zenith Angles and Atmospheric Haziness, International Journal of Remote Sensing, 15 (13), 2531-2542, 1994.

Lucht, W., C.B. Schaaf, and A.H. Strahler, An algorithm for the retrieval of albedo from space using semiempirical BRDF models, Ieee Transactions on Geoscience and Remote Sensing, 38 (2), 977-998, 2000.

Martin, M.E., and J.D. Aber, High spectral resolution remote sensing of forest canopy lignin, nitrogen, and ecosystem processes, Ecological Applications, 7 (2), 431-443, 1997.

Martonchik, J.V., C.J. Bruegge, and A. Strahler, A review of reflectance nomenclature used in remote sensing, Remote Sensing Reviews, 19, 9-20, 2000.

Mutanga, O., A.K. Skidmore, and H.H.T. Prins, Predicting in situ pasture quality in the Kruger National Park, South Africa, using continuum-removed absorption features, Remote Sensing of Environment, 89 (3), 393-408, 2004.

Myneni, R.B., S. Hoffman, Y. Knyazikhin, J.L. Privette, J. Glassy, Y. Tian, Y. Wang, X. Song, Y. Zhang, G.R. Smith, A. Lotsch, M. Friedl, J.T. Morisette, P. Votava, R.R. Nemani, and S.W. Running, Global products of vegetation leaf area and fraction absorbed PAR from year one of MODIS data, Remote Sensing of Environment, 83 (1-2), 214-231, 2002.

Nagler, P.L., C.S.T. Daughtry, and S.N. Goward, Plant litter and soil reflectance, Remote Sensing of Environment, 71 (2), 207-215, 2000.

Nemani, R.R., C.D. Keeling, H. Hashimoto, W.M. Jolly, S.C. Piper, C.J. Tucker, R.B. Myneni, and S.W. Running, Climate-driven increases in global terrestrial net primary production from 1982 to 1999, Science, 300 (5625), 1560-1563, 2003.

Nicodemus, F.E., J.C. Richmond, J.J. Hsia, I.W. Ginsberg, and T. Limperis, Geometrical Considerations and Nomenclature for Reflectance, National Bureau of Standards, US Department of Commerce, Washington, D.C., 1977.

North, P.R.J., Three-dimensional forest light interaction model using a Monte Carlo method, Ieee Transactions on Geoscience and Remote Sensing, 34 (4), 946-956, 1996.

Otterman, J., T. Brakke, and J. Smith, Effects of Leaf-Transmittance Versus Leaf-Reflectance on Bidirectional Scattering from Canopy Soil Surface - an Analytical Study, Remote Sensing of Environment, 54 (1), 49-60, 1995.

Painter, T.H., B. Paden, and J. Dozier, Automated spectro-goniometer: A spherical robot for the field measurement of the directional reflectance of snow, Review of Scientific Instruments, 74 (12), 5179-5188, 2003.

Palacios Orueta, A., and S.L. Ustin, Multivariate statistical classification of soil spectra, Remote Sensing of Environment, 57 (2), 108-118, 1996.

Panferov, O., Y. Knyazikhin, R.B. Myneni, J. Szarzynski, S. Engwald, K.G. Schnitzler, and G. Gravenhorst, The role of canopy structure in the spectral variation of transmission and absorption of solar radiation in vegetation canopies, Ieee Transactions on Geoscience and Remote Sensing, 39 (2), 241-253, 2001.

Pinty, B., N. Gobron, J.L. Widlowski, S.A.W. Gerstl, M.M. Verstraete, M. Antunes, C. Bacour, F.

Gascon, J.P. Gastellu, N. Goel, S. Jacquemoud, P. North, W.H. Qin, and R. Thompson, Radiation transfer model intercomparison (RAMI) exercise, Journal of Geophysical Research-Atmospheres, 106 (D11), 11937-11956, 2001.

Pinty, B., M.M. Verstraete, and R.E. Dickinson, A Physical Model for Predicting Bidirectional Reflectances over Bare Soil, Remote Sensing of Environment, 27 (3), 273-288, 1989.

Pinty, B., J.L. Widlowski, M. Taberner, N. Gobron, M.M. Verstraete, M. Disney, F. Gascon, J.P. Gastellu, L. Jiang, A. Kuusk, P. Lewis, X. Li, W. Ni-Meister, T. Nilson, P. North, W.H. Qin, L. Su, S. Tang, R. Thompson, W. Verhoef, H. Wang, J. Wang, G. Yan, and H. Zang, Radiation Transfer Model Intercomparison (RAMI) exercise: Results from the second phase, Journal of Geophysical Research-Atmospheres, 109 (D06210), 2004.

Richardson, A.J., C.L. Wiegand, H.W. Gausman, J.A. Cuellar, and A.H. Gerbermann, Plant, Soil, and Shadow Reflectance Components of Row Crops, Photogrammetric Engineering and Remote Sensing, 41 (11), 1401-1407, 1975.

Rouse, J.W., R.H. Haas, J.A. Schell, and D.W. Deering, Monitoring vegetation systems in the Great Plains with ERTS-1, in Third Earth Resour. Tech. Satell. Symp., pp. 309-317, 1973.

Sandmeier, S.R., Acquisition of bidirectional reflectance factor data with field goniometers, Remote Sensing of Environment, 73 (3), 257-269, 2000a.

Sandmeier, S.R., and K.I. Itten, A field goniometer system (FIGOS) for acquisition of hyperspectral BRDF data, Ieee Transactions on Geoscience and Remote Sensing, 37 (2), 978-986, 1999.

Sandmeier, S.R., and A. Strahler, BRDF Laboratory Measurements, Remote Sensing Reviews, 18, 481-502, 2000b.

Schaepman-Strub, G., M. Schaepman, S. Dangel, T. Painter, M. Verstraete, and J.V. Martonchik, Review of reflectance nomenclature used in optical remote sensing with quantitative comparisons, submitted.

Sellers, P.J., B.W. Meeson, F.G. Hall, G. Asrar, R.E. Murphy, R.A. Schiffer, F.P. Bretherton, R.E. Dickinson, R.G. Ellingson, C.B. Field, K.F. Huemmrich, C.O. Justice, J.M. Melack, N.T. Roulet, D.S. Schimel, and P.D. Try, Remote-Sensing of the Land-Surface for Studies of Global Change - Models, Algorithms, Experiments, Remote Sensing of Environment, 51 (1), 3-26, 1995.

Serrano, L., J. Penuelas, and S.L. Ustin, Remote sensing of nitrogen and lignin in Mediterranean vegetation from AVIRIS data: Decomposing biochemical from structural signals, Remote Sensing of Environment, 81 (2-3), 355-364, 2002.

Serrano, L., S.L. Ustin, D.A. Roberts, J.A. Gamon, and J. Penuelas, Deriving water content of chaparral vegetation from AVIRIS data, Remote Sensing of Environment, 74 (3), 570-581, 2000.

Serrot, G., M. Bodilis, X. Briottet, and H. Cosnefroy, Presentation of a new BRDF measurement device, in SPIE, Europto series, Barcelona, Spain, 1998.

Sims, D.A., and J.A. Gamon, Relationships between leaf pigment content and spectral reflectance across a wide range of species, leaf structures and developmental stages, Remote Sensing of Environment, 81 (2-3), 337-354, 2002.

Sims, D.A., and J.A. Gamon, Estimation of vegetation water content and photosynthetic tissue area from spectral reflectance: a comparison of indices based on liquid water and chlorophyll absorption features, Remote Sensing of Environment, 84 (4), 526-537, 2003.

Strachan, I.B., E. Pattey, and J.B. Boisvert, Impact of nitrogen and environmental conditions on corn as detected by hyperspectral reflectance, Remote Sensing of Environment, 80 (2), 213-224, 2002.

Stricker, N.C.M., A. Hahne, D.L. Smith, J. Delderfield, M.B. Oliver, and T. Edwards, Atsr-2 - the Evolution in Its Design from Ers-1 to Ers-2, Esa Bulletin-European Space Agency (83), 32-37, 1995.

Strub, G., U. Beisl, M. Schaepman, D. Schlaepfer, C. Dickerhof, and K. Itten, Evaluation of diur-

nal hyperspectral HDRF data acquired with the RSL field goniometer during the DAISEX'99 campaign, Isprs Journal of Photogrammetry and Remote Sensing, 57 (3), 184-193, 2002.

Strub, G., M.E. Schaepman, Y. Knyazikhin, and K.I. Itten, Evaluation of spectrodirectional Alfalfa canopy data acquired during DAISEX'99, Ieee Transactions on Geoscience and Remote Sensing, 41 (5), 1034-1042, 2003.

Thompson, R., and N. Goel, Two models for rapidly calculating bidirectional reflectance: Photon spread (ps) model and statistical photon spread (sps) model, Remote Sensing Reviews, 16, 157-207, 1998.

Tian, Y.H., Y.J. Wang, Y. Zhang, Y. Knyazikhin, J. Bogaert, and R.B. Myneni, Radiative transfer based scaling of LAI retrievals from reflectance data of different resolutions, Remote Sensing of Environment, 84 (1), 143-159, 2003.

Tsay, S.C., M.D. King, G.T. Arnold, and J.Y. Li, Airborne spectral measurements of surface anisotropy during SCAR-B, Journal of Geophysical Research-Atmospheres, 103 (D24), 31943-31953, 1998.

Tucker, C.J., and L.D. Miller, Soil Spectra Contributions to Grass Canopy Spectral Reflectance, Photogrammetric Engineering and Remote Sensing, 43 (6), 721-726, 1977.

Underwood, E., S. Ustin, and D. DiPietro, Mapping nonnative plants using hyperspectral imagery, Remote Sensing of Environment, 86 (2), 150-161, 2003.

United Nations Framework Convention on Climate Change (UNFCCC). Full text of the Convention and the Kyoto Protocol. www.unfccc.de/resource/conv/index.html, 1999.

Ustin, S.L., G. Scheer, D. DiPietro, E. Underwood, and K. Olmstead, Hyperspectral remote sensing for invasive species detection and mapping., Abstracts of Papers of the American Chemical Society, 221, U50-U50, 2001.

Valeriano, M.M., J.C.N. Epiphanio, A.R. Formaggio, and J.B. Oliveira, Bidirectional Reflectance Factor of 14 Soil Classes from Brazil, International Journal of Remote Sensing, 16 (1), 113-128, 1995.

Verbrugghe, M., and J. Cierniewski, Influence and modelling of view angles and microrelief on surface temperature measurements of bare agricultural soils, Isprs Journal of Photogrammetry and Remote Sensing, 53 (3), 166-173, 1998.

Verhoef, W., Light-Scattering by Leaf Layers with Application to Canopy Reflectance Modeling - the Sail Model, Remote Sensing of Environment, 16 (2), 125-141, 1984.

Vogt, P., Bestimmung des Blattflächenindexes und der absorbierten, photosynthetisch aktiven Strahlung der Vegetation aus bidirektionalen Reflexionsfaktoren am Oberrand der Pflanzendecke, PhD thesis, Freie Universität, Berlin, 1997.

Weiss, M., F. Baret, M. Leroy, O. Hautecoeur, C. Bacour, L. Prevot, and N. Bruguier, Validation of neural net techniques to estimate canopy biophysical variables from remote sensing data, Agronomie, 22 (6), 547-553, 2002.

Weiss, M., F. Baret, R.B. Myneni, A. Pragnere, and Y. Knyazikhin, Investigation of a model inversion technique to estimate canopy biophysical variables from spectral and directional reflectance data, Agronomie, 20 (1), 3-22, 2000.

Wessman, C.A., J.D. Aber, D.L. Peterson, and J.M. Melillo, Remote-Sensing of Canopy Chemistry and Nitrogen Cycling in Temperate Forest Ecosystems, Nature, 335 (6186), 154-156, 1988.

Yankee Environmental Systems, I., Multi-filter rotating shadow band radiometer model MFR-7, 8 pp., Yankee Environmental Systems, Inc., Turner's Fall, MA, 2002.

Zarco-Tejada, P.J., J.R. Miller, J. Harron, B.X. Hu, T.L. Noland, N. Goel, G.H. Mohammed, and P. Sampson, Needle chlorophyll content estimation through model inversion using hyperspectral data from boreal conifer forest canopies, Remote Sensing of Environment, 89 (2), 189-199, 2004.

Zarco-Tejada, P.J., J.R. Miller, T.L. Noland, G.H. Mohammed, and P.H. Sampson, Scaling-up and model inversion methods with narrowband optical indices for chlorophyll content

estimation in closed forest canopies with hyperspectral data, Ieee Transactions on Geoscience and Remote Sensing, 39 (7), 1491-1507, 2001.

Zhang, X.Y., M.A. Friedl, C.B. Schaaf, A.H. Strahler, J.C.F. Hodges, F. Gao, B.C. Reed, and A. Huete, Monitoring vegetation phenology using MODIS, Remote Sensing of Environment, 84 (3), 471-475, 2003.

Chapter 2

The DAISEX Campaigns in Support of a Future Land-Surface-Processes Mission

Berger, M., M. Rast, P. Wursteisen, E. Attema, J. Moreno, A. Muller, U. Beisl, R. Richter, M. Schaepman, G. Strub, M.P. Stoll, F. Nerry, and M. Leroy, The DAISEX campaigns in support of a future land-surface-processes mission, Esa Bulletin-European Space Agency (105), 101-111, 2001.

Reprinted with permission from ESA, 2004.

The contribution of G. Schaepman-Strub to this journal consists of the planning, acquisition, analysis and visualization of the Swiss field goniometer system (FIGOS) measurements in the frame of the ESA DAISEX'99 field campaigns.

Abstract

In the last ten years, the retrieval of geo-/biophysical parameters from airborne imaging-spectrometer data has made significant progress. ESA therefore decided to investigate the feasibility of quantitatively retrieving geo-/biophysical variables as the requisite inputs for process models. For three years in succession (1998 to 2000), therefore, the Agency has conducted an airborne imaging spectrometer campaign called 'The Digital Airborne Imaging Spectrometer Experiment (DAISEX)' in support of a possible future spaceborne mission. The instruments flown included DAIS 7915, HYMAP, ROSIS, POLDER and LEANDRE. This article describes the state of the art in retrieving variables relevant to land-surface processes from hyperspectral data cubes, outlines the scientific objectives, and demonstrates the first results of the DAISEX campaigns.

2.1 Introduction

Part of ESA's Earth Observation Envelope Programme (EOEP) is intended to advance our understanding of the various processes occurring in the Earth's biosphere/geosphere, and their interactions with the atmosphere. Thus, the Programme's 'Theme 3: Geosphere/ Biosphere' focusses on the modelling and monitoring of land-surface processes, the study of interactions, and the analysis of climate impacts on the biosphere, with the objective of enhancing our skills in predicting the evolution of the Earth system.

Real-life applications such as weather forecasting, crop-yield estimation, precision farming, the management of renewable and non-renewable resources, as well as environmental-hazard monitoring/forecasting, would all benefit from improved process model descriptions.

A spaceborne scientific mission addressing the provision of information on geospheric/ biospheric processes and their interactions with the atmosphere is currently being formulated. This mission implies the need for an instrument with high spectral and angular resolution and a very high radiometric performance, operating in the reflective and thermal parts of the spectrum, not only to identify but also to quantify the key variables driving the processes.

2.2 Background

The Earth's environment is a complex system that couples, on various temporal and spatial scales, the atmosphere, the oceans, the land and the cryosphere. Many aspects of the functioning of the Earth system are still not fully understood. In order to enhance still further our capacity to predict the evolution of the Earth's environment under the influence of both natural variability and human activities, the provision of data and their integration into appropriate models is of paramount importance. To better understand and predict processes occurring in the different ecosystems, estimates of process-driving' variables are needed. The capability to observe the Earth with a range of instruments providing different spatial, radiometric, temporal and angular resolutions is expected to result in major advances in process monitoring and management. Such considerations underlie the formulation of ESA's Earth Observation Envelope Programme.

For this Programme, two classes of Earth Observation missions have been identified for the post-2000 time frame: the Earth Watch and the Earth Explorer missions. Earth Watch missions are pre-operational missions concerned with operational needs requiring continuous data provision. Earth Explorer missions are focussed on research and demonstration. They are further subdivided into Earth Explorer Core Missions, which are larger missions led by ESA, and Earth Explorer Opportunity Missions, which are smaller and more flexible missions, not necessarily led by ESA.

One of the first set of Earth Explorer Core Missions, which were the subject of Phase-A studies, was the Land-Surface Processes and Interaction Mission (LSPIM). This mission's core instrument was a hyper-spectral imager covering the visible, near-infrared, shortwave infrared and thermal-infrared spectral ranges.

Following the User Consultation Meeting in Granada (Spain) in October 1999, LSPIM was not selected, but was assessed as being of high scientific merit. SPECTRA – a mission with similar but more focussed and refined objectives – was proposed to the Agency in response to the Call for Ideas for the next Earth Explorer Core Missions. Its scientific objectives and technical and programmatic feasibility are currently under evaluation.

Within the framework of the Earth Observation Preparatory Programme (EOPP), ESA carries out various airborne campaigns to support the development of geo-/biophysical retrieval algorithms, calibration and validation and simulation for future spaceborne Earth Observation missions. It was within this framework that the DAISEX campaigns were organised in 1998, 1999 and 2000, involving test sites in Spain, France and Germany and exploiting a range of airborne instruments. The overflights were accompanied by an intensive field-measurement programme.

DAISEX is intended to provide airborne hyperspectral measurements over land, to demonstrate the retrieval of variables as required for future land-surface-process missions.

2.3 Information gathering

Passive optical sensors operate in the reflective and thermal parts of the electromagnetic spectrum. The sources of information they observe are the radiance fields emitted or reflected from the Earth's surface. On its path through the atmosphere, the irradiance interacts with the atmospheric particles and gases before reaching the sensor. Assuming that all interactions caused by the atmosphere can be accounted for, information on the surface should be retrievable. These 'disturbing interactions' caused by the atmospheric constituents (gaseous molecules and aerosols) contain information useful for atmospheric research.

The chemical and physical condition of the surface defines the intrinsic information in the reflected or emitted radiance field. Its retrievability depends on the spatial, spectral, angular and radiometric resolution of the observing instrument. The basic concept of an imaging spectrometer is shown in Figure 2.1.

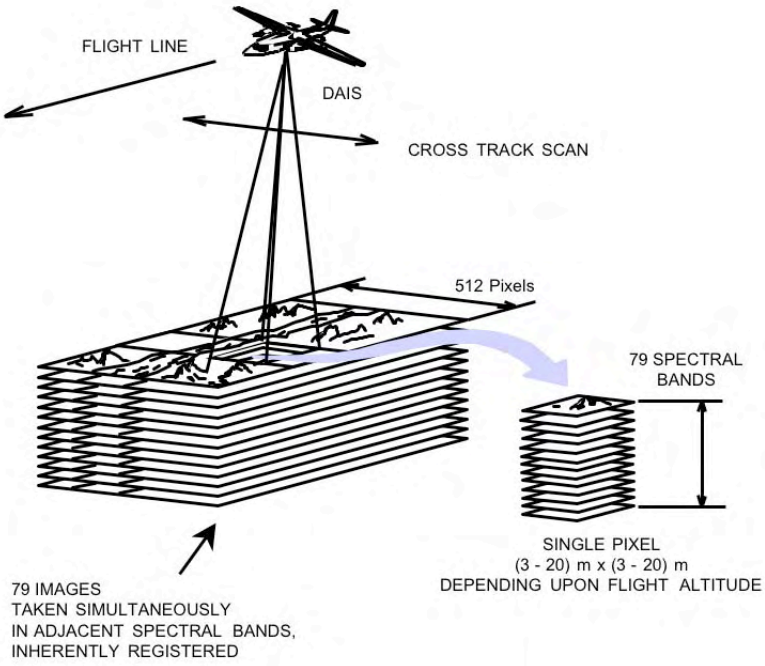

Figure 2.1: Illustration of hyperspectral data cube acquisition.

The sensor scans the top-of-the-atmosphere radiance within its instantaneous field of view (IFOV). The flight altitude and the IFOV define the footprint size of each pixel, often referred to as the ground instantaneous field of view (GIFOV). The incoming radiance is dispersed into its spectral components by a spectrometer. As the instrument moves forward it records line-by line, building up an image data cube.

As already mentioned, the chemical and physical condition of the surface defines the information intrinsic in hyperspectral data cubes. Generally, the reflectance ρ can be described as a function of the wavelength λ, the location $\vec{r}$, the time of observation t, the viewing direction ϑ and the polarisation p, such that

$$\rho = f(\lambda,\vec{r},t,\vartheta,p) \tag{2.1}$$

Polarisation plays an important role for atmospheric scattering, but is of minor influence for natural surfaces and thus can be neglected.

The viewing direction and the directional anisotropy behaviour of different surfaces were only marginally addressed in the early days of remote sensing due to lack of data, but are currently the subject of much on-going research. Sensors like MISR and POLDER foster these research topics by providing multiangular and multi-spectral data sets.

Anisotropic reflectance is caused by multiple scattering within the surface (e.g. canopy) and is thus a function of the structure of the interacting media. It may contain meaningful information about, for example, the number and size of the leaves (Leaf Area Index – LAI), their orientation (Leaf Inclination Distribution Function – LIDF), and the height of the canopy. It may therefore be able to provide indicators of the condition of the vegetation. A prominent feature of the directional anisotropy effect is called the 'hot spot', which is the increased reflectance when the surface is viewed in the same direction as it is illuminated by the Sun (same line of sight). Recent research showed that the half-width of the hot spot contains useful information about the condition of the vegetation. Usually, there is a parameter 'q' associated with the hot spot, defined as its width/height ratio. In order to get a good estimate of q, one of the aims is to observe from as many different viewing directions as close to the hot spot as possible.

Anisotropic effects can be assessed via the experimental Bidirectional Reflectance Factor (BRF), which is the ratio of the directionally reflected radiance from the surface target and the nadir radiance of a Lambertian-scattering reference target. The Bidirectional Reflectance Distribution Function (BRDF) describes the angular behaviour of the surfaces, and it can be assessed by measuring the BRF.

Compared with the limited angular range of airborne and spaceborne data sets, experimental directional reflectance factors (acquired with field goniometers) are quite plentiful and enable us to determine the BRDFs of the objects for quite a number of viewing and illumination geometries.

Figure 2.2 and Figure 2.3 show two examples of experimental directional reflectance factors, namely those for bare soil and for alfalfa acquired during DAISEX '99 with the Swiss field goniometer. Note that the highest reflectance, which forms the peak of the hot spot, cannot be measured with the field goniometer due to the shading of the target by the instrument.

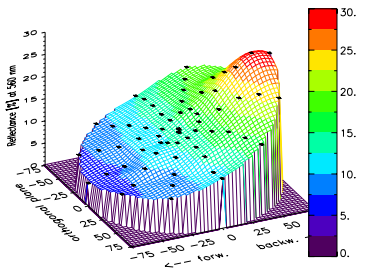

Figure 2.2: Bidirectional Reflectance Factors (BRFs) of bare soil for 65 different viewing angles at 560 nm (Sun azimuth 94° and zenith angle 49°; symbols indicate measured data points).

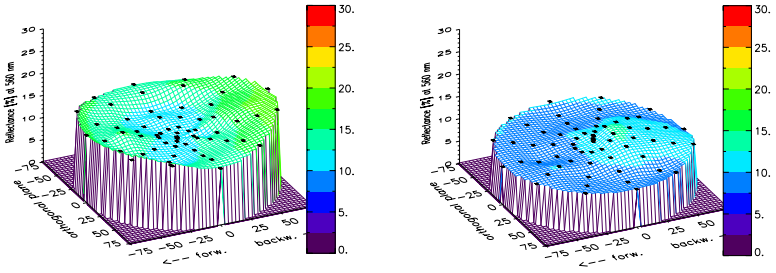

Figure 2.3: Bidirectional Reflectance Factors of a dense alfalfa canopy for two different illumination angles at 560 nm (left: Sun azimuth 90°, zenith 53°; right: Sun azimuth 182°, zenith 17°).

Diurnal directional measurements show the variability of the reflectance factors due to changing illumination geometry, i.e. changing solar zenith angle.

The spectral effects of the anisotropy can be analysed by normalising the BRF with a representative spectrum of the object (e.g. a nadir-view spectral signature or the spectral hemispherical albedo derived from the BRF measurements). Figure 2.4 shows an example of the spectral dependence of anisotropic effects for the measured alfalfa canopy with different solar zenith angles.

One of the objectives of DAISEX was to assess the use of multiangular-hyperspectral data to enhance the retrieval of structural biophysical variables such as the LAI.

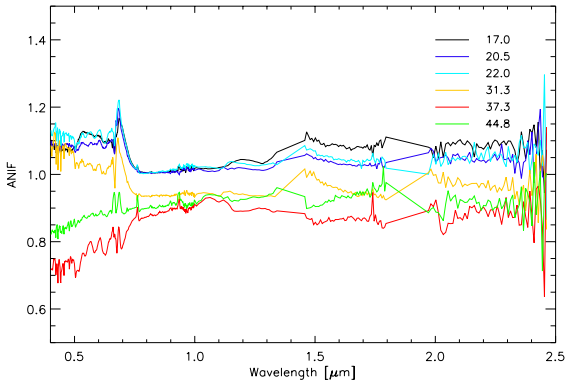

Figure 2.4: Comparison of alfalfa nadir reflectances ratioed with the spectral albedo for six different solar zenith angles.

2.4 Information retrieval

Basically, three different types of retrievals can be distinguished:

2.4.1 Classical retrievals

Classical retrievals use system, atmospherically and geometrically corrected data sets as input data. Each pixel represents the reflectance on the ground within the footprint of the sensor. Different correction schemes are used to atmospherically correct the data. Semiempirical methods are mainly used to correct for atmospheric scattering effects. These techniques are considered sufficient for broadband sensors, which are affected to only a minor extent by atmospheric gaseous absorption features. More sophisticated techniques are required for the narrowband hyperspectral data sets. For these data, atmospheric radiative transfer models, constrained by radiosonde measurements or the use of standard atmospheric profiles, are used. High calibration accuracy is a prerequisite. Calibrations are performed to convert the recorded digital counts into radiance values. The latest developments in the atmospheric-correction schemes consider the different viewing directions within one scanning line, as well as the topography of the terrain. Ongoing research focusses on the inclusion of the anisotropic reflectance effects of different surface types.

The derived reflectance values are used to produce higher-level products (Level-2), which may in turn be used to derive further products (Level-3), for instance estimating LAI from vegetation indices. The latter were derived by relating the increased reflectance values of vegetation in the near-infrared to the reflectance of vegetation in the visible red (red edge), and using an established empirical relationship between the indices and LAI. Another technique fits the red edge to a Gaussian function, the coefficients of which are then related to vegetation variables in a semiempirical way.

Currently, the most commonly used techniques for quantitatively retrieving variables from hyperspectral data are un-mixing and differential absorption techniques. The latter use the fact that the depth of the absorption is correlated with the weight percentage of the material observed. Thus, absorption depths in specific spectral bands can be used to quantify the amount of the material present. For this technique, the absorption feature needs to be fully observed, including both of the inflection points left and right of the absorption feature. Un-mixing techniques assume that the observed spectrum within the footprint of the sensor is a combination of the spectra of all pure spectral end-members (spectrally ‘pure’ material) within this footprint. Even though the combination is unlikely to be linear, it has been proved that the assumption of a linear combination (as often applied) gives reasonably good results. End-members can be selected from the data set itself by identifying ‘pure’ pixels within the scene, or using spectral libraries.

It should be noted here that spectral libraries are also being used to train 'classifiers', e.g. neural networks. In this case it is the image that is classified rather than variables quantitatively retrieved. Another technique that falls into this category is the Spectral Angle Mapper (SAM). This method determines the similarity of each pixel in the image to known library spectra by computing their angle within the spectral space, where the number of spectral bands defines the dimension of the latter.

2.4.2 Inversion of coupled radiative transfer models

Intensive research is currently in progress in this area and major advances have been achieved during the past few years. Instead of using a radiative transfer model only for the atmospheric correction, radiative transfer models are developed to describe the optical properties of vegetation and soils. These models are coupled with the atmospheric transfer models, resulting in complete radiative transfer codes describing the interactions over the entire path of the radiation from the emitted solar irradiance to the Top of the Atmosphere (TOA) radiance recorded by satellite sensors. Variables can then be retrieved by model inversion constrained by ancillary data (e.g. atmospheric profiles measured by a radiosonde, in-situ measured micro-climatic data, a-priori knowledge of some of the canopy and soil variables, e.g. gathered by campaign activities). Moreover, comparison of the modelled TOA radiances constrained by ancillary data with the observed TOA radiances makes it possible to analyse and further improve the models.

TOA radiances are used as inputs in the inversion process. Different approaches are proposed for the inversion, such as look-up tables, neural networks, golden-section 3D and Gauss-Newton techniques. It should be noted that the models also consider illumination- and viewing-angle dependent effects. This means that the inversion process is further constrained by feeding in additional angular observations. This in turn reduces the number of degrees of freedom available during the inversion, and may enhance the accuracy of the retrieved variables. The latter will then be used as inputs to surface-process models to derive variables of interest to researchers, such as canopy state, fluxes, crop production, etc. These models can be used both for monitoring and forecasting the state of the ecosystem.

2.4.3 Assimilation of remote-sensing data into radiative transfer and canopy or soil functioning coupled models

A further development of the technique discussed above is the coupling of the complete radiative transfer models with the surface-process models themselves (canopy and soil functioning models) and assimilating the remote-sensing observations from different sources (optical and SAR data with different spectral and spatial resolutions) in a multitemporal manner.

Assimilation involves tuning (by means of a cost function) some of parameters of the coupled models so that the simulation matches the observations as closely as possible. This facilitates optimum exploitation of the complementary features of the different sensors. This technique is potentially the most promising because it makes best use of available information, both on the physical or biological processes and any ancillary data.

This technique follows a new philosophy. Instead of retrieving variables directly, it rather aims at stabilising the coupled process models by adjusting variables within the models, making use of assimilation techniques. The stabilised models make it possible to predict the future state of the ecosystem more accurately. The frequent feeding of the models with remote-sensing data accounts for unforeseen events such as hailstorms or other natural hazards, thereby ensuring that the model remains 'on-track'.

This, of course, is a rather ambitious and challenging idea and many scientific questions still remain unanswered. These include the refinements to be introduced into the models, the non-linearity of model scales and the related optimum spatial resolutions, the optimum temporal coverage of the different sensors, the optimum spectral resolution, the optimum number of viewing directions and the required spectral resolution of angular observations, the optimum SAR (band, polarisations and incident angle), etc. Some of these questions were already addressed within the framework of the LSPIM Phase-A.

ESA plans to investigate these questions further through dedicated study activities. The DAISEX campaigns provided suitable data to start addressing some of these questions. A future land-surface-processes mission will certainly help in refining these ideas. Programmes like APEX and CHRIS/PROBA will be useful assets.

2.5 The DAISEX campaigns

The main scientific objective of the DAISEX campaigns was to demonstrate the feasibility of quantitatively retrieving geo-/biophysical variables by accounting for atmospheric effects, whilst at the same time analysing the data for possible additional information on directional anisotropy. Bio-/geophysical variables included the leaf area index, biomass, leaf water content, canopy height, chlorophyll content, surface temperatures and emissivity. Since accurate calibration and atmospheric corrections are essential to quantitatively retrieve these variables, in-situ atmospheric measurements (needed to derive the atmospheric corrections) were performed in addition to the field measurements for validating calibration and retrieval. The atmospheric modelling for airborne hyper-spectral sensors was carried out based on the ATCOR model. Three airborne campaigns were organised over test sites in Spain, France and Germany, in 1998, 1999 and 2000, exploiting a range of different airborne instruments.

2.5.1 DAISEX Test Sites and Teams

a) The Barrax Site

The Barrax test site is a well-described agricultural site close to the town of Albacete in Spain. It was formerly used in such international programmes as EFEDA, RESRAPS, RESMEDES, RESYSMED, RISMOP and STAAARTE, which included the exploitation of a range of airborne instruments, e.g. AVIRIS, DAEDALUS, TMS, and AIRSAR. Data from SIR-C/X-SAR as well as operational sensors such as ERS-SAR, Landsat-TM, SPOT-HRV, NOAA-AVHRR, and Meteosat are available. Detailed thematic maps and long-term data records exist. In addition, there are two permanent meteorological stations in the area continuously recording the energy and water fluxes. The School of Agronomical Engineering of the University of Castilla-La Mancha permanently monitors the fields. An additional advantage of the Barrax site is its topography and geomorphology. It is relatively flat, which eases the pre-processing required to correct for geometric and radiometric distortions (needed for the analysis of multi-angular observations).

b) The Colmar and Hartheim Sites

The Colmar site is an agricultural one operated by the Institute National de Recherches Agronomiques (INRA), located south of the city of Colmar in France. The Hartheim site is about 20 km southwest of Freiburg in Germany, and is directly adjacent to the Colmar site. During DAISEX, both sites were referred to collectively as the DAISEX 'Upper Rhine Super Site (URSS)'. The URSS is located in the southern part of the Upper Rhine Valley, extending from Karlsruhe to Basel, and from the Vosges to the Black Forest. The area is a highly uniform flood plain, lying about 200 m above sea level. Much information has been collected on the atmosphere, soil, hydrology, radiation, land occupation and use, and air quality over the years. Remote sensing has been used over the last 15 years (Landsat-TM, SPOT-HRV, NOAA-AVHRR, Meteosat, ERS-SAR). It has been an important area for both national and international research programmes, such as the Regio Klima Project (REKLIP). The Colmar site includes experimental test fields producing a variety of crops, and experimental vineyards. The site is well characterised in terms of the physical and chemical properties of its soil and its hydrology, and it includes meteorological stations.

Hartheim is a coniferous forest site (pinus sylvestris, about 40 years old) run by the Meteorological Institute of the University of Freiburg. It is about 10 km in extent north-south, and about 1.5 km east-west. Intensive measurements have been conducted since 1970, including tree-characterisation (height, density, etc.) and flux measurements. Two towers (30 m and 15 m high) within the site are instrumented with radiometers, ultrasonic anemometer thermometers and fast hygrometers, enabling mass- and energy-flux estimates to be derived. Hartheim has been used for both national and international research programmes such as REKLIP.

c) Teams Involved in the Campaigns

ESA Earth Sciences Division:
Campaign Unit (APP-FSS): Overall management
Land Unit (APP-FSL): Scientific support

DLR, Oberpfaffenhofen:
Flight operation of DAIS 7915, HYMAP and ROSIS. Pre-flight and in-flight calibration of airborne instruments. Radiometric, geometric and atmospheric corrections of DAIS 7915, HYMAP and ROSIS data.

University of Valencia:
Management of ground measurement programme in Barrax, Spain. Data analysis, including data-quality assessment and algorithm validation.

University of Strasbourg:
Management of ground measurement programme in Colmar and Hartheim. Data analysis including quality assessment and algorithm validation.

University of Zurich:
Goniometer measurements in Barrax and Colmar. Analysis of goniometer measurements.

CESBIO:
Flight operation of POLDER. Radiometric, geometeric and atmospheric correction of POLDER data.

2.5.2 Airborne sensors, flight patterns and acquired data sets

The core instruments used in the DAISEX campaigns were the Digital Airborne Imaging Spectrometer (DAIS 7915), the High-Resolution Imaging Spectrometer (HYMAP), the Reflective Optics System Imaging Spectrometer (ROSIS), and the Polarisation and Directionality of the Earth's Reflectance (POLDER) airborne instrument.

DAIS 7915 is a 79-channel imaging spectrometer operating in the 0.5 to 12.5 µm wavelength range with four grating spectrometers. With the exception of the 1.05 – 1.4 µm region, all atmospheric windows are covered, which is a unique feature of this system. The instrument, purchased from GER Corporation (USA) jointly by the EC Joint Research Centre (JRC) and DLR, has already been flown in Europe since 1995 for a number of different research and commercial projects.

HYMAP is an Australian instrument, built by Integrated Spectronics Pty. Ltd. The sensor provides 126 bands across the reflective solar wavelength region (0.45–2.5 µm) with contiguous spectral coverage (except in the atmospheric water-vapour bands) and bandwidths of 15 – 20 nm. The system operates on a three-axis stabilised platform to minimise image distortion due to aircraft motion. It provides a high signal-to-noise ratio (>500:1) and thus an industry-standard- setting image quality. Laboratory calibration and operational system monitoring ensure the radiometric performance required for demanding spectral mapping tasks.

ROSIS is a compact airborne imaging spectrometer developed jointly by German industry and research organisations. It provides 115 spectral bands in the spectral

range 430 – 860 nm, with 4 nm spectral sampling. It was recently redesigned to provide greater radiometric and spectral stability.

POLDER is a wide field of view radiometer equipped with a 2D CCD array and a filter wheel providing eight spectral bands from 443 to 865 nm. The airborne version has a similar concept to the spaceborne version, but a different spectral band configuration. A given pixel on the ground is projected to different locations on the 2D CCD array, and therefore has different view-angles in successive images.

With a specific flight pattern such as that operated by ARAT during DAISEX'99, up to 50 view directions are acquired per pixel. After pre-processing, the BRDF of every pixel is reconstructed up to a 60° viewing angle at 20 m spatial resolution of an area of typically 3 km x 3 km.

The complementary nature of the various instruments is illustrated in Figure 2.5, which shows their different spectral layouts in the context of atmospheric transmission.

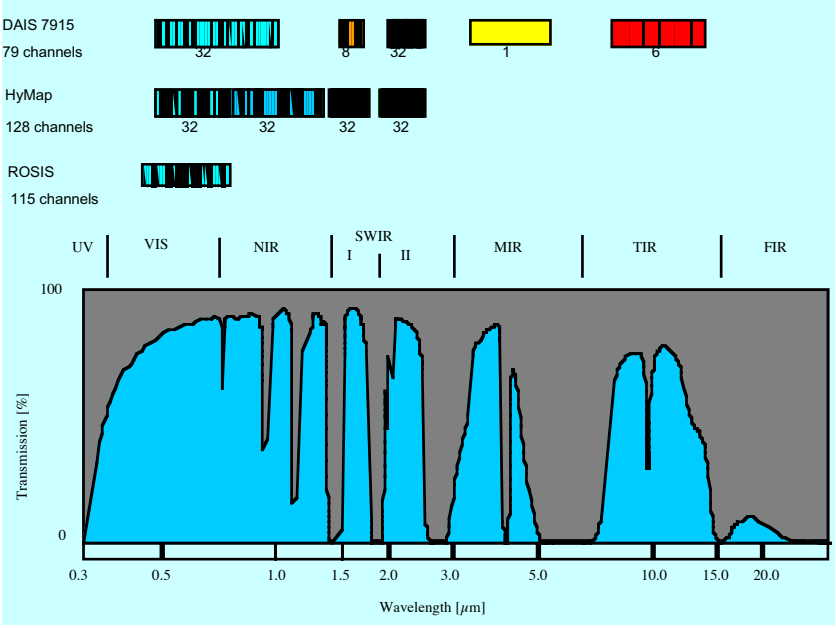

Figure 2.5: Atmospheric transmission and spectral layout of DAIS 7915, HYMAP and ROSIS.

Data have been acquired under different observation geometries by using crossing flight paths, as illustrated in Figure 2.6.

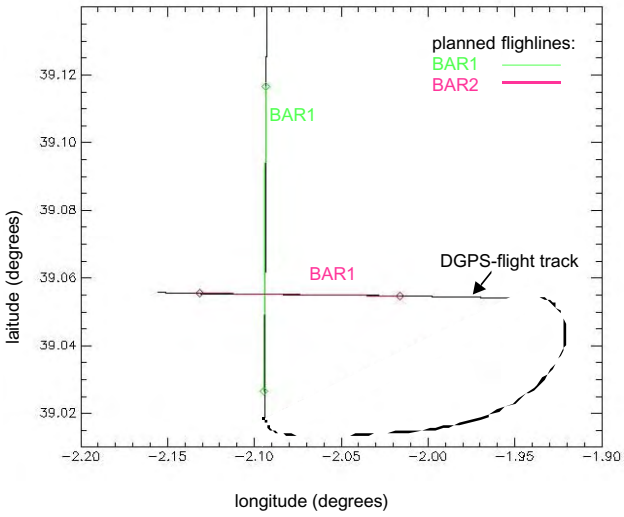

Figure 2.6: Flight pattern used during DAISEX'98 over the Barrax test site.

In particular, the 1999 campaign focussed on the acquisition of multi-angular data, by using three pairs of crossing flight paths – one in the morning, one at midday, and one in the afternoon – over the Barrax site for HYMAP and DAIS 7915. This provided a total of six different view-illumination angles for each pixel in the overlapping area of the flight paths. Observation of the hot spot was assured by the east-west flight line at noon. Table 2.1 summarises the data acquired by each sensor during the three campaigns.

DAIS 7915
HYMAP
POLDER
ROSIS

Year	Barrax, Spain				Colmar, France				Hartheim, Germany			
	D	H	P	R	D	H	P	R	D	H	P	R
1998												
1999												
2000												

Table 2.1: Airborne data acquired during DAISEX campaigns.

The most complete data set was acquired over the Spanish test site. Thanks to an EC-funded project, the French ARAT aircraft, equipped with the LEANDRE atmospheric-measurement instrument, could be operated simultaneously with DAIS and HYMAP over the Spanish site in 1999. This allowed the acquisition of a complimentary data set, something that had never been done before. The combination of HYMAP (VNIR, SWIR component), DAIS (VNIR, SWIR, TIR component) and POLDER (angular component) data enabled us to simulate the

instrument as it was proposed by LSPIM. The ARAT instrument provided a 3D characterisation of the atmosphere at the time of the overflight.

2.5.3 Ground measurements

The field measurements involved a suite of instruments operated by the various research teams. The direct and diffuse solar irradiation was measured with high spectral resolution (6 nm) for atmospheric characterisation. In-situ aerosol characterisation was also performed by a particle counter and nephelometer on ARAT, enabling us to estimate aerosol extinction profiles. Ground-based reflectance measurements were mainly acquired for two reasons: (a) those of relatively homogeneous targets for system-calibration purposes, and (b) those to radiometrically characterise principal soils and vegetation. The latter were also performed under different viewing geometries exploiting a field goniometer. Figure 2.7 shows the Swiss goniometer for BRDF measurements as operated during the DAISEX'99 campaign. All field measurements were geo-referenced using GPS for later integration of the data into Geographical Information Systems (GIS).

Figure 2.7: The Swiss goniometer at the Barrax site.

Detailed mapping included crop identification, phenological state description and soil- roughness measurements. Soil and crop samples were collected for later laboratory analysis of the soil's mineral composition and the biochemical contents. Validation measurements included LAI, fPAR, chlorophyll content, surface temperature, surface emissivity and evapotranspiration.

At the URSS (the DAISEX Upper Rhine Super Site) particular attention was paid to measurement of the radiative-balance, energy- flux and directional TIR-radiance components for modelling and evaluating the surface energy balance. In-situ radiosonde measurements were made to obtain temperature, ozone, pressure and humidity profiles up to an altitude of 30 km. These measurements are used to

constrain the atmospheric transfer codes used for atmospheric corrections. Radio sounding was supported by the Spanish National Institute of Meteorology and Meteo France.

2.5.4 Preliminary results

Pre-processing of DAIS 7915, HYMAP and ROSIS data included radiometric, geometric and atmospheric corrections, carried out by DLR. First results are presented in Figure 2.8, where HYMAP data with a spatial resolution of about 6 m x 6 m, acquired over Barrax during DAISEX'99, are shown. The image is a 'true-colour' composite using bands 18,9,3 (0.685, 0.549, 0.457 μm) for red, green and blue, respectively. For visualisation purposes, the image was enhanced using standard image-processing tools. Irrigated field patterns of different sizes (circled objects) are shown. Different shades of green indicate different types and growing stages of vegetation and crops. Brownish to greyish colours show fields with sparse vegetation and bare soil; gravel roads appear as white lineaments.

Figure 2.8: HYMAP data acquired over Barrax.

Data acquired during the DAISEX'99 campaign show the 'hot spot' in hyperspectral data cubes for the first time; it appears as a bright horizontal line in the upper part of the image.

POLDER images of the 3 km x 3 km Barrax area at 865 nm for three positions of the plane (along the same flight line, within a time interval of a few seconds) are presented in Figure 2.9.

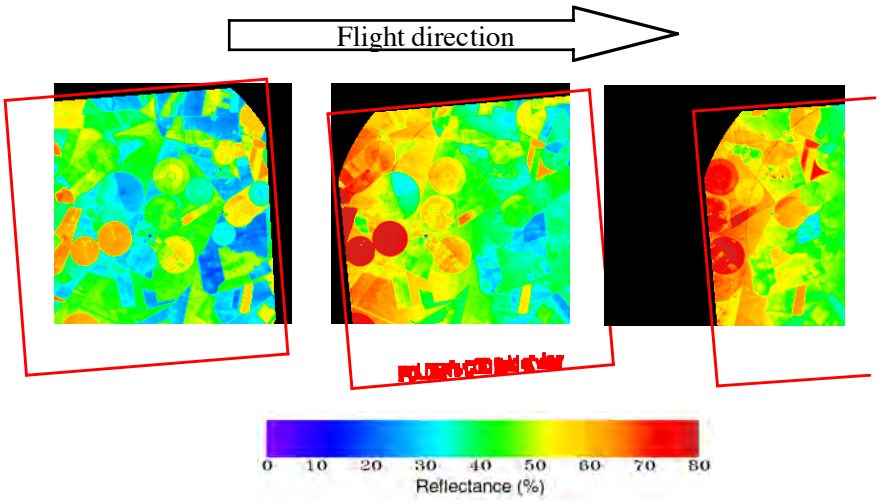

Figure 2.9: POLDER images of the 3 km x 3 km Barrax area at 865 nm for three positions of the viewing plane (courtesy of Luis Alonso, Univ. of Valencia).

The different aspects of the three images are due to the different view-target-Sun configurations (the Sun is located to the bottom-right of the images). The image sequence shows the hot spot, characterised by a sharp increase in surface directional reflectance when illumination and viewing geometry are in coincidence. The processing of all images acquired during the flight permits the full BRDF of every 20 m pixel of the area to be reconstructed.

Figure 2.10 shows the reflectance at 2200 nm (SWIR-II) extracted from the HYMAP image for different viewing zenith angles. Several fields with the same vegetation coverage were used for this purpose. The hot spot is clearly visible at a view zenith angle of 16.8°, also in the SWIR-II, which proves the good radiometric performance of the HYMAP sensor. Note that the image was acquired on 4 April, when the Sun was close to latitude 20°N, which with the observed hot spot at 16.8° adds up to about 37°, which is the latitude of the test site.

Figure 2.11a shows a cross-section of two geocoded, atmospherically corrected, and co- registered HYMAP data acquisitions in Barrax. The chess-board-like pattern in the overlapping area is obtained by alternating squares in the north-south image, which is superimposed on top of the east-west image. Both images have been processed in the same way (calibration, geocoding/correction, atmospheric correction, image processing), and the differences are due solely to angular effects.

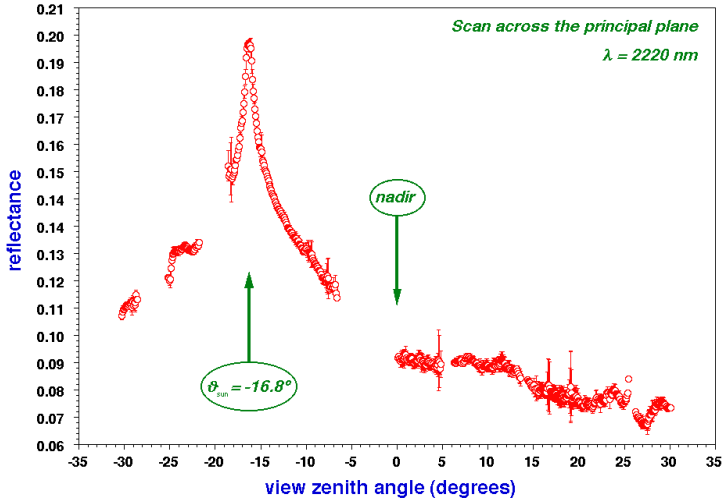

Figure 2.10: Reflectance of alfalfa at 2200 nm for different view zenith angles extracted from HYMAP data.

The angular effects are most pronounced in the hot-spot region (a bright horizontal band in the upper third of the image) and disappear in the nadir viewing direction (slightly below image centre). Images without any directional components would not exhibit any pattern-like structure. In this case, the hot spot in the east- west direction is not present in the north-south image. Also, no pattern-like structure can be observed close to nadir in the centre of the image.

Figure 2.11b is an example of a new method for normalising hyperspectral images to a single viewing geometry (BRDF correction). The BRDF correction takes place after geo- and atmospheric correction and a statistical method is used to extract BRF measurements for each surface type. The Ambrals Model is applied to the data and correction factors are calculated. The procedure currently requires user supervision, but has the potential to be automated in the future.

As a result, most of the differences disappear in the right-hand image (Figure 2.11b). Only some vegetated areas show residual differences, which are smaller than the original ones. These classes have a large internal reflectance variation. Improving the classification will reduce the errors. A prerequisite for separating a class is to have enough occurrences at different viewing angles within the image.

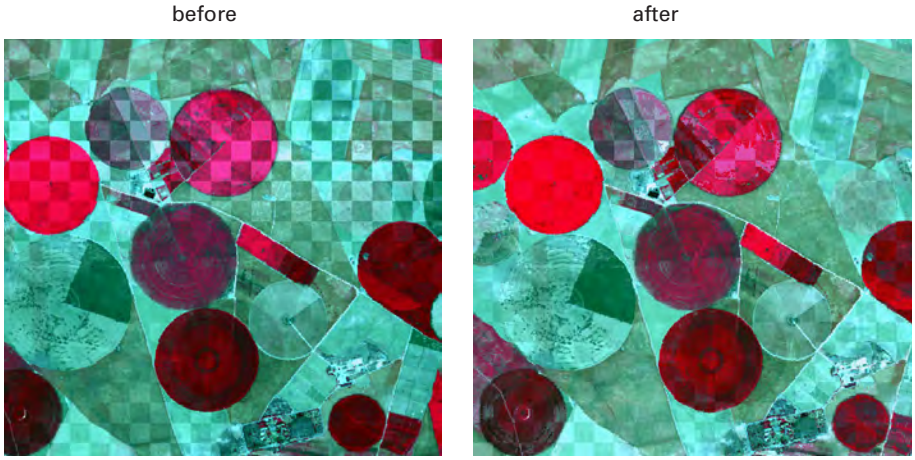

Figure 2.11: BRDF correction with a class- specific Ambral Model fit.

The ability to discriminate between green vegetation (Figure 2.12a), senescent vegetation (Figure 2.12b), and soil background is essential not only to retrieve critical biophysical parameters, but also for the assimilation of data into models describing the terrestrial carbon cycle, where the different roles of the green (photosynthetically active) vegetation, the senescent vegetation (carbon assimilation) and soil (mostly for soil respiration) must be properly accounted for.

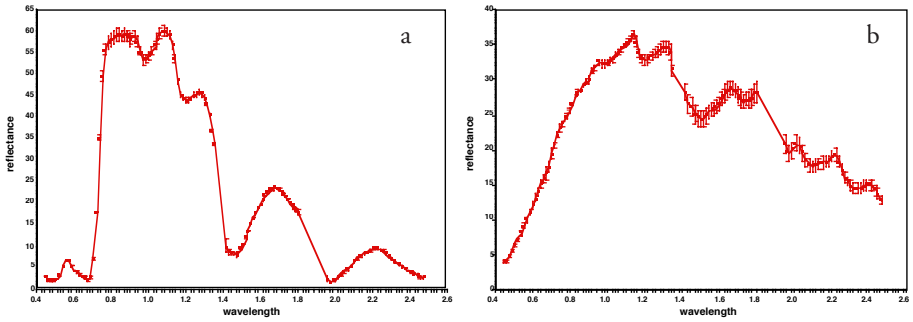

Figure 2.12: Spectral response of the HYMAP sensor for (a) green vegetation, and (b) senescent vegetation, for the Barrax study area during DAISEX '99.

Figure 2.13 compares actual HYMAP reflectance data, derived from raw data after calibration and atmospheric correction, and simulated reflectance data, by means of a theoretical radiative transfer code driven by elementary inputs describing the leaves, the soil background and the canopy structure. The good fit that has been obtained is an indication both of the accurate radiometric calibration and atmospheric correction of the HYMAP data, and the stability achieved across

the whole spectral range. The fit also illustrates our present capabilities for modelling hyperspectral data by means of radiative transfer codes. The code is based on the scattering and absorption properties of elementary leaf constituents. The combined soil-canopy response is obtained by modelling the transport of photons across the medium. Any deficiency in the theoretical modelling and/or the calibration of HYMAP data would show up in this plot.

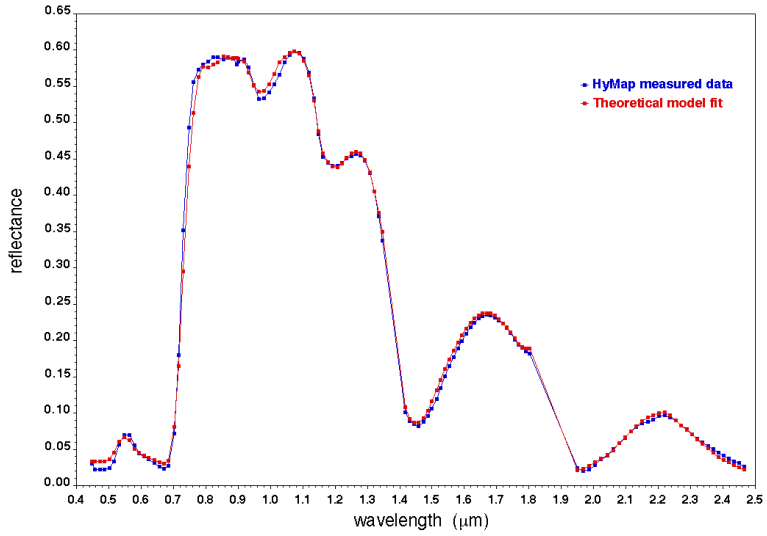

Figure 2.13: Comparison between actual HYMAP reflectance data, after calibration and atmospheric correction, and simulated reflectance data by means of a theoretical radiative transfer code.

The ability to understand the theory behind the role of each individual variable in the combined spectral response finally measured by the sensor is important for retrievals of bio-/geochemical parameters and for assimilating hyperspectral data into models of land-surface processes.

2.5.5 Outlook

Data acquired during the DAISEX campaigns are currently being further analysed and validated. In particular, validation of higher-level products accounting for different viewing and illumination geometries will be analysed, by comparing measured and modelled BRDFs and by inverting a full radiative transfer code.

Results of the campaigns will be aggregated into process models describing the vegetation growth and energy/water balance over time. This will further demonstrate the feasibility of a future land mission aimed at advancing our knowledge of land-surface processes and interactions with the atmosphere.

A workshop summarising the results is planned for the beginning of 2001. In addition, ESA plans to fund dedicated studies addressing some of the open questions discussed in this article by exploiting the data acquired during the DAISEX campaigns.

2.6 Acknowledgment

The authors wish to acknowledge the work of all team members involved in the DAISEX campaigns. The cooperation of the Institute for Regional Development at Albacete and the Agricultural Research Centre in Barrax were essential to campaign success. We are also grateful to the Spanish Air Force authorities, in particular the commander and personnel of the Military Airfield at Albacete, to the DLR flight operations manager Heinz Finkenzeller, to Christian Tardieu (IGN) and Christian Allet (INSU) for the operation of ARAT, to Jean-Yves Balois (LOA, Lille) for the installation and calibration of POLDER, to Meteo France, to the Spanish National Institute of Meteorology (which contributed the local radio soundings), and to the Remote Sensing Laboratory of Zurich University for their support.

The ARAT/LEANDRE flights over Barrax were supported by the European Commission's STAAARTE project, funded by the Fourth Framework Research Programme. The DAISEX experiment in Barrax was also supported by a Fulbright project of the Commission for Cultural, Educational and Scientific exchange between the USA and Spain. The US contribution was partially supported by a grant from the US Department of Agriculture.

Chapter 3

Evaluation of Diurnal Hyperspectral HDRF Data Acquired with the RSL Field Goniometer During the DAISEX'99 Campaign

Strub, G., U. Beisl, M. Schaepman, D. Schlaepfer, C. Dickerhof, and K. Itten, Evaluation of diurnal hyperspectral HDRF data acquired with the RSL field goniometer during the DAISEX'99 campaign, ISPRS Journal of Photogrammetry and Remote Sensing, 57 (3), 184-193, 2002.

Reprinted with permission from ISPRS, 2004.

Abstract

A directional data set of bare soil and Alfalfa acquired using the FIeld GOniometer System (FIGOS) during the DAIS Experiment 1999 (DAISEX'99) campaign is preprocessed and analyzed for its quality. Two different normalization methods to derive anisotropy factors, i.e., dividing by nadir reflectance and by spectral albedo, are tested and discussed. The effect of varying reflectances on the prediction of vegetation variables due to changing Sun and viewing geometries is demonstrated by the derivation of the weighted difference vegetation index (WDVI) for Alfalfa multiangular data and proves to be significant. The results described in this work are a contribution to the preprocessing and validation of ground-based directional remote sensing data, with a special emphasis on the spectral component and the diurnal dynamics of multiangular ground-based observations of soil and an Alfalfa canopy. The study is a step towards the generation of BRDF databases for the validation and calibration of air- and spaceborne remote sensing data.

3.1 Introduction

Multiangular ground based spectroradiometer measurements are a tool to calibrate, validate or correct anisotropy effects present in air- and spaceborne remote sensing data. Recent works showed good agreement between directional ground based and airborne imaging spectrometer HDRF (hemispherical directional reflectance factor) and radiance data (Abdou et al., 2001b; Beisl, 2001).

BRDF a priori knowledge based on field observations improve the retrieval of surface bidirectional reflectance and spectral albedo from satellite data (Li et al., 2001). Further, in situ ground measurements are needed to address heterogeneity and scaling issues (Walthall et al., 2000). Spectro-directional reflectance measurements were performed during field campaigns in the past, but the employed instruments often were limited to a few spectral bands and view angles (Abdou et al., 2001a; Breon et al., 2001; Cierniewski et al., 2002) or the analysis focussed on a limited number or region of wavelengths, e.g., to investigate the influence of view and Sun angles on vegetation indices (Epiphanio and Huete, 1995; Walter-Shea et al., 1997). Even though first studies were performed on hyperspectral directional data (Sandmeier and Deering, 1999), there is still a lack of spectro-directional ground based reflectance data with corresponding systematic analysis of spectral effects of the anisotropy, especially in the context of vegetation canopy investigations. To generate BRDF a priori knowledge databases, directional field measurements have to be acquired, preprocessed and analyzed in a consistent manner to guarantee high quality standards.

For this reason, goniometer measurements were performed during DAISEX'99 (ESA Contract No. 13390/NL/GD), an airborne imaging spectrometer campaign in the framework of ESA's Earth Observation Preparatory Programme.

The main scientific objective of the campaign was to demonstrate the estimation of geobiophysical variables, such as surface temperature, LAI, canopy biomass, leaf water content and canopy height from imaging spectrometer data (ESA, 1999). The agricultural test site Barrax (Spain) included a variety of crops such as wheat, barley, maize and Alfalfa. Remote sensing data were acquired using the imaging spectrometers DAIS 7915 and HyMap, as well as the multispectral instrument POLDER. Simultaneous intensive ground truth measurements were carried out, including the measurement of biophysical and -chemical quantities, soil characteristics, and spectro-directional reflectance signatures (Berger et al., 2000). The latter was measured by the RSL field goniometer.

The concept of the goniometer allows the observation of the surface reflectance under changing view angles. For the study of the effect of different Sun angles, HDRF data of bare soil, a dense Alfalfa canopy and non-irrigated ripe barley were acquired over the day. The selected fields were located in the crossing area of different flight lines. Thus, the reference fields observed by the airborne sensors were represented under different illumination and viewing geometries.

The aim of this study is to present the processing of the ground based soil and Alfalfa directional reflectance data, including quality assessment tests. Further, two different methods for the normalization of multiangular reflectance are presented and discussed. Resulting anisotropy factors enable the analysis of spectral effects of the anisotropy and thus will be a tool to verify BRDF modelling output. The last part contains the assessment of solar and view angle effects on the calculation of a vegetation index (i.e., the weighted difference vegetation index, WDVI (Clevers, 1989)) used to derive the leaf area index of a vegetation canopy.

3.2 Methods

3.2.1 Measurement setup

FIGOS is a transportable goniometer designed to measure HDRF under natural illumination conditions (Sandmeier and Itten, 1999). The goniometer is operated with a GER3700 spectroradiometer with a FOV of 3° and a spectral range from 0.4 to 2.5 µm (Schaepman, 1998; Sandmeier and Itten, 1999). Mounted on the zenith arc of the goniometer, the footprint of the radiometer at ground level has a radius of 5.2 cm at nadir position.

At the beginning of the measurements, the azimuth arc is directed to magnetic north, and the zenith arc is adjusted to the solar principal plane. The azimuth angle refers to the solar principle plane and is defined as zero on the position opposite to the Sun whereas the zenith angle is defined as zero at nadir position. Negative view zenith angles indicate a direction opposite to the Sun (forward scattering), positive view zenith angles indicate a direction towards the Sun (backward scattering).

To retrieve reflectances of the target surface and to determine irradiance conditions, a Spectralon reference panel (Labsphere, 1997) is measured from the nadir position once for each zenith arc. In increments of 15° in the zenith and 30° in the azimuth direction, 66 target and seven panel measurements covering a full hemisphere are taken in about 23 minutes.

Single view angle FIGOS observations are referred to as ‘measurements’ in the following, whereas a ‘hemisphere’ includes all view angle reflectances of a full scan of the hemisphere (i.e., 66 measurements from different view angles for a single Sun angle configuration).

The goniometer is placed directly onto the soil, whereas on the Alfalfa field, boxes are put underneath the azimuth arc. By this means, plant height and the azimuth arc are situated on the same level (cf., Figure 3.1).

Figure 3.1: FIGOS on the Alfalfa field at the Barrax test site.

The data resulting from the goniometer deployment at the Barrax test site is listed in Table 3.1

Target	No. of observed hemispheres	Range of solar zenith angle
Bare soil	13	17.5 - 79.0
Alfalfa	8	17.0 - 55.0

Table 3.1: Overview of HDRF data acquired at the Barrax test site from 2 June to 4 June, 1999.

3.2.2 Data quality assessment

a) Preprocessing

Quantities measured with the FIGOS correspond to the surface-leaving radiance reflected by the target and the Spectralon panel. Following the nomenclature of Martonchik et al. (2000), the preprocessing procedure is resulting in hemispherical directional reflectance factors (HDRF).

In addition to the division of the target radiances by the Spectralon radiance, the preprocessing included the correction of the deviation of the Spectralon reference panel from an ideal Lambertian reflector using a calibration coefficient determined in the laboratory (Sandmeier et al., 1998a). Spectral regions with atmospheric transmittance values lower than 20% were determined in a MODTRAN 4 (Berk et al., 1999) run for standard atmospheric conditions and were excluded from further analysis. FIGOS measurements do not include an adequate repre-

sentation of the hot spot feature, because a segment of approximately 10° is shaded by the sensor. The shaded target measurements were excluded and the hot spot was not interpolated for further analysis.

b) Consistency of nadir reflectances

During the 66 target measurements (approx. 23 minutes), the Sun angles are changing due to the non zero time frame required for the hemispherical measurements. The range of the deviations further depends on the time of day, the day of the year and the geographical location. For the available goniometer data from Barrax, maximum values for the change of the solar azimuth angle were reached around noon (up to 20°) in combination with relatively low change (1°) of the zenith angle, whereas in the morning and evening the deviations of the azimuth decreased to a minimum of 4° and the zenith angle changes reached up to 6°.

To assess the effect of the angular variations of the Sun, the standard deviation for all nadir target reflectances of each hemisphere were computed, which should be zero for invariant Sun geometry and stable object properties. The deviation of the nadir target reflectances was computed for all hemispheres over the entire spectral range (cf., Figure 3.2). For soil nadir measurements and Alfalfa, the mean standard deviations were related to the solar zenith angle change (cf., Figure 3.3). The larger the zenith angle change, the larger the standard deviation of the nadir measurements. The computed mean relative standard deviations for Alfalfa are obviously larger than for bare soil. The results implicate, that the time for a full hemispherical scan has to be reduced as much as possible, especially for large solar zenith angles or the exact Sun angle of the time has to be taken into account for the analysis. Further studies have to relate view angle dependent HDRF variations to the variations caused by the changing Sun angle during a hemispherical scan.

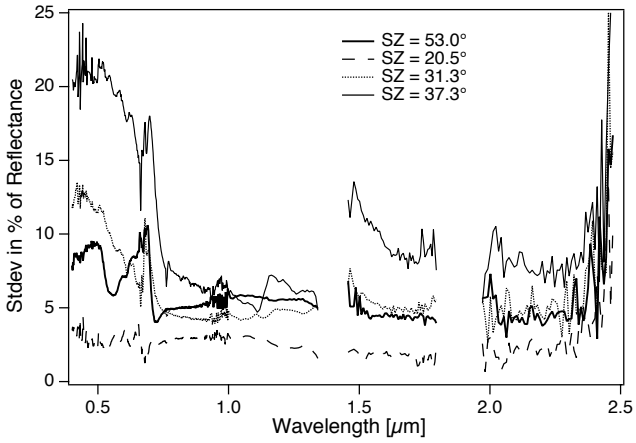

Figure 3.2: Relative standard deviation of nadir reflectances throughout a full hemispherical scan of the Alfalfa canopy at four solar zenith angles.

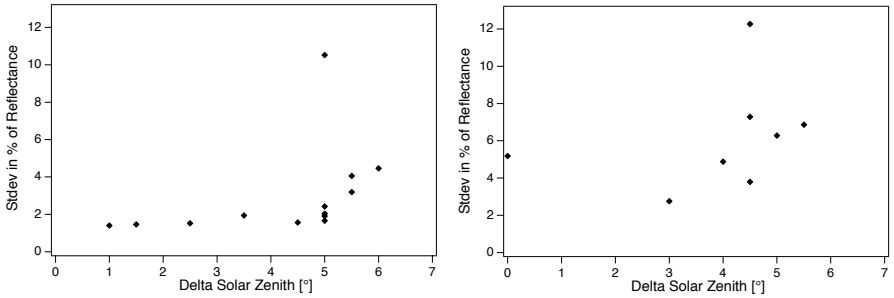

Figure 3.3: Relative standard deviations of nadir measurements during one hemisphere averaged over the whole spectral range related to the deviation of the solar zenith during the hemispherical scan, for the targets bare soil (left) and Alfalfa (right).

3.2.3 Normalization methods

To derive the relative deviation from a perfect lambertian object, the measured HDRF is compared to a target standard spectrum. This normalization is a means to separate the spectral variability of directional remote sensing data from the spectral signature of the target. Two main methods for field goniometer data are in use: the normalization by nadir reflectance and by hemispherical reflectance (Jackson et al., 1990; Sandmeier et al., 1998b; Cierniewski et al., 2002).

For the comparison of the two approaches, only the solar principle plane, where the anisotropy is most pronounced, was taken into account.

a) Normalization by nadir target reflectance

The anisotropy factor $ANIF$ describes the portion of reflectance in a specific view direction in relation to the nadir reflectance. It is used to analyze the spectral variability of HDRF (R^{hem}) data and is defined as follows (Sandmeier and Itten, 1999):

$$ANIF(\theta_i,\varphi_i,\theta_r,\varphi_r,\lambda) = \frac{R^{hem}(\theta_i,\varphi_i,\theta_r,\varphi_r,\lambda)}{R^{hem}(\theta_i,\varphi_r,\theta_r = 0,\varphi_r = 0,\lambda)}, \qquad (3.1)$$

whereas $\theta_i,\varphi_i,\theta_r,\varphi_r$ denote the zenith and azimuth angle of the direction of illumination and reflection, respectively, and λ refers to the wavelength. All reflectance data of bare soil and Alfalfa were divided by the nadir target reflectance to derive the ANIF.

b) Normalization by hemispherical reflectance

The hemispherical reflectance A_{BHR} is the ratio of total hemispherical reflected radiation to incident radiant flux and is also referred to as 'spectral albedo'. It is approximated by the integration of the measured HDRFs over the hemisphere (Sandmeier and Itten, 1999):

$$A_{BHR}(\theta_i,\varphi_i,\lambda) \approx \frac{1}{\pi}\int_0^{2\pi}\int_0^{\pi/2} R^{hem}\theta_i,\varphi_i,\theta_r,\varphi_r,\lambda \times \cos\theta_r \sin\theta_r d\theta_r d\varphi_r \ . \qquad (3.2)$$

The spectral albedo was derived for each hemisphere observed with the goniometer. The computed hemispherical reflectance is expected to be lower than the real albedo, because the reflectance values of the hot spot region were not included in the goniometer data.

For all hemispheres of bare soil and Alfalfa, the spectral albedo and their statistics were computed. The albedo was nearly constant for solar zenith angles lower than 60°. For hemispheres with larger solar zenith angles, larger hemispherical reflectance values were obtained (cf., Figure 3.4).

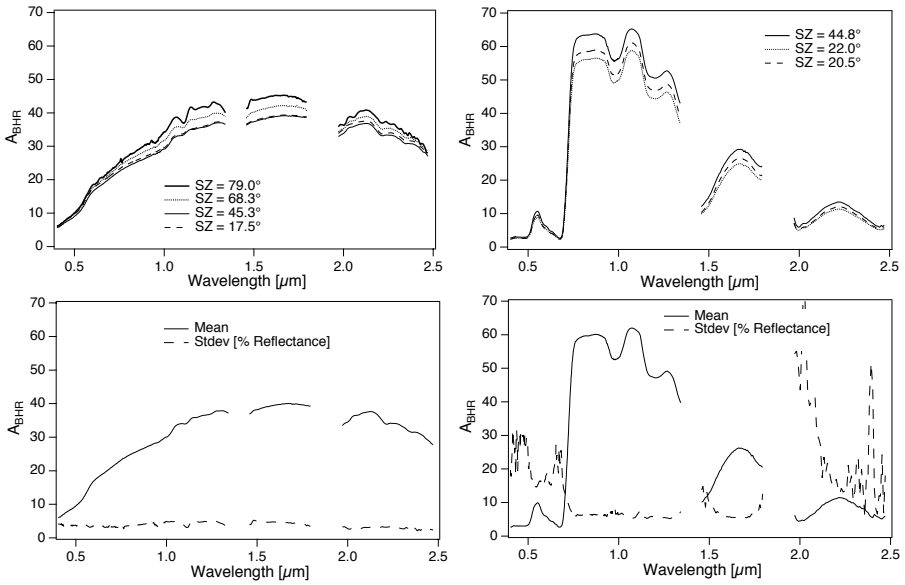

Figure 3.4: For all hemispheres of bare soil (left) and Alfalfa (right), the spectral albedo (top) was computed. Statistical analysis show the standard deviation in percentage reflectance over the measured wavelength range (bottom).

The quotient of the directional reflectance values and the spectral albedo, $ANIF_{BHR}$, refers to the deviation of the reflection behavior in a specific view direction from a mean hemispherical reflectance for the irradiance conditions at the time. It is used to analyze the spectral variability of HDRF data and is derived as follows:

$$ANIF_{BHR}(\theta_i,\varphi_i,\theta_r,\varphi_r,\lambda) = \frac{R^{hem}(\theta_i,\varphi_i,\theta_r,\varphi_r,\lambda)}{A_{BHR}(\theta_i,\varphi_i,\lambda)} \ . \qquad (3.3)$$

3.3 Results

3.3.1 Comparison of normalization methods

Both anisotropy factors, normalized by nadir reflectance and by hemispherical reflectance, can be used to analyze the spectral variability of BRDF effects, but show differences in their range for different Sun zenith angles. As an example, the reflectance of soil at 0.8 µm was normalized with nadir reflectance and spectral albedo. It can be demonstrated that for reflectances acquired at low Sun zenith angles (with a hot spot lying close to nadir (e.g., 17.5°)), the derived ANIF for view zenith angles in the region of the hot spot was lower than the $ANIF_{BHR}$, i.e., reflectances normalized by the spectral albedo (cf., Figure 3.5).

The concept of normalizing directional reflectance data by nadir reflectance is applicable if a low angular resolution of directional data is available which does not allow the derivation of the spectral albedo. Further, it is the most convenient projection center. Nevertheless, the normalization with hemispherical reflectance has the advantage that it does not depend on the Sun zenith angle and therefore allows the comparison of different hemispheres. For the following analysis only anisotropy factors derived with hemispherical reflectances will be considered.

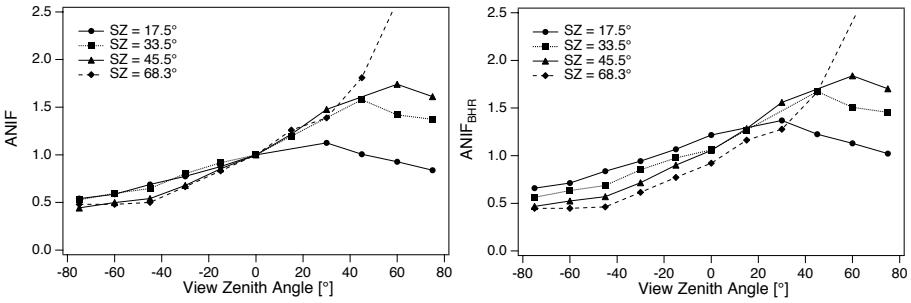

Figure 3.5: Comparison of normalized reflectance factors (0.8 µm) of bare soil in the solar principle plane. Normalization by nadir reflectance (left) and spectral albedo (right).

3.3.2 Results from normalization by hemispherical reflectance

The reflectance factors normalized by hemispherical reflectance are a means to demonstrate wavelength dependent effects caused by the variation of Sun and viewing geometry. Deviations which are not caused by the changing geometry, such as variations of the biochemicals over the day, should be eliminated because they are represented in the spectral albedo derived for each hemisphere and thus divided out.

The measured soil revealed a distinct spectral behavior depending on the Sun zenith angle compared to the dense Alfalfa canopy data (cf., Figure 3.6). Soil ani-

sotropy factors mainly showed an offset for different solar zenith angles, with the exception of the highest zenith angle of 79°, whereas Alfalfa demonstrated a distinct spectral behavior for different Sun angles. These findings could be related to the different mechanisms causing the BRDF as explained by Strahler et al. (1999). Bare soil anisotropy is dominated by geometric-optical surface scattering, driven by shadow-casting and mutual obscuration of three-dimensional surface elements, i.e., furrows in the harrowed field. Dense vegetation, instead, is dominated by volume scattering by finite scatterers (leaves of plant canopies) that are uniformly distributed, potentially nonuniformly inclined and themselves have anisotropic reflectance. The spectral behavior of the vegetation anisotropy factors could be related to the different scattering mechanisms. To further analyze ANIF anomalies, more precise information on the canopy optical and biophysical properties throughout the day are needed.

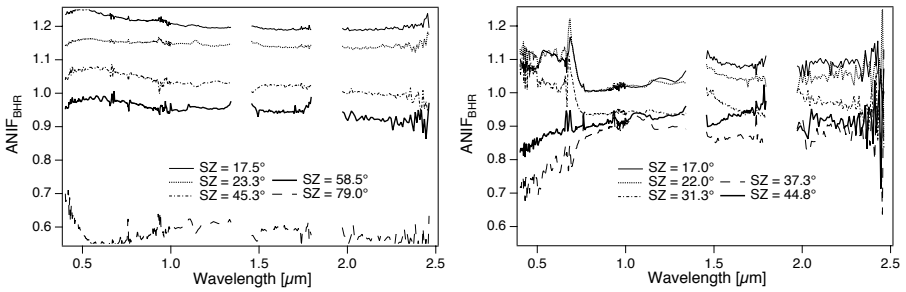

Figure 3.6: Comparison of the reflectances of soil (left) and Alfalfa (right) normalized by the spectral albedo for different Sun zenith angles (view zenith angle = 0°, view azimuth angle = 0°).

Anisotropy factors of Alfalfa observed for different view angles show a similar shape for different wavelengths but clearly other ranges (cf., Figure 3.7).

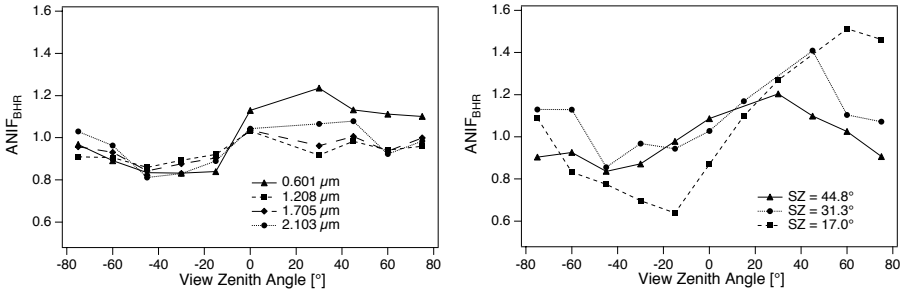

Figure 3.7: Comparison of normalized reflectances of Alfalfa in different wavelength ranges for a Sun zenith angle of 22° and a view azimuth angle of 0° (left) and at the wavelength of 0.55 µm for different Sun zenith angles (right).

3.3.3 Directional effects present in the weighted difference vegetation index

To test the potential influence of directional data for the prediction of vegetation variables, the behavior of the reflectance in two spectral bands (0.67 µm and 0.78 µm) which are used for the derivation of the weighted difference vegetation index WDVI (Clevers, 1989) was observed over the day. All Alfalfa reflectance measurements from nadir position for different Sun zenith angles were compared, as well as the anisotropy factors normalized by spectral albedo (cf., Figure 3.8). Reflectance values at 0.78 µm varied between 58% and 50%. The *WDVI* was determined as follows:

$$WDVI = R^{hem}(\theta_i,\varphi_i,\theta_r,\varphi_r,\lambda_1) - 1.5R^{hem}(\theta_i,\varphi_i,\theta_r,\varphi_r,\lambda_2) \qquad (3.4)$$

whereas λ_1 corresponds to 0.78 µm and λ_2 is located at 0.67 µm. The resulting relation between the derived WDVI and the directional reflectance revealed the following conclusions: The derived WDVI followed the directional behavior of the reflectance at 0.78 µm, with a maximum value of 54 and a minimum of 47. Because of the low reflected signal, the absolute differences of the reflectance at 0.67 µm caused by different view angles were low as well. For the presented case, the directional effects at 0.67 µm could be ignored. Thus, directional effects are represented in reflectance as well as in WDVI data at about the same dimension and cannot be overlooked, if the reflectance measurements are performed at different Sun zenith angles throughout the day. Special attention has to be paid to the deviation introduced by directional effects if vegetation variables are derived from the WDVI. Depending on the range of the WDVI, due to the proposed exponential relation of the WDVI to the leaf area index (LAI) (Clevers, 1989), the variation of the LAI can be even larger than in the original reflectance data.

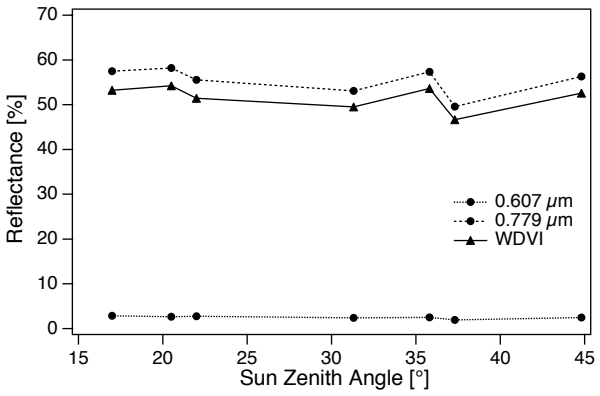

Figure 3.8: Comparison of reflectances of a dense Alfalfa canopy used for the derivation of the WDVI over a day.

3.4 Conclusions and outlook

The diurnal directional reflectance data acquired with the Swiss Field Goniometer at the test site of Barrax enabled the study of the influences of Sun and viewing geometry on the anisotropy of bare soil and a dense Alfalfa canopy.

The large standard deviation of nadir reflectances during a single hemisphere especially at large Sun zenith angles showed that the effect of changing Sun geometry has to be addressed and taken into account for further work, if such HDRF measurements are exploited.

Normalization methods allow the generation of anisotropy factors which point out the spectral variation of BRDF effects. Two different methods, namely the normalization by nadir reflectances and by hemispherical reflectance (i.e., spectral albedo), were tested. For a high resolution of directional measurements, the normalization by hemispherical reflectance is highly preferred because it is independent of the position of the hot spot for a specific Sun zenith angle. The normalization with spectral albedo allows the comparison of different hemispheres throughout the day, due to the elimination of effects which are not caused by the changes of the Sun geometry.

Future work will address the quantification of the above described effects and the improvement of the measurement setup covering the hot spot region more precisely. Diurnal hemispherical reflectance data for varying canopy types and phenological stages have to prove the presented results. This will allow the comparison and transfer of the knowledge of the anisotropy of vegetation canopies to imaging spectrometer data.

Variability of vegetation canopy reflectances can have a strong effect on the range of derived quantities, such as the LAI. Therefore directional effects have to be addressed and their influence on secondary variables has to be determined to improve the methodology of vegetation variables prediction.

The need for the correction of BRDF effects was illustrated by the results of the WDVI analysis, based on field goniometer data. Imaging spectrometer data show the same tendencies and therefore have to be normalized to a reference Sun and viewing geometry (Beisl, 2001). Field based spectro-directional observations are essential to calibrate, validate and eventually normalize air- and spaceborne remote sensing data. This experiment is a contribution to the preprocessing of the ground data to enable the comparison with remote observations, with a special emphasis on spectral and diurnal dynamics of anisotropy effects.

3.5 Acknowledgements

The authors greatly acknowledge the institutions who partly supported the presented study: University of Valencia [J. Moreno under ESA Contract No. 13390/NL/GD], Astrium GmbH, the Paul Scherrer Institut and the GFZ Potsdam. The reviewers are thanked for their valuable comments.

3.6 References

Abdou, W.A., Helmlinger, M.C., Conel, J.E., Bruegge, C.J., Pilorz, S.H., Martonchik, J.V., Gaitley, B.J., 2001a. Ground measurements of surface BRF and HDRF using PARABOLA III. Journal of Geophysical Research 106 (11), 11967-11976.

Abdou, W.A., Conel, J.E., Pilorz, S.H., Helmlinger, M.C., Bruegge, C.J., Gaitley, B.J., Ledeboer, W. C., Martonchik, J.V., 2001b. Vicarious calibration. A reflectance-based experiment with AirMISR. Remote Sensing of Environment 77, 338-353.

Beisl, U., 2001. Correction of bidirectional effects in imaging spectrometer data. Remote Sensing Series 37, Dept. of Geography, University of Zurich, 189 p.

Berk, A., Anderson, G.P., Bernstein, L.S., Acharya, P.K., Dothe, H., Matthew, M.W., Adler-Golden, S.M., Chetwynd, J.H., Richtsmeier, S.C., Pukall, B., 1999. MODTRAN 4 Radiative transfer modeling for atmospheric correction. Proc. 8th JPL Airborne Earth Science Workshop, Pasadena, USA, pp. 55-61.

Berger, M., Moreno, J., Müller, A., Schaepman, M., Wursteisen, P., Rast, M., Attema, E., 2000. The digital imaging spectrometer experiment - DAISEX'99. Proc. IGARSS, Hawaii, USA, pp. 3039-3041.

Breon, F.M., Maignan, F., Leroy, M., Grant, I., 2001. A statistical analysis of hot spot directional signatures measured from space. Proc. 8th International Symposium Physical Measurements and Signatures in Remote Sensing, Aussois, France, pp. 343-353.

Cierniewski, J., Verbrugghe, M., Marlewski, A., 2002. Effects of farming works on soil surface bidirectional reflectance measurements and modelling. International Journal of Remote Sensing 23 (6), 1075-1094.

Clevers, J., 1989. The application of a weighted infrared-red vegetation index for estimating leaf area index by correcting for soil moisture. Remote Sensing of Environment 29, 25-37.

Epiphanio, J.C., Huete, A.R., 1995. Dependence of NDVI and SAVI on Sun/sensor geometry and its effect on FAPAR relationships in Alfalfa. Remote Sensing of Environment 51, 351-360.

ESA, 1999. DAISEX-99 experimenters handbook. Draft 3, 27 May 1999, ESA Scientific Campaign Unit, ESTEC.

Jackson, R.D., Teillet, P.M., Slater, P.N., Fedosejevs, G., Jasinski, M.F., Aase, J.K., Moran, M.S., 1990. Bidirectional measurements of surface reflectance for view angle corrections of oblique imagery. Remote Sensing of Environment 32, 189-202.

Labsphere, 1997. Diffuse reflectance coating and materials. Catalogue 1. Labsphere, Shaker St., North Sutton, NH 03260, USA.

Li, X., Gao, F., Wang, J., Strahler, A., 2001. A priori knowledge accumulation and its application to linear BRDF model inversion. Journal of Geophysical Research 106 (11), 11925-11935.

Martonchik, J.V., Bruegge, C.J., Strahler, A.H., 2000. A review of reflectance nomenclature used in remote sensing. Remote Sensing Reviews 19, 9-20.

Sandmeier, S., Müller, C., Hosgood, B., Andreoli, G., 1998a. Sensitivity analysis and quality assessment of laboratory BRDF data. Remote Sensing of Environment 64 (2), 176-191.

Sandmeier, St., Mueller, Ch., Hosgood, B., Andreoli, G., 1998b. Physical mechanisms in hyperspectral BRDF data of grass and watercress. Remote Sensing of Environment 66, 222-233.

Sandmeier, S.R., Itten, K. I., 1999. A field goniometer system (FIGOS) for acquisition of hyperspectral BRDF data. IEEE Transactions on Geoscience and Remote Sensing 37 (2), 978-986.

Sandmeier, S., Deering, D., 1999. Structure analysis and classification of boreal forests using airborne hyperspectral BRDF data from ASAS. Remote Sensing of Environment 69 (3), 281-295.

Schaepman, M. E., 1998. Calibration of a field spectrometer. Remote Sensing Series 31, Dept. of Geography, University of Zurich, 146 p.

Schlaepfer, D., 1998. Differential absorption methodology for imaging spectroscopy of atmospheric water vapor. Remote Sensing Series 32, Dept. of Geography, University of Zurich, 131 p.

Strahler, A.H., Muller, J.-P. et al, 1999. MODIS BRDF/Albedo product: algorithm theoretical basis document version 5.0. MODIS product ID: MOD43. NASA EOS MODIS.

Walter-Shea, E.A., Privette, J., Cornell, D., Mesarch, M.A., Hays, C.J., 1997. Relations between directional spectral vegetation indices and leaf area and absorbed radiation in Alfalfa. Remote Sensing of Environment 61 (1), 162-177.

Walthall, C., Roujean, J.L., Morisette, J., 2000. Field and landscape BRDF optical wavelength measurements: experience, techniques and the future. Remote Sensing Reviews 18 (24), 503-531.

Chapter 4

Evaluation of Spectro-Directional Alfalfa Canopy Data Acquired During DAISEX'99

Strub, G., M.E. Schaepman, Y. Knyazikhin, and K.I. Itten, Evaluation of spectrodirectional Alfalfa canopy data acquired during DAISEX'99, Ieee Transactions on Geoscience and Remote Sensing, 41 (5), 1034-1042, 2003.

Abstract

Field goniometer measurements are a tool to generate a priori Bidirectional Reflectance Distribution Function (BRDF) knowledge for correction and validation of directional reflectance data acquired by air- and spaceborne sensors. This study analyzes diurnal Hemispherical-Directional Reflectance Factor (HDRF) data of an Alfalfa canopy measured during the Digital Airborne Imaging Spectrometer EXperiment 1999 (DAISEX'99). We analyze the variation of measured and modeled spectro-directional vegetation data, revealing that measurement noise is negligible compared to the variation due to the canopy's anisotropy. The deviations of the spectral albedo (bihemispherical reflectance (BHR)) and of field spectrometer nadir measurements throughout a day prove to be larger than modeled deviations. Calculated anisotropy factors quantify the spectral dependent effects of the vegetation reflectance anisotropy. This is a contribution towards the generation of a reliable BRDF database by suggesting methods to preprocess and analyze observed directional vegetation reflectance data, with special emphasis on the spectral dimension.

4.1 Introduction

Field goniometer measurements are used to validate, calibrate, or correct bidirectional effects present in air- and spaceborne sensor data. Recent works show good agreement between directional ground based and airborne imaging spectrometer HDRF and radiance data [1][2]. Further, a priori knowledge of directional reflectance properties in the form of field measurements improve the retrieval of surface bidirectional reflectance and spectral albedo from satellite data [3]. Results of early field campaigns (e.g., LACIE (Large Area Crop Inventory Experiment) and AgRISTARS (Agriculture and Resources Inventory Surveys Through Aerospace Remote Sensing)) already recognized the importance of spectro-directional measurements [4]. Although such data of Alfalfa canopies were acquired in the past, the performed analysis focused on integrated broadband red and near-infrared directional reflectances in order to determine the influence of the view and Sun direction on vegetation indices [5][6].

This paper aims at the quantification of additional information contained in diurnal spectral HDRFs of an Alfalfa (Medicago sativa) canopy, in contrast to multispectral unidirectional reflectance data. FIeld GOniometer System (FIGOS) [7] measurements were performed during DAISEX'99, a campaign in the framework of the European Space Agency's Earth Observation Preparatory Programme [8][9]. From 1998 through 2000, this campaign was conducted on an agricultural test site in Spain (39°03' N, 2°05' W) to demonstrate the estimation of geo-/biophysical variables from imaging spectrometer data. In 1999, the airborne sensors DAIS7915 [10], HYMAP [11] and POLDER [12] were flown at three times throughout the day. Simultaneous diurnal HDRF measurements of the Alfalfa canopy exhibit the effect of changing view and Sun direction, whereas their high spectral resolution allows analyzing wavelength dependent anisotropy effects.

A description of the experimental design, the preprocessing and quality analysis methodology is followed by the presentation of reflectance simulations. The PROSPECT model [13] is used to simulate leaf optical properties needed to calculate the reflectance of the canopy with the SAILH model (Scattering by Arbitrarily Inclined Leaves, with Hot spot effect, [14]). The statistical analysis of the observed data is a prerequisite to quantify the influence of directional effects on the vegetation variable estimation using empirical and semi-empirical methodologies (e.g., vegetation indices) neglecting the anisotropy.

Spectro-directional reflectance data of crops serve as input to radiative transfer models, coupled with canopy functioning models, applied in precision farming and yield prediction [15]. Thus, measured and simulated reflectances are compared quantitatively with the objective of predicting canopy structure variables, using vegetation models in inverse mode. Modeled reflectances serve as a reference to analyze directional observations' uncertainties and determine differences in their representation of spectro-directional effects. A methodology for the nor-

malization of measured HDRF data is presented, simplifying the analysis of wavelength dependence of the anisotropy of canopy reflectance.

4.2 Experimental site and instruments

4.2.1 Alfalfa characteristics

The study concentrates on the bidirectional reflectance characterization of the agricultural crop Alfalfa, a mainstay in the production of livestock products, and recognized as the oldest plant grown solely for forage. The estimate of worldwide acreage amounted to 32 million ha in 1988. The worldwide importance of Alfalfa is attributed to its high yield of nutritious herbage, rapid recovery after cutting, longevity, and tolerance to environmental stress [16].

Alfalfa is a heliotropic plant, which means that architectural changes occur caused by the movement of the Sun during the day [17]. Both diaheliotropic (i.e., leaf surface perpendicular to the direction of incident radiation) and paraheliotropic (leaf orientation parallel to incident radiation) movements are reported [18][19].

The observed Alfalfa canopy was irrigated and dense, in the late bud stage (Figure 4.1). The height of the canopy was 50 cm, the fresh biomass 1880 g/m2 and the leave's Dry Matter (DM) per ground area 22.3 mg/cm2. Measurements performed using a Licor LAI 2000 instrument [20] indicated a leaf area index (LAI) of 3. Calculating the Specific Leaf Mass (SLM) from the given leave's dry matter and the LAI (SLM = DM/LAI), a SLM of 7.4 mg/cm2 results, a value which is considered too high compared to published ranges for Alfalfa at about the same maturity stage [21][22]. LAI 2000 measurements taken under direct illumination conditions can result in an underestimation of LAI values, up to a factor 1.8 [20]. Thus, a true LAI could be between 3 and 5.5. The upper bound of the LAI variation is used in model calculations (Section 4.4.2), leading to a more realistic SLM of 4 mg/cm2. In the case of dense canopies (LAI>3) its reflectance can be insensitive to LAI [23][24]. Therefore, setting LAI value to 5.5 does not lead to a significant mistake in the modeled canopy reflectance.

Figure 4.1: Alfalfa stem photograph ([25] © Oregon State University, Forage Information System) (a), projected nadir ground instantaneous field of view of the GER3700 spectrometer onto the Alfalfa canopy [26] (b), and side view of the observed canopy [26] (c).

4.2.2 Experimental design of FIGOS measurements

The FIGOS goniometer [7] is operated with a GER3700 having a field of view of 3° and a spectral range from 0.4 to 2.5 µm, calibrated for absolute radiance traceable to a NIST (National Institute of Standards and Technology, USA) calibration standard [27]. Mounted on the zenith arc of the goniometer, the footprint of the spectroradiometer has a radius of 5.2 cm at nadir position. In increments of 15° in zenith and 30° in azimuth direction, 66 target and seven Spectralon panel measurements covering a full hemisphere are recorded in about 23 minutes. The reference panel nadir view measurements allow for the derivation of the surface HDRF. A Reagan sunphotometer measuring the direct irradiance is set up next to FIGOS, enabling the simulation of the diffuse part of the total irradiance.

4.3 Methodology

4.3.1 Preprocessing of measured directional reflectance data

Following the reflectance nomenclature of Martonchik et al. [28], quantities measured with FIGOS correspond to the surface-leaving radiance reflected by the target L_r and the Spectralon panel L_r^{ref}. Due to the sensors Ground Instantaneous Field of View (GIFOV) exceeding the area of the Spectralon for large view zenith angles, panel measurements are performed only from the nadir view direction.

To derive the hemispherical-directional reflectance factor (HDRF, R^{hem}) for each view angle, the surface-leaving radiance is divided by the radiance from a lambertian reflector illuminated under the same ambient conditions. Due to deviations from a perfectly lambertian and lossless reflectance behavior of the Spectralon panel, a correction factor is introduced, which ideally corresponds to the Bidirectional Reflectance Factor (BRF, R^{ref}) of the panel. By introducing the actual Sun zenith angle θ_i of the directional measurements in the following equation, the correction factor k is derived [29]:

$$k(\theta_i,\lambda) = a_0(\lambda) + a_1(\lambda)\theta_i + a_2(\lambda)\theta_i^2, \tag{4.1}$$

where θ_i is the solar zenith angle, λ is the wavelength, and a_0, a_1, and a_2 represent the coefficients for the polynomial fit of the Spectralon panel BRDF derived in a laboratory experiment [29]. For solar zenith angles of 17° to 53°, k varies from 0.89 to 0.926, respectively with minor differences among wavelengths. Thus, the HDRF (R^{hem}) calculation from field measurements results in the following formula:

$$R^{hem}(\theta_i,\varphi_i,\theta_r,\varphi_r,\lambda) = \frac{L_r(\theta_i,\varphi_i,\theta_r,\varphi_r,\lambda)}{L_r^{ref}(\theta_i,\varphi_i,\theta_r = 0,\varphi_r = 0,\lambda)} \times k(\theta_i,\lambda), \tag{4.2}$$

whereas $\theta_i,\varphi_i,\theta_r,\varphi_r$ are the zenith and azimuth angles of the direction of illumination and reflection, respectively.

Due to self-shadowing of the target by the sensor in the hot spot direction for view angles located 10° around the actual Sun zenith angle, corresponding HDRF data in the solar principle plane cannot be measured with FIGOS. Wavelength regions with sensor artifacts (cf., [27]) and low atmospheric transmittance (< 20%) are excluded from further analysis. Gaseous transmittance was derived from forward simulations using MODTRAN4 [30] with atmospheric conditions derived from inverted sunphotometer data acquired simultaneously with the FIGOS measurements and the spectral response function of the GER3700 spectrometer.

In the following, single view angle FIGOS observations will be referred to as 'measurements', whereas a FIGOS hemisphere includes reflectances of a full scan of the view hemisphere (i.e., 66 measurements from different view angles for a single Sun angle configuration).

The spectral albedo (BiHemispherical Reflectance, BHR, A_{BHR}) is computed to characterize the radiation budget over the whole hemisphere. The bihemispherical reflectance (A_{BHR}) is the ratio of the flux Φ_r of light reflected from surface area dS to the incident flux Φ_i [28]:

$$A_{BHR}(\lambda) = \frac{d\Phi_r(\lambda)}{d\Phi_i(\lambda)} = \frac{dS \int_{2\pi} L_r(\theta_r,\varphi_r,\lambda)\cos\theta_r \sin\theta_r d\theta_r d\varphi_r}{dS \int_{2\pi} L_i(\theta_i,\varphi_i,\lambda)\cos\theta_i \sin\theta_i d\theta_i d\varphi_i}. \quad (4.3)$$

During the DAISEX'99 experiment the irradiance Φ_i, required for the calculation of A_{BHR} using (3), was not observed and therefore A_{BHR} is derived by integrating the HDRF data over all directions of the view hemisphere [29]:

$$A_{BHR}(\theta_i,\varphi_i,\lambda) \approx \frac{1}{\pi} \int_0^{2\pi} \int_0^{\pi/2} R^{hem}\theta_i,\varphi_i,\theta_r,\varphi_r,\lambda \times \cos\theta_r \sin\theta_r d\theta_r d\varphi_r. \quad (4.4)$$

4.3.2 Quality assessment: sources of uncertainties of measured HDRF

The observed surface's BRDF and experimental artifacts, reducing the additional information content of multiangular data, cause the variation of HDRF field measurements. Therefore the quantification of uncertainties of the HDRF introduced by sources as discussed in the following paragraphs is a prerequisite for further analysis of the data.

a) Sensor uncertainties

FIGOS deploys a radiance-calibrated GER3700 spectroradiometer, with determined detector specific uncertainties for reflectance measurements (i.e., +- 2.9 to +- 6.16% with a 10% changing atmosphere between reference and target measurement) [27].

b) Panel correction uncertainties

As described in Section 4.3.1, the HDRF calculation includes a Spectralon panel correction with a polynomial fit representing it's BRF where angles have not been measured. The root mean square error of the fit with regard to the measured BRF varied from 1.4 to 2.2% reflectance for the wavelength range 0.45 to 1.0 μm.

c) Not quantified additional sources of variation

Even though the Sun's geometry is changing during the time of the 66 target measurements of a hemisphere (see Section 4.2.2), it is assumed to be constant. Maximum values for the change of the azimuth were reached around noon (up to 20°), whereas in the morning and evening the deviations of the azimuth decreased and the zenith angle changes reached up to 6°.

Due to the constant focal length of the GER3700 optics, the extent of the GIFOV changes with the view zenith angle according to the cosine projection law. For nadir measurements, the ellipse of the sensor's footprint has a length of 10 cm and increases to 40 cm for a view angle of 75°. Thus, inhomogeneity of the target introduces additional uncertainties.

A still poorly understood effect of the BRDF is its scale dependence. For the characterization of the Alfalfa canopy BRDF, the scattering elements (i.e., the indi-

vidual leaves) could be at a critical size with respect to the limited GIFOV of FIGOS.

Throughout the day, changes in vegetation structural properties (e.g., leaf angle distribution [18]) due to physiological and biochemical variations of the plants may cause variations of the measured directional reflectance. Due to missing information about the vegetation properties throughout the day it is not possible to quantify this part of the variation.

4.3.3 Vegetation canopy HDRF simulations

To establish a reference for the measured Alfalfa HDRF data, leaf optical properties and canopy reflectance were calculated using PROSPECT [13] and SAILH [14]. Vegetation and actual atmospheric conditions as well as soil reflectance measured on the test site served as model input.

4.3.4 Statistical analysis

To assess the range of variation of HDRF data due to the changing view and Sun direction throughout the day, a statistical analysis of measured and modeled HDRFs is performed, with a special emphasis on the wavelength specific behavior. The results reveal the variation of directional data corresponding to structural information about the vegetation canopy, compared to the data uncertainties introduced by artifacts mentioned in Section 4.3.2.

The first analysis includes the overall variation of all preprocessed HDRFs, i.e., the calculation of the mean, standard deviation, and coefficient of variation (standard deviation divided by mean) over all view and Sun directions. Thereafter, the variation of the HDRFs of each hemisphere is calculated, showing the information content of all view angles for an approximately constant solar position. A third analysis demonstrates the deviation of nadir view measurements acquired at different Sun zenith angles from the nadir view spectrum around solar noon (i.e., solar zenith angle of 17°). The difference of the noon spectrum minus the actual spectrum is divided by the noon spectrum to obtain the normalized deviation.

4.3.5 Analysis of wavelength dependence

Vegetation canopy HDRF data exhibit pronounced wavelength dependent effects, which can be described by anisotropy factors [31]. In order to derive the relative deviation of each view angle reflectance, measured HDRF data are divided by a standard target spectrum. In this study the calculated bihemispherical reflectance of each observed hemisphere is chosen as standard spectrum instead of the usually applied nadir reflectance [29][31]. The anisotropy factor $ANIF_{BHR}$ refers to the deviation of the reflection behavior in a specific view direction from the BHR, for the actual irradiance conditions of the measured hemisphere:

$$ANIF_{BHR}(\theta_i,\varphi_i,\theta_r,\varphi_r,\lambda) = \frac{R^{hem}(\theta_i,\varphi_i,\theta_r,\varphi_r,\lambda)}{A_{BHR}(\theta_i,\varphi_i,\lambda)}. \quad (4.5)$$

4.4 Observed spectro-directional data and model simulations

4.4.1 Preprocessing and resulting Alfalfa HDRF data

Measured directional reflectance is converted to HDRF data as in Section 4.3.1, accounting for the non-lambertian and absorbing behavior of the Spectralon panel, shaded target measurements, and wavelength ranges with sensor artifacts and low atmospheric transmittance. Low total gaseous transmittance wavelength ranges were identified at 1.3 µm and 1.8 to 1.9 µm. The preprocessing resulted in eight hemispheres of Alfalfa HDRF data used for further analysis (Table 4.1).

Hemisphere	sa [°]	sz [°]	no. m.	Hemisphere	sa [°]	sz [°]	no. m.
1	90.0	53.0	59	5	224.5	22.0	63
2	107.0	35.8	64	6	246.5	31.3	66
3	140.8	20.5	64	7	254.8	37.3	66
4	181.5	17.0	66	8	262.5	44.8	66

Table 4.1: Hemispheres of the Alfalfa canopy after preprocessing (sa = average sun azimuth relative to geographic North, sz = average sun zenith angle, no. m. = number of reflectance measurements per hemisphere after preprocessing).

4.4.2 PROSPECT/SAILH simulation description

Using the modeling approach as defined in Section 4.3.3, the input parameters for PROSPECT and SAILH are determined. An average leaf angle of the Alfalfa canopy and the leaf structure parameter N [13] are derived from literature [6]. The LAI is used to calculate the leaf chlorophyll, and leaf water from observed canopy amounts (see Section 4.2.1). A PROSPECT run for the identified leaf biochemical and structural characteristics (structure parameter N = 1.8, chlorophyll a and b content Cab = 41.4 µg/cm2, equivalent water thickness Cw = 0.022 cm, dry matter content Cm = 0.004 g/cm2, brown pigment content = 0.1) is performed. The resulting leaf reflectance and transmittance serve as input to SAILH, together with the canopy architecture characteristics, the observed soil reflectance, and the ratio of diffuse to total irradiance. The latter was derived from sunphotometer data for each FIGOS hemisphere using the optical depth from the sunphotometer as input to MODTRAN4 [30]. The resulting ratio for the actual conditions is wavelength (between 0.26 and 0.36 at 0.4 µm and decreasing to 0.05 at 0.8 µm) and time dependent, with a minimum around solar noon.

Finally, a run of SAILH for the geometry of each goniometer measurement is performed (Table 4.2). Resulting HDRF data are resampled to the spectral resolution of the preprocessed FIGOS measurements.

SAILH parameter	Input value	
Leaf area index	5.5	Constant
Average leaf angle	50°	Constant
Hot spot parameter	0.057	Constant
Leaf reflectance	PROSPECT output	Constant
Leaf transmittance	PROSPECT output	Constant
Soil reflectance	Nadir reflectance measured at test site	Constant
View zenith angle	Angular position of FIGOS	Variable
Sun zenith angle	Corresponding to mean solar angle of individual FIGOS hemisphere	Variable
Relative azimuth Sun-sensor	Angular position of FIGOS	Variable
Diffuse fraction	From MODTRAN 4	Variable

Table 4.2: SAILH input parameters used for simulation runs of Alfalfa HDRF for all view and sun angles of the day.

4.5 Results

4.5.1 Resulting HDRF data and their quality

a) Statistical analysis

Calculated mean values of measured and modeled Alfalfa HDRF data over all view and Sun directions show similar shapes, especially in the visible wavelength region (Figure 4.2). The standard deviation and coefficient of variation of the measured HDRF are wavelength dependent. The mean variation over all wavelengths amounts to 17.7% and therefore is larger than the mean variation of the modeled HDRF data (11.1%).

Wavelength regions with low mean reflectance (e.g., the red spectral region around 680 nm) exhibit a larger variation in HDRF data, compared to high reflectance values with a rather small variation (e.g., the Near-Infrared (NIR) region). This behavior of the HDRF data cannot be explained as an instrumental artifact, because modeled data show the same tendency. The explanation is found in the decreased anisotropy for wavelength regions with high reflectance and

therefore a higher amount of multiple scattering. These findings are consistent with a study describing the anisotropy of an Alfalfa canopy in the red and NIR spectral region assessing the influence of Sun and sensor geometry on NDVI and SAVI [5].

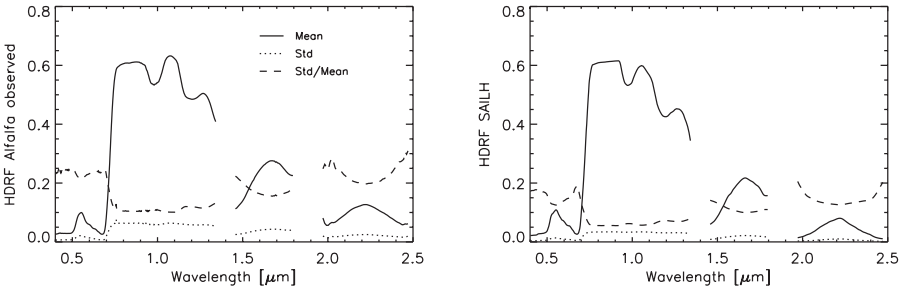

Figure 4.2: Overall statistics for measured (a) and simulated (b) Alfalfa HDRF data over all Sun and view directions.

The analysis of the mean HDRF data and their variation with respect to diurnal dynamics shows that the range of variation of the different view angles is related to the Sun zenith angle (Figure 4.3). HDRFs exhibit a larger variation for large Sun zenith angles, i.e., a more pronounced directional behavior than HDRF data acquired around solar noon.

b) Nadir Alfalfa HDRF variations throughout the day

Field spectrometer measurements serve as a reference for air- and spaceborne remote sensing data and are used for vicarious calibration purposes. Therefore they are optimally acquired simultaneously to the overflight. The following analysis derives the deviations of the diurnal nadir Alfalfa HDRFs from a perfectly timed measurement.

The differences between the nadir view HDRF around solar noon (Sun zenith angle of 17°) and nadir view HDRFs measured at different Sun zenith angles throughout the day, normalized by the solar noon HDRF are shown in Figure 4.4. The relative HDRF deviations are wavelength dependent and considerably larger for wavelength regions with low reflectance values (e.g., red spectral bands around 0.6 μm) compared to spectral regions with high canopy reflectance (e.g., NIR). In the visible part of the spectrum HDRF data are up to 40% below solar noon measurements. The deviations in measured data result from the changing Sun direction, atmospheric and vegetation conditions as well as spectroradiometer uncertainties. Even though simulations account for changing Sun angles and atmospheric conditions, modeled HDRF deviations are much smaller and within 20% of the reference noon reflectance. Further, measured data do not follow the trend of simulations, where absolute deviations increase with increasing solar zenith angle. Nadir observations are biggest for illumination geometries

corresponding to solar noon and early morning, thus lying in the hot spot area, and exhibit the lowest reflectances for solar zenith angles around 36°. The difference between simulated and measured data could be found in the changes of vegetation structure throughout the day, which was neither assessed in the field nor taken into account in the simulations. The analysis illustrate the need of measurements at the exact time of the overflight for vicarious calibration purposes of imaging spectrometer data and the necessity of taking into account the Sun angle geometries for field spectrometer measurements.

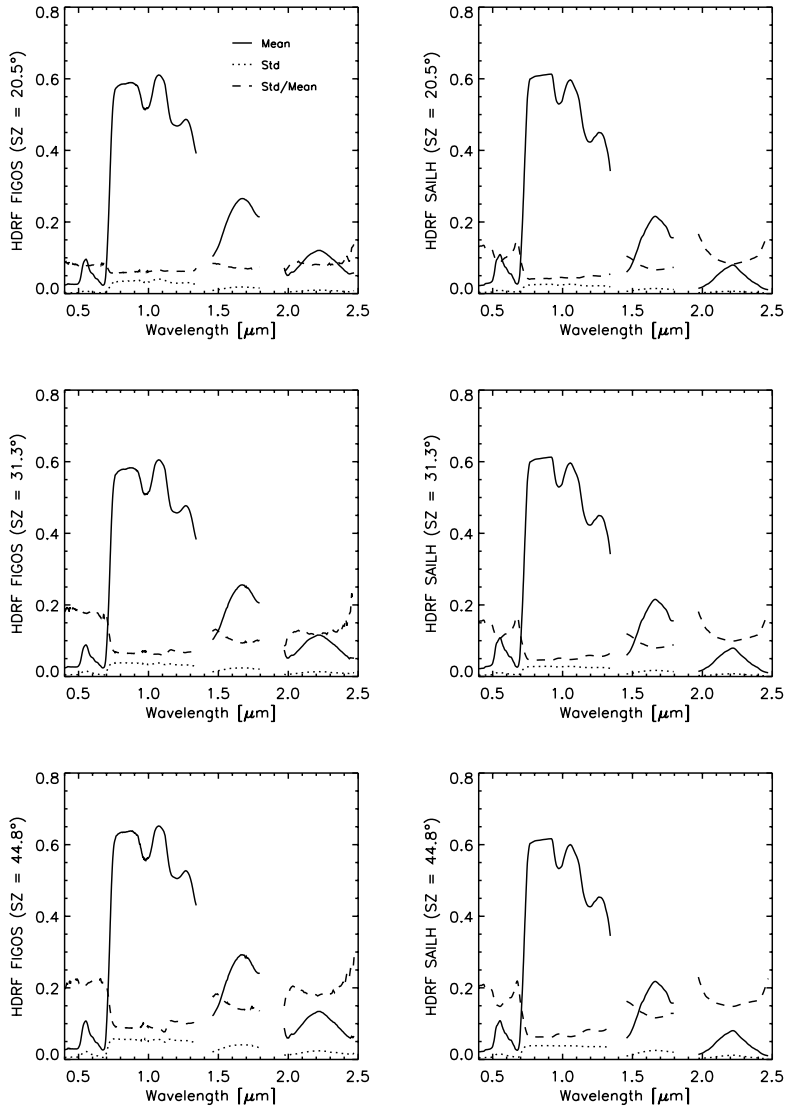

Figure 4.3: Statistics for measured (a-c) and simulated (d-f) Alfalfa HDRF data of the whole hemisphere for three Sun zenith angles throughout the day.

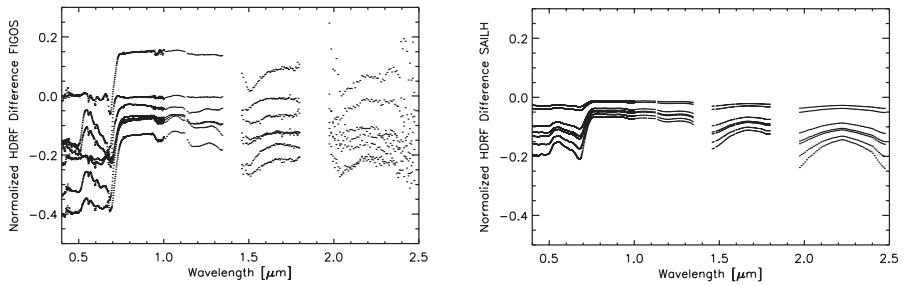

Figure 4.4: Deviations of nadir view HDRF measurements (a) (HDRF difference for solar zenith angles of 53.0°, 20.5°, 44.8°, 31.3°, 22.0°, 35.8°, 37.3° (from top to bottom)) and simulations (b) (HDRF difference for solar zenith angles of 20.5°, 22.0°, 31.3°, 35.8°, 37.3°, 44.8°, 53.0° (from top to bottom)) of the Alfalfa canopy from corresponding HDRF around solar noon (i.e., nadir view HDRF for solar zenith angle of 17.0°), normalized by the solar noon HDRF.

4.5.2 BHR results

The calculated BHR for measured and simulated Alfalfa canopy hemispheres basically increases with growing Sun zenith angle (Figure 4.5), in accordance with albedo trends reported in other studies [32][33][34]. The average variation of the BHR derived from measured data reaches 12.7% over all wavelengths, whereas simulated data varies only by 1%, even though changes of the Sun position and atmospheric conditions are accounted for in the simulations.

The albedo basically is an increasing function of the solar zenith angle, but shows an asymmetric behavior with regard to solar noon [32]. Analyzing morning and afternoon spectral albedos derived from measurements (Figure 4.5), the BHR averaged over the measured wavelength range is considerably larger for morning conditions (e.g., solar zenith angle of 20.5°) than the corresponding afternoon albedo (e.g., solar zenith angle of 22.0°).

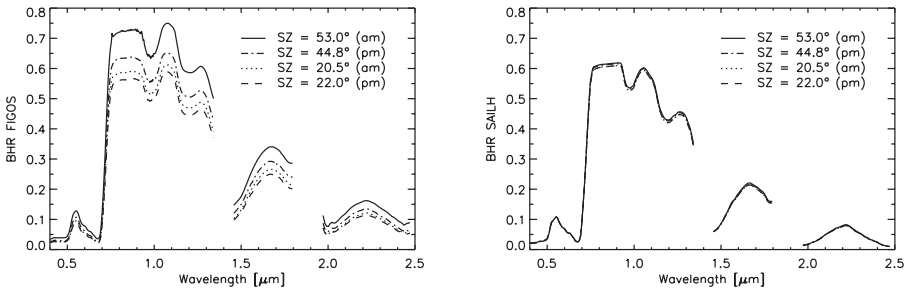

Figure 4.5: BHR results of the dense Alfalfa canopy for different solar angles throughout the day derived from measured (a) and simulated (b) HDRF data. Note the higher albedo for the morning solar zenith angle of 20.5° compared to the lower albedo of the afternoon albedo at a solar zenith of 22.0°.

Large solar zenith angles evoke a more pronounced variation of the HDRF over the whole view angle hemisphere compared to Sun positions around noon (Figure 4.3). HDRF data were related to the corresponding BHR to analyze their spectral behavior (Figure 4.6). SAILH simulated HDRF variations are large for wavelengths with a low BHR. In highly reflecting spectral regions the anisotropy is much less pronounced in terms of variation of the HDRF, most likely due to multiple scattering effects smoothing directional effects. Comparing measured HDRF data to the BHR, the above-mentioned relation exists for large solar zenith angles, whereas small solar zenith angles show a less pronounced anisotropy (Figure 4.6).

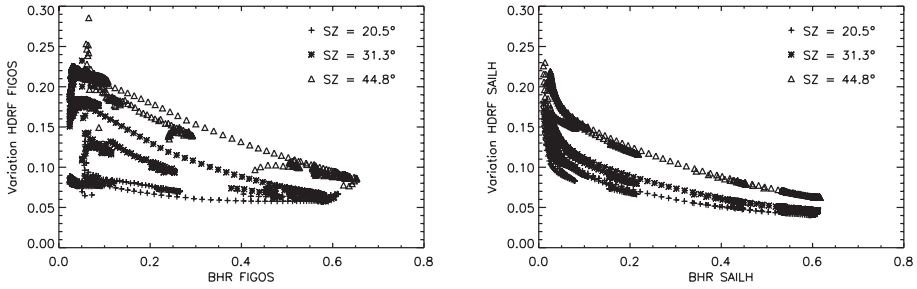

Figure 4.6: Variation of HDRF versus BHR for each wavelength of measured (a) and simulated (b) Alfalfa canopy data for three solar zenith angles.

The variation of the HDRF measured at a solar zenith of 20.5° amounts to 6 to 10% for most wavelength regions, being almost constant with regard to the actual canopy BHR. The various variation levels for different wavelengths with the same BHR exposed in measured data indicate that anisotropy effects not correlated to the spectral albedo do exist.

4.5.3 Results from normalization procedure

Normalizing HDRF data with the corresponding BHR emphasizes wavelength dependence of the anisotropy. Anisotropy factors, $ANIF_{BHR}$ (see Equation 4.5), from SAILH nadir view simulations show a very similar wavelength dependent behavior for different Sun zenith angles, i.e., mainly an offset of the anisotropy factors for the three different times of the day, with higher values for highly absorbing wavelength regions (Figure 4.7). $ANIF_{BHR}$ derived from measured data exhibit a more complex shape, especially in the visible spectral range.

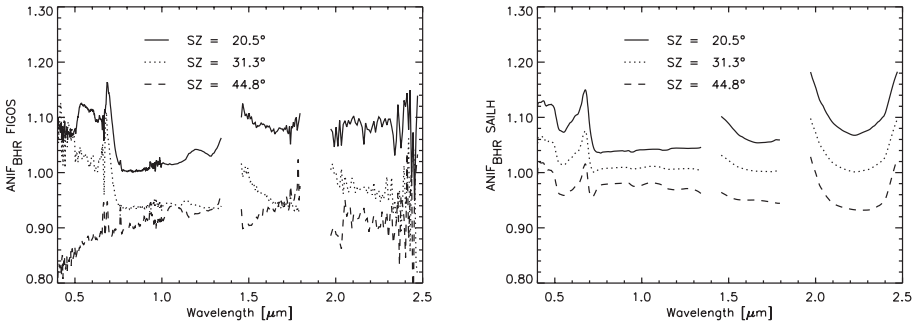

Figure 4.7: $ANIF_{BHR}$ from FIGOS measurements (a) and SAILH simulations (b) for the nadir view angle at three different Sun zenith angles of the day.

4.6 Conclusions

This study suggests a standard procedure to analyze field goniometer data for their quality and quantify their information content with regard to observations' uncertainties. The preprocessing includes the derivation of HDRFs from measured radiances, taking into account the deviations of the Spectralon panel from a perfect lambertian reflector, as well as system and atmosphere properties. An overall characterization of the target's spectral anisotropy is performed using statistical analysis, the spectral albedo, BHR, and the anisotropy factor, $ANIF_{BHR}$. The comparison of modeled and observed data is a tool to assess differences in their representation of spectro-directional effects and assign corresponding uncertainties to HDRF data.

Nadir HDRF measurements throughout the day exhibit large deviations due to a changing solar position and canopy architecture, whereas simulations show smaller deviations. Thus the HDRF should be measured in field experiments and vicarious calibration procedures at the time it is needed, rather than simulated. The results on the BHR substantiate previous studies: the albedo increases with growing Sun zenith angle and an asymmetry with respect to solar noon exists.

The presented procedure guarantees the quality and uncertainty assessment required for the use of spectro-directional reflectance available in a priori BRDF knowledge databases. Even though observed and modeled Alfalfa canopy data show similar trends for the overall statistical analysis, spectral effects are not fully reproduced by simulations.

Future analyses of the spectral effects in the anisotropy of vegetation reflectance require simultaneous measurements of the canopy transmittance and leaf optical properties. They will allow to verify more complex algorithms for estimating vegetation variables, which are based on theories explaining the canopy reflectance

in the solar reflected spectral region using leaf optical properties in combination with wavelength independent variables, characterizing the architecture of the canopy [14][35]. Laboratory measurements with joint outdoor observations are planned to separate the illumination components for deriving BRFs and the BRDF and eliminating spectral effects introduced by the atmosphere, and thus enabling investigations on the separated vegetation dependent spectral effects of the canopy anisotropy.

4.7 Acknowledgements

The authors would like to thank the DAISEX field team, J. Moreno (University of Valencia), W. Verhoef (National Aerospace Center), J. Keller (PSI), S. Dangel, U. Beisl, and C. Dickerhof for their support and fruitful discussions. The authors thank the reviewers for helpful comments on the manuscript, allowing for substantial improvements.

4.8 References

[1] W. A. Abdou, J.E. Conel, S.H. Pilorz, M.C. Helmlinger, C.J. Bruegge, B.J. Gaitley, W. C. Ledeboer, and J.V. Martonchik, Vicarious calibration. A reflectance-based experiment with AirMISR, Remote Sens. Environ., vol. 77, pp. 338-353, 2001.

[2] U. Beisl, Correction of bidirectional effects in imaging spectrometer data, Remote Sensing Series, RSL, Zürich, vol. 37, pp. 189, 2001.

[3] X. Li, F. Gao, J. Wang, and A. Strahler, A priori knowledge accumulation and its application to linear BRDF model inversion, J. Geophys. Res., vol. 106, no. 11, pp. 11925-11935, 2001.

[4] M.E. Bauer, C. Daughtry, L. Biehl, E. Kanemasu, and F. Hall, Field spectroscopy of agricultural crops, IEEE Trans. Geosci. Remote Sensing, vol. GE-24, no. 1, pp. 65-75, 1986.

[5] J.C. Epiphanio and A.R. Huete, Dependence of NDVI and SAVI on Sun/ sensor geometry and its effect on FAPAR relationships in Alfalfa, Remote Sens. Environ., Vol. 51, pp. 351-360, 1995.

[6] A. Walter-Shea, J. Privette, D. Cornell, M. A. Mesarch, and C. J. Hays, Relations between directional spectral vegetation indices and leaf area and absorbed radiation in Alfalfa, Remote Sens. Environ., vol. 61, pp. 162-177, 1997.

[7] S.R. Sandmeier and K. I. Itten, A field goniometer system (FIGOS) for acquisition of hyperspectral BRDF data, IEEE Trans. Geosci. Remote Sensing, vol. 37, pp. 978-986, 1999.

[8] M. Berger, M. Rast, P. Wursteisen, E. Attema, J. Moreno, A. Mueller, U. Beisl, R. Richter, M. Schaepman, G. Strub, M.P. Stoll, F. Nerry, and M. E. Leroy, The DAISEX campaigns in support of a future land-surface-processes mission, ESA Bulletin, vol. 105, pp. 101-111, 2001.

[9] Remote Sensing Unit, University of Valencia, Spain (2001). The DAISEX project home page. http://io.uv.es/projects/daisex/

[10] S.H. Chang, M.J. Westfield, F. Lehmann, D. Oertel, and R. Richter, 79- channel airborne imaging spectrometer, SPIE, vol. 1937, pp. 164-172, 1993.

[11] Integrated Spectronics Pty Ltd. (2002, January 22). HYMAP – Airborne hyperspectral scanner. http://www.intspec.com/hymap.htm

[12] J.L. Deuze, F.M. Breon, J.C. Roujean, P.Y. Deschamps, C. Devaux, M. Herman, and A. Podaire, Analysis of the POLDER (POLarization and Directionality of Earth's Reflectances) airborne instrument observations over land surfaces, Remote Sens. Environ., vol. 45, pp. 137-154, 1994.

[13] S. Jacquemoud and F. Baret, PROSPECT: A model of leaf optical properties spectra, Remote Sens. Environ., vol. 34, pp. 75-91, 1990.

[14] W. Verhoef, Theory of radiative transfer models applied in optical remote sensing of vegetation canopies, Ph.D. thesis, National Aerospace Laboratory NLR, pp. 320, 1998.

[15] M. Weiss, D. Troufleau, F. Baret, H. Chauki, L. Prevot, A. Olioso, N. Bruguier, and N. Brisson, Coupling canopy functioning and radiative transfer models for remote sensing data assimilation, Remote Sens. Environ., vol. 108, pp. 113-128, 2001.

[16] Alfalfa and Alfalfa improvement, ed. A.A. Hanson, co-ed. D.K. Barnes and R.R. Hill, Agronomy, no. 29, American Society of Agronomy, Madison, Wisconsin, USA, 1084 p., 1988.

[17] J.R. Ehleringer and I.N. Forseth, Solar tracking by plants, Science, vol. 210, pp. 1094-1098, 1980.

[18] R.L. Travis and R. Reed, The solar tracking pattern in a closed Alfalfa Canopy, Crop Science, vol. 23, pp. 664-668, 1983.

[19] M.S. Moran, P.J. Pinter, B.E. Clothier, and G.A. Stephen, Effect of water stress on the canopy architecture and spectral indices of irrigated Alfalfa, Remote Sens. Environ., vol. 29, no. 3, pp. 251-261, 1989.

[20] J.M. Welles and J. M. Norman, Instrument for indirect measurement of canopy architecture, Agronomy Journal, vol. 83, no. 5, pp. 818-825, 1991.

[21] I.M. Ray, M.S. Townsend, and J.A. Henning, Variation for yield, water-use efficiency, and canopy morphology among nine Alfalfa germplasms, Crop Sci., vol. 38, pp. 1386-1390, 1998.

[22] R.H. Hart, R.B. Pearce, N.J. Chatterton, G.E. Carlson, D.K. Barnes, and C.H. Hanson, Alfalfa yield, specific leaf weight, CO2 exchange rate, and morphology, Crop Sci., vol. 18, pp. 649-653, 1978.

[23] N. Gobron, B. Pinty, M. Verstraete, and Y. Govaerts, A semidiscrete model for the scattering of light by vegetation, J. Geophys. Res., vol. 102, no. 8, pp. 9431-9446, 1997.

[24] Y. Knyazikhin, J.V. Martonchik, D.J. Diner, R.B. Myneni, M. Verstraete, B. Pinty, and N. Gobron, Estimation of vegetation canopy leaf area index and fraction of absorbed photosynthetically active radiation from atmosphere-corrected MISR data. J. Geophys. Res., vol. 103, no. 24, pp. 32239-32256, 1998.

[25] D.B. Hannaway. (2000, April 10). National Alfalfa Information System: Stems. http://forages.orst.edu/IS/NAIS/main.cfm?PageID=41

[26] J. Moreno, et al., DAISEX-1999 field experiment report, ESA/ESTEC Contract 13390/NL/GD, Univ. Valencia, 90 pp., 1999.

[27] M. E. Schaepman and S. Dangel, Solid laboratory calibration of a nonimaging spectroradiometer, Applied Optics, vol. 39, no. 1, pp. 3754-3764, 2000.

[28] J.V. Martonchik, C.J. Bruegge and A.H. Strahler, A review of reflectance nomenclature used in remote sensing, Remote Sensing Reviews, vol. 19, pp. 9-20, 2000.

[29] St. Sandmeier, Ch. Müller, B. Hosgood, and G. Andreoli, Sensitivity analysis and quality assessment of laboratory BRDF data, Remote Sens. Environ., vol. 64, pp. 176-191, 1998.

[30] A. Berk, G. Anderson, L. Bernstein, P. Acharya, H. Dothe, M. Matthew, S. Adler-Golden, J. Chetwynd, and S. Richtsmeier, MODTRAN 4 radiative transfer modeling for atmospheric correction, Proc. of 8th JPL Airborne Earth Science Workshop, Pasadena, pp. 55-61, 1999.

[31] S.R. Sandmeier, E.M. Middleton, D.W. Deering, and W. Qin, The potential of hyperspectral bidirectional reflectance distribution function data for grass canopy characterization, J. Geophys. Res., vol. 104, no. 8, pp. 9547-9560, 1999.

[32] P. Minnis, S. Mayor, W.L. Smith, and D.F. Young, Asymmetry in the diurnal variation of surface albedo, IEEE Trans. Geosci. Remote Sensing, vol. 35, pp. 879-891, 1997.

[33] W. Lucht, C.B. Schaaf, and A.H. Strahler, An algorithm for the retrieval of albedo from space using semiempirical BRDF models, IEEE Trans. Geosci. Remote Sensing, vol. 38, pp. 977-998, 2000.

[34] S. Liang, J.C. Stroeve, I.F. Grant, A.H. Strahler, and J.P. Duvel, Angular corrections to satellite data for estimating Earth radiation budget, Remote Sensing Reviews, vol. 18, no. 24, pp. 103-136, 2000.

[35] O. Panferov, Y. Knyazikhin, R.B. Myneni, J. Szarzynski, S. Engwald, K.G. Schnitzler, and G. Gravenhorst, The role of canopy structure in the spectral variation of transmission and absorption of solar radiation in vegetation canopies, IEEE Trans. Geosci. Remote Sensing, vol. 39, pp. 241-253, 2001.

Chapter 5

Review of Reflectance Nomenclature Used in Optical Remote Sensing with Quantitative Comparisons

Schaepman, G., M.E. Schaepman, T. Painter, S. Dangel, J. Martonchik, M. Verstraete, Review of Reflectance Nomenclature Used in Optical Remote Sensing with Quantitative Comparisons, 2004, in preparation.

Abstract

Demand for consistent definitions of reflectance quantities has increased in the remote sensing user community with the increased availability of spectro-directional sensors. Even though more recent satellite programs such as NASA's MODIS and MISR sensors take into account the directional dimension of different reflectance products, there are still many published studies remaining rather unspecific on the particular reflectance quantity that they are based on. One example is the term 'albedo' that ranges from the simple use of ‘nadir measured reflectance’ to sophisticated approximations of albedo, based on a directional model as well as the integrated narrow band to broadband conversion of reflectance. This renders it difficult to evaluate and compare published results with respective uncertainties. In this paper, we summarize basic reflectance nomenclature and list a spectro-directional processing chain, while separating conceptual from measurable quantities. We exemplify resulting differences of these quantities by using a threefold approach that is based on real data (e.g., MISR), on simulation of natural targets (e.g., vegetation canopy and snow cover), and finally on simulation of an artifical target in a laboratory environment. For all approaches, real measurements are being used from satellite and goniometric measurements respectively. Results from the case study comparison demonstrate the difference between directional-hemispherical reflectance versus bihemispher-

ical reflectance and bidirectional reflectance factors versus hemispherical-directional reflectance factors. The presented case studies give a detailed insight into the dimension of the problem and are quantified accordingly. We conclude that the actual differences in reflectance products of a remotely sensed surface are significant and depend not only on atmospheric conditions, the object's surroundings, and the topography, but as well on the scattering properties of the surface itself. The results give a clear indication that reflectance quantities shall be treated with outmost care and consistency to allow future comparison between results, and a consistent data quality of spectrodirectional (derived) products.

5.1 Introduction

The Earth-looking remote sensing community has developed over the past few years an increased appreciation of the effects that are induced by change of solar illumination geometry and sensor viewing geometry on airborne and satellite data due to the anisotropic reflectance of the Earth's surface and the atmosphere. It has also been noted, that not only the direction of illumination and observation influence the measured reflectance, but also the (instantaneous) field of view ((I)FOV) of the particular instrument used. In the past, various reflectance quantities have been defined to describe the corresponding conditions of the measurements and their transformation into a common terminology (Nicodemus, 1977; Martonchik, 2000).

Nevertheless, these conditions are often partly or even fully neglected in the processing applied by end-users, resulting in different reflectance quantities that will be compared. This is particularly true for the so-called surface reflectance versus albedo discussion. The term albedo is often used for these quantities interchangeably, mainly due to the lack of a unified reflectance terminology and missing awareness of the inherent uncertainty of directional measurements, when assuming them to be acquired at nadir. (e.g., Breuer, 2003). The albedo is one important source of radiative transfer induced uncertainties in general circulation models in climate research [Lucht, 2000]. These models may require an absolute accuracy of +-0.02 of the albedo for a monthly average, equivalent to an energy flux density of +- 10 Wm^{-2} [Sellers, 1995]. This requirement usually cannot be met using state-of-the-art approaches, but significant advances in the estimation and validation of the albedo have been made recently [Kimes, 1987; Kimes, 1992; Asrar, 1993; Lewis, 1994; Liu, 1994; Russell, 1997b; Lyapustin, 1999; Barnsley, 2000; Lucht, 2000; Zhou, 2003].

The adequate usage of reflectance data requires a precise, widely distributed and easy to use reflectance nomenclature, coupled with an indepth understanding of spectro-directional effects. Historically, many authors have identified these problems; nevertheless they often restricted themselves to a single quantity, or did not cover newer setups such as laboratory measurements [Nicodemus, 1977; Diner, 1999; Martonchik, 2000; Snyder, 2002; Di Girolamo, 2003]. In addition, there is inconsistency to be observed in definitions and properties of reflectance quantities used, that are derived from different sensor systems. Recent advances originating from the Multi-angle Imaging SpectroRadiometer (MISR) science team have lead to a more uniform reflectance terminology usage that has been intrinsically based on the work of Nicodemus [1977], and disseminated to the user community by recent works of Diner [1999]. Further, operational MISR data products include different reflectance products, giving users the opportunity to apply the appropriate quantity for their investigations the first time.

The reflectance anisotropy of observed surfaces contains unique information about its structure and the optical properties of the scattering elements. The un-

derlying concept for the characterization of the anisotropy is the bidirectional reflectance distribution function (BRDF). It describes the radiance reflected by a surface as a function of a parallel beam of incident light from a single direction into another direction of the hemisphere. Under natural conditions, i.e. for all field, airborne and spaceborne sensor measurements, the assumption of a single direction of the incident beam does not hold true. Natural light is composed of a direct part, thus uncollided radiation, as well as a diffuse component scattered by the atmosphere, and/ or the surroundings of the observed target. The amount and spectral character of the diffuse light irradiating the observed surface is thus depending on the atmospheric conditions, as well as on the topography and the scattering properties of the surroundings. Previous studies have shown the effects of different atmospheric conditions in simulated and measured data. Without correction of the diffuse component of the irradiance, the resulting products will always be dependent on actual atmospheric conditions, especially in the Rayleigh scattering dominated wavelength region (400-800 nm), and are not limited to the desired intrinsic directional characteristics of the observed surface. The derivation of the bidirectional reflectance distribution function (BRDF) using multiangular measurements performed under ambient sky illumination will result in considerable shape distortion of the resulting surface BRDF in the visible and near-infrared when no correction for the diffuse part of the illumination is performed, even under clear sky conditions [Lyapustin, 1999]. Subsequently, Martonchik [1994] and Lyapustin [1999] have developed methods for an accurate atmospheric correction to enhance the experimental research of anisotropic surface reflectance.

Several studies analyzed simulated reflectance data under different ratios of direct and diffuse irradiance conditions [Asrar, 1993; Lewis, 1994; Lyapustin, 1999]. The analysis of illumination effects present in measured reflectance data is discussed in Kriebel [1976], Ranson [1985], Deering [1987], and Liu [1994]. The aim of this paper is to highlight the differences in reflectance caused by different geometries of the opening angle of the illumination, i.e., directional and hemispherical extent. We are using an approach that is based on common and emerging applications for spectrodirectional problems. First, we perform an in-depth analysis of real data using the Multi-angle Imaging SpectroRadiometer (MISR), where we discuss the results of a comparison between directional and hemispherical reflectance products for selected biomes on the terrestrial surface. from the (MISR) are presented for selected test sites. Secondly we perform a modelling exercise for two significantly different natural land covers, forest and snow. Based on field goniometric measurements using PARABOLA and ASG respectively as well as the RPV and DISORT models, we will obtain a quantiative result of the influence of the diffuse component that is included in the hemispherical extent. Finally we are using a laboratory setup based on LAGOS, where an artificial aluminum target is measured and the MPRV model used. This has been included due to the increasing availability of laboratory instruments and their potential im-

pact on performing weather-independent experiments for the proper determination of BRDF's. We include where possible a variation of different direct to diffuse irradiance scenarios in these case studies.

This paper finally allows full access to the basic concepts of reflectance quantities used, by summarizing the nomenclature articles of Nicodemus (1977) and Martonchik (2000). It highlights the importance of a proper usage of definitions through quantitative comparisons of different reflectance products.

5.2 Definitions

Based on the initial definitions by Nicodemus [1977] and Martonchik [2000], we propose the individual directional quantities, using the following notations:

S distribution of direction of radiation

ρ reflectance $\equiv d\Phi_r / d\Phi_i$ [dimensionless]

R reflectance factor $\equiv d\Phi_r / d\Phi_{rid}$ [dimensionless]

θ zenith angle, in a spherical coordinate system [rad]

ϕ azimuth angle, in a spherical coordinate system [rad]

ω solid angle $\equiv \int d\omega \equiv \iint \sin\theta \cdot d\theta \cdot d\phi$ [sr]

Ω projected solid angle $\equiv \int \cos\theta \cdot d\omega \equiv \iint \cos\theta \cdot \sin\theta \cdot d\theta \cdot d\phi$ [sr]

λ wavelength of the radiation [nm]

E irradiance, incident flux density $\equiv$ dΦ/dA [Wm^{-2}]

L radiance $\equiv d^2\Phi/(dA \cdot \cos\theta \cdot d\omega)$ [$Wm^{-2}sr^{-1}$]

A surface area [m^2]

Φ radiant flux [W]

f() function

with the following sub- and superscripts used in combination with the above mentioned parameters:

i incident

r reflected

id *i*deal (lossless) and *d*iffuse (isotropic or Lambertian).

a) Radiance, reflectance, reflectance factors

Spectral radiance is the most important quantity to be measured in spectroradiometry. The surface leaving radiance is usually ratioed by the incident radiation onto the surface, resulting in the so-called reflectance. Following the concept of energy conservation, the values of the reflectance are in the inclusive interval 0 to 1. The reflectance factor is the ratio of the radiant flux reflected by a surface to that reflected into the same reflected-beam geometry by an ideal (lossless) and dif-

fuse (lambertian) standard surface, irradiated under the same conditions. For measurement purposes, a Spectralon panel commonly approximates the ideal diffuse standard surface. Reflectance factors may reach values beyond 1, especially for highly specular reflecting surfaces.

b) Conceptual and measurable reflectance quantities

Since in most applications in Earth related remote sensing the reflected spectral radiance is measured, we define

$\rho(S_i, S_r, \lambda)$ = reflectance, and

$R(S_i, S_r, \lambda)$ = reflectance factor

where S_i and S_r describe the distribution of the direction of *all* incoming and the *part of* the reflected radiance observed by the sensor or considered to be of interest, respectively. S_i and S_r can depend on λ, in cases where a sensor has a different field of view (FOV) depending on the wavelength. In addition, S_i and S_r only describe a set of angles occurring with the incoming/reflected radiation and not its power distribution. No sensor weight functions are included here. Thus, S_r describes a cone with a certain solid angle corresponding to a sensor's FOV. If the sensitivity of the sensor decreases towards the rim of the cone, a convolution function must be given.

Maintaining the wavelength dependency of reflectance, the terms S_i and S_r can be expanded into a more specific notation, for the reflectance and reflectance factor, adapted to the remote sensing problem and respecting particular directional issues:

$\rho(\theta_i, \phi_i, \omega_i; \theta_r, \phi_r, \omega_r; \lambda)$, and

$R(\theta_i, \phi_i, \omega_i; \theta_r, \phi_r, \omega_r; \lambda)$,

where the direction of the incoming and the reflected radiance, as well as the solid angle of the cone are indicated. This notation follows the definition of a general cone. For the special condition of a circular cone, please refer to the notation of McCamy [1966].

This expanded definition can furthermore be subdivided into a number of subcategories. From a physical point of view, there is the possibility to define special cases of ρ and R, namely conceptual quantities and measurable quantities. Conceptual quantities of reflectance include the assumption that the size/ distance ratio of the illuminating source (usually the sun or lamp) and the observing sensor is assumed to be zero and are usually labelled *directional* in the general terminology. Since infinitesimal elements of solid angle do not include *measurable* amounts of radiant flux, and unlimited small light sources and sensor FOVs do not exist, all measurable quantities of reflectance are performed in the *conical* or *hemispherical* domain of geometrical considerations. Thus, actual measurements always involve non-zero intervals of direction and the underlying basic quantity for all radiance and reflectance measurements is the conical case, including the special case of a cone with hemispherical extent ($\omega = 2\pi$ [sr]). The integration of

the incoming radiance over a solid angle of conical or hemispherical extent accounts for the diffuse illumination. Under field conditions, the irradiance can be divided into a direct sunlight component and a second irradiance component scattered by the atmosphere and terrain, which leads to an anisotropic, diffuse sky illumination. Being a function of wavelength, the ratio of diffuse/direct incident irradiance highly influences the spectral dependence of directional effects as shown in the snow case study below.
The integration of the reflected radiance over a solid angle of conical or hemispherical extent corresponds e.g. to the opening angle of the sensor.

In spectroradiometry, the quantities most commonly measured are spectral irradiance and spectral radiance. The latter is the radiant flux in a beam per unit wavelength and per unit area and solid angle of that beam. It is usually expressed in the SI units [$Wm^{-2}sr^{-1}nm^{-1}$]. It is the quantity required for quantitatively analyzing directional effects and the baseline of most airborne and satellite measurements.

A refinement of the above reflectance and reflectance factor definition leads to the following special cases:

- ω_i or ω_r are omitted when either is zero (directional quantities).
- if $0 < (\omega_i \text{ or } \omega_r) < 2\pi$, then θ, ϕ describe the direction of the center axis of the cone (e.g. the line from a sensor to the center of its ground field of view).
- if $\omega_i = 2\pi$, the angles θ_i, ϕ_i indicate the direction of the incoming direct radiation (e.g., the position of the sun). However, for remote sensing applications, it is often useful to separate the natural incoming radiation into a direct (neglecting the sun's size) and hemispherical diffuse part. One may also include terrain reflected diffuse component that is calculated with a topographic radiation model such as TOPORAD [Dozier, 1980]. The preferred notation for the geometry of the incoming radiation is then $\theta_i, \phi_i, 2\pi$, thus keeping the position of the sun. It must be noted that in this case, θ_i, ϕ_i do not describe the center of the cone (2π), except if the sun's position is at nadir. For the white-sky case, corresponding to the configuration of an isotropic diffuse downward radiation field, without any direct irradiance component (closest approximated in the case of a deep cloud deck), θ_i, ϕ_i are omitted.
- If $\omega_r = 2\pi$, θ_r and ϕ_r are omitted.

Finally, according to Nicodemus, 1977, the angular characteristics of the incoming radiance are named first in the term and are followed by the angular characteristics of the reflected radiance. This leads to the following nomenclature of spectro-directional quantities (Table 5.1):

Reflected Incoming	**Directional**	**Conical**	**Hemispherical**
Directional	Bidirectional reflectance Case 1	Directional-conical reflectance Case 2	Directional-hemispherical reflectance Case 3
Conical	Conical-directional reflectance Case 4	Biconical reflectance Case 5	Conical-hemispherical reflectance Case 6
Hemispherical	Hemispherical-directional reflectance Case 7	Hemispherical-conical reflectance Case 8	Bihemispherical reflectance Case 9

Table 5.1: Relation of incoming and reflected radiance terminology used to describe reflectance quantities. The labelling with 'Case' corresponds to the nomenclature of Nicodemus [1977]. Grey fields correspond to measurable quantities (Cases 5, 8), the others (Cases 1-4, 6, 7, 9) denote conceptual quantities.

5.2.1 Examples for measurable quantities and derived products

Referring to Table 5.1, typical measurement instrumentation with resulting reflectance products can be listed for the individual cases. The biconical reflectance (Case 5) is a typical laboratory setup, where a collimated light source illuminates a target that is measured using a non-imaging spectroradiometer (e.g., EGO [Koechler, 1994], and LAGOS [Dangel, 2003]). The hemispherical-conical reflectance (Case 8) corresponds to the most common measurement of satellites or airborne and field instruments (e.g., MERIS, ASD FieldSpec). Finally, bihemispherical reflectance (Case 9) is approximated by measurements using albedometers [e.g., Kipp, 2000].

Even though measurable quantities only reflect Cases 5 and 8 in Table 5.1 above, the non-zero interval of the sensor's field of view may be neglected and resulting quantities are reported as being bidirectional or hemispherical-directional measurements. Most satellite reflectance products delivered after atmospheric correction procedures are labelled 'surface reflectance' (e.g., Moderate Resolution Imaging Spectroradiometer (MODIS) [Vermote, 1999]). Nevertheless, in many cases the underlying concept of the used reflectance nomenclature is unclear or undocumented, resulting in significant difficulties to assign the proper terminology to the delivered data product. As long as data from satellite or airborne sensors and field spectrometers are not corrected for the hemispherical angular extent of the incoming radiance, the reflected measured quantity always depends on the actual direct and diffuse components of the irradiance over the whole hemisphere. As a consequence, data without a proper specification of the correspond-

ing beam geometries are subject to misinterpretation and subsequently their uncertainties increase.

Table 5.2 lists the most important data products as they are distributed from satellite and airborne sensors.

Reflected Incoming	**Directional**	**Conical**	**Hemispherical**
Directional	BRF (Bidirectional Reflectance Factor) BRDF (Bidirectional Reflectance Distribution Function) Case 1	 Case 2	DHR (Directional-Hemispherical Reflectance Case 3
Conical	Case 4	Case 5	Case 6
Hemispherical	HDRF (Hemispherical-Directional Reflectance Factor) Case 7	Hemispherical-Conical Reflectance Case 8	BHR (BiHemispherical Reflectance Case 9

Table 5.2: Tabular description of typical data products delivered from satellite and airborne measurements. Empty fields denote no products delivered in the respective category, the grey field denotes a typical satellite measurement.

Figure 5.1 shows the derivation of the products from the satellite measurement. The integration of the HDRF (Case 7) over the viewing hemisphere results in the BHR (Case 9). Using a modelling approach (e.g., Martonchik, 1994; Martonchik, 1998; Lyapustin, 1999), the HDRF data (Case 7) is further used to derive BRF (Case 1), and finally, DHR (Case 3) can be derived from BRF (Case1) by hemispherical integration over the viewing hemisphere. A special case is the derivation of the BRDF from the BRF (again Case 1), which is simply scaling the BRF by $1/\pi$.

The abovementioned derivations of conceptual reflectance quantities from measured reflectance data include the application of a BRDF model. Thus, derived conceptual quantities depend not only on the sampling scheme, availability and accuracy of measured data, but also on the model itself.

Note that the previously cited Nicodemus [1977] bases his nomenclature on an available BRDF. The BRDF can be considered as the most important description

of spectro-directional data, since all other quantities can be derived from it by integration.

We will now describe above-cited commonly used quantities and allocate the respective case number where appropriate.

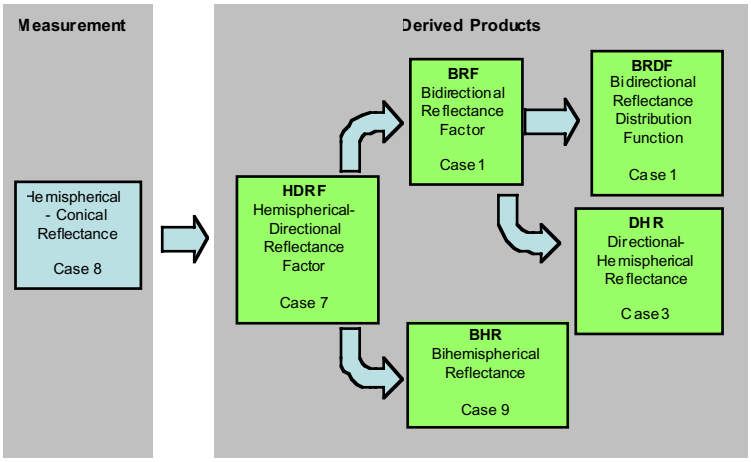

Figure 5.1: Conceptual data processing chain of airborne and satellite measurements to convert a spectrodirectional measurement (Case 8) into BHR, BRDF, and DHR respectively.

5.2.2 The Bidirectional Reflectance Distribution Function (BRDF) – Case 1

The bidirectional reflectance distribution function (BRDF) describes the scattering of a parallel beam of incident light from one direction in the hemisphere into another direction in the hemisphere. The term BRDF was first used in the literature in the early 1960s [Nicodemus, 1965]. It also describes the intrinsic scattering properties of a surface and thus enables to derive many other relevant quantities. The spectral BRDF can be expressed as

$$BRDF = f_r(\theta_i,\phi_i;\theta_r,\phi_r;\lambda) = \frac{dL_r(\theta_i,\phi_i;\theta_r,\phi_r;\lambda)}{dE_i(\theta_i,\phi_i;\lambda)}[sr^{-1}] \tag{5.1}$$

For reasons of clarity, we will ignore the spectral dependence in the following. The spectral dependence of the BRDF of vegetation canopies and snow cover has been documented in literature [Middleton, 1992; Russell, 1997a, Sandmeier, 1999; Painter, 2004], but is not subject of this contribution. We therefore write for the BRDF

$$BRDF = f_r(\theta_i,\phi_i;\theta_r,\phi_r) = \frac{dL_r(\theta_i,\phi_i;\theta_r,\phi_r)}{dE_i(\theta_i,\phi_i)}[sr^{-1}] \tag{5.2}$$

5.2.3 Reflectance Factors – Definition of Case 1 and Case 7

When directional properties of a surface are being measured, the procedure usually follows the definition of a reflectance factor. The reflectance factor is the ratio of the radiant flux reflected by a sample surface to the radiant flux reflected into the identical beam geometry by an ideal (lossless) and diffuse (Lambertian) standard surface, irradiated under the same conditions as the sample surface. Following the different beam geometries of the incident and reflected radiant fluxes as mentioned above, we define the *bidirectional reflectance factor*, the *hemispherical-directional reflectance factor*, the *biconical reflectance factor*, and the *hemispherical-conical reflectance factor*.

The **bidirectional reflectance factor** (**BRF; Case 1**) can be written as the ratio of the reflected flux by the surface area *dA* to the reflected flux from an ideal and diffuse surface of the same area *dA* under identical view and illumination geometry, including the single direction of the illumination and reflected radiant flux.

$$BRF = R(\theta_i,\phi_i;\theta_r,\phi_r) = \frac{d\Phi_r(\theta_i,\phi_i;\theta_r,\phi_r)}{d\Phi_r^{id}(\theta_i,\phi_i)} \tag{5.3}$$

$$= \frac{\cos\theta_r \sin\theta_r dL_r(\theta_i,\phi_i;\theta_r,\phi_r)d\theta_r d\phi_r dA}{\cos\theta_r \sin\theta_r dL_r^{id}(\theta_i,\phi_i)d\theta_r d\phi_r dA} \tag{5.4}$$

$$= \frac{dE_i(\theta_i,\phi_i)}{dL_r^{id}(\theta_i,\phi_i)} \cdot \frac{dL_r(\theta_i,\phi_i;\theta_r,\phi_r)}{dE_i(\theta_i,\phi_i)} \tag{5.5}$$

$$= \frac{f_r(\theta_i,\phi_i,\theta_r,\phi_r)}{f_r^{id}(\theta_i,\phi_i)} = \pi \cdot f_r(\theta_i,\phi_i;\theta_r,\phi_r) \tag{5.6}$$

An ideal lambertian surface reflects the same radiance in all view directions, and its BRDF is $1/\pi$. Thus, the BRF [unitless] of any surface can be expressed as its BRDF [sr^{-1}] times π (Equation 5.6). For $\Phi^{id}{}_r$ and $L^{id}{}_r$, we omit the view zenith and azimuth angles, because there is no angular dependence for the ideal and Lambertian surface.

The concept of the **hemispherical-directional reflectance factor** (**HDRF; Case** 7) is similar to the definition of the BRF, but includes the illumination from the entire hemisphere. This makes the quantity more dependent on the actual, simulated or assumed atmospheric conditions and topographic reflectance, including spectral effects introduced by the variation of the diffuse to direct irradiance ratio with wavelength (e.g., Strub, 2003). For clarity, the wavelength is omitted in the following expressions.

$$HDRF = R(\theta_i,\phi_i,2\pi;\theta_r,\phi_r) = \frac{d\Phi_r(\theta_i,\phi_i,2\pi;\theta_r,\phi_r)}{d\Phi_r^{id}(\theta_i,\phi_i,2\pi)} \tag{5.7}$$

$$= \frac{\cos\theta_r \sin\theta_r L_r(\theta_i,\phi_i,2\pi;\theta_r,\phi_r)d\theta_r d\phi_r dA}{\cos\theta_r \sin\theta_r L_r^{id}(\theta_i,\phi_i,2\pi)d\theta_r d\phi_r dA} \tag{5.8}$$

$$= \frac{L_r(\theta_i,\phi_i,2\pi;\theta_r,\phi_r)}{L_r^{id}(\theta_i,\phi_i,2\pi)} = \frac{\int_{2\pi} f_r(\theta_i,\phi_i;\theta_r,\phi_r)d\Phi_i(\theta_i,\phi_i)}{\int_{2\pi}(1/\pi)d\Phi_i(\theta_i,\phi_i)} \tag{5.9}$$

$$= \frac{\int_0^{2\pi}\int_0^{\pi/2} f_r(\theta_i,\phi_i;\theta_r,\phi_r)\cos\theta_i \sin\theta_i L_i(\theta_i,\phi_i)d\theta_i d\phi_i}{(1/\pi)\int_0^{2\pi}\int_0^{\pi/2}\cos\theta_i \sin\theta_i L_i(\theta_i,\phi_i)d\theta_i d\phi_i} \tag{5.10}$$

If we divide L_i into a direct (E_{dir} with angles θ_0,ϕ_0) and diffuse part, we may continue

$$= \frac{f_r(\theta_0,\phi_0;\theta_r,\phi_r)E_{dir}(\theta_0,\phi_0) + \int_0^{2\pi}\int_0^{\pi/2} f_r(\theta_i,\phi_i;\theta_r,\phi_r)\cos\theta_i \sin\theta_i L_i^{diff}(\theta_i,\phi_i)d\theta_i d\phi_i}{(1/\pi)(E_{dir}(\theta_0,\phi_0) + \int_0^{2\pi}\int_0^{\pi/2}\cos\theta_i \sin\theta_i L_i^{diff}(\theta_i,\phi_i)d\theta_i d\phi_i)}$$

(5.11)

$$= \frac{f_r(\theta_0,\phi_0;\theta_r,\phi_r)E_{dir}(\theta_0,\phi_0) + \int_0^{2\pi}\int_0^{\pi/2} f_r(\theta_i,\phi_i;\theta_r,\phi_r)\cos\theta_i \sin\theta_i L_i^{diff}(\theta_i,\phi_i)d\theta_i d\phi_i}{(1/\pi)(E_{dir}(\theta_0,\phi_0) + \int_0^{2\pi}\int_0^{\pi/2}\cos\theta_i \sin\theta_i L_i^{diff}(\theta_i,\phi_i)d\theta_i d\phi_i)}$$

(5.12)

$$= R(\theta_0,\phi_0;\theta_r,\phi_r)d + R(2\pi;\theta_r,\phi_r)(1-d) \tag{5.13}$$

where $R(2\pi;\theta_r,\phi_r)$ could be called white-sky HDRF and d corresponds to the relative amount of direct radiation (i.e. $d \in [0, 1]$).

Of major importance for laboratory measurements is the biconical reflectance factor (conical-conical reflectance factor, CCRF; Case 5) defined as

$$CCRF = R(\theta_i,\phi_i,\omega_i;\theta_r,\phi_r,\omega_r) = [\pi/(\Omega_i \cdot \Omega_r)] \cdot \int_{\omega_i}\int_{\omega_r} f_r(\theta_i,\phi_i;\theta_r,\phi_r) \cdot d\Omega_r \cdot d\Omega_i \tag{5.14}$$

where $\Omega = \int d\Omega = \int \cos\theta d\omega = \int\int \cos\theta \sin\theta d\theta d\phi$ is the projected solid angle of the cone. We refer to [McCamy, 1966; Nicodemus, 1977] for the special case of a circular cone.

Formally, the CCRF can be seen as the most flexible quantity, because its expression contains all other cases as special ones: for $\omega = 0$ the integral collapses and

we obtain the directional case, for $\omega = 2\pi$ we obtain the hemispherical case. However, the BRF and BRDF remain the most fundamental and desired quantities because they are the only quantities not integrated over a range of angles. All other quantities are averages of the BRF/BRDF, and therefore generally contain *less* information.

For large field of view sensors, outdoor measurements cannot hold the assumption of a zero interval of the solid angle for the measured reflected radiance beam. Thus, the resulting measurement quantity is the hemispherical-conical reflectance factor (HCRF; Case 8), obtained from Equation 5.14 by setting $\omega_i = 2\pi$:

$$HCRF = R(\theta_i,\phi_i,2\pi;\theta_r,\phi_r,\omega_r) = [1/\Omega_r]\cdot \int_{2\pi}\int_{\omega_r} f_r(\theta_i,\phi_i;\theta_r,\phi_r)\cdot d\Omega_r \cdot d\Omega_i \tag{5.15}$$

5.2.4 Reflectance – Case 3 and Case 9

For the complete characterization of the energy fluxes, the reflected radiance is integrated over the view hemisphere, resulting in the so-called albedo. It is the ratio of reflected to incident solar irradiance. In the following, the hemispherical reflectance is described as a function of the incoming radiation, including (i) the special condition of pure direct irradiance, (ii) actual irradiance, composed of diffuse and direct components, and (iii) pure diffuse irradiance.

The directional-hemispherical reflectance (DHR; Case 3) corresponds to the special case of pure direct illumination and thus is sometimes referred to as black-sky albedo. It is the ratio of the flux for light reflected by a surface area *dA* into the view hemisphere to the illumination flux, when the surface is illuminated with a parallel beam of light from a single direction.

$$DHR = \rho(\theta_i,\phi_i;2\pi) = \frac{d\Phi_r(\theta_i,\phi_i;2\pi)}{d\Phi_i(\theta_i,\phi_i)} = \frac{dA\int_0^{2\pi}\int_0^{\pi/2} dL_r(\theta_i,\phi_i;\theta_r,\phi_r)\cos\theta_r \sin\theta_r d\theta_r d\phi_r}{d\Phi_i(\theta_i,\phi_i)} \tag{5.16}$$

$$= \frac{d\Phi_i(\theta_i,\phi_i)\int_0^{2\pi}\int_0^{\pi/2} f_r(\theta_i,\phi_i;\theta_r,\phi_r)\cos\theta_r \sin\theta_r d\theta_r d\phi_r}{d\Phi_i(\theta_i,\phi_i)} \tag{5.17}$$

$$= \int_0^{2\pi}\int_0^{\pi/2} f_r(\theta_i,\phi_i;\theta_r,\phi_r)\cos\theta_r \sin\theta_r d\theta_r d\phi_r \tag{5.18}$$

The bihemispherical reflectance (BHR; Case 9), generally called albedo, is the ratio of the flux of light reflected from the surface area *dA* into the whole hemisphere to the incident flux, when the area is illuminated by an arbitrary radiation field of hemispherical angular extent.

$$BHR = \rho(\theta_i,\phi_i,2\pi;2\pi) = \frac{d\Phi_r(\theta_i,\phi_i,2\pi;2\pi)}{d\Phi_i(\theta_i,\phi_i,2\pi)} \tag{5.19}$$

$$= \frac{dA\int_0^{2\pi}\int_0^{\pi/2} dL_r(\theta_i,\phi_i,2\pi;\theta_r,\phi_r)\cos\theta_r \sin\theta_r d\theta_r d\phi_r}{dA\int_0^{2\pi}\int_0^{\pi/2} dL_i(\theta_i,\phi_i)\cos\theta_i \sin\theta_i d\theta_i d\phi_i} \tag{5.20}$$

$$= \frac{\int_0^{2\pi}\int_0^{\pi/2}\int_0^{2\pi}\int_0^{\pi/2} f_r(\theta_i,\phi_i;\theta_r,\phi_r)\cos\theta_r \sin\theta_r d\theta_r d\phi_r L_i(\theta_i,\phi_i)\cos\theta_i \sin\theta_i d\theta_i d\phi_i}{\int_0^{2\pi}\int_0^{\pi/2} L_i(\theta_i,\phi_i)\cos\theta_i \sin\theta_i d\theta_i d\phi_i} \tag{5.21}$$

$$= \frac{\int_0^{2\pi}\int_0^{\pi/2} \rho(\theta_i,\phi_i;2\pi) L_i(\theta_i,\phi_i)\cos\theta_i \sin\theta_i d\theta_i d\phi_i}{\int_0^{2\pi}\int_0^{\pi/2} L_i(\theta_i,\phi_i)\cos\theta_i \sin\theta_i d\theta_i d\phi_i} \tag{5.22}$$

If as before we divide L_i into a direct (E_{dir} with angles θ_0, ϕ_0) and diffuse part, and assume that L_i^{diff} is isotropic we can write

$$= \frac{\rho(\theta_0,\phi_0;2\pi)E_{dir}(\theta_0,\phi_0) + L_i^{diff}\pi(1/\pi)\int_0^{2\pi}\int_0^{\pi/2}\rho(\theta_i,\phi_i;2\pi)\cos\theta_i \sin\theta_i d\theta_i d\phi_i}{E_{dir}(\theta_0,\phi_0) + \pi L_i^{diff}} \tag{5.23}$$

$$= \rho(\theta_0,\phi_0;2\pi)d + \rho(2\pi;2\pi)(1-d) \tag{5.24}$$

where d again corresponds to the relative amount of direct radiation.

For the special case of isotropic illumination we can describe the resulting BHR (referred to as white-sky albedo) as follows

$$BHR = \rho(2\pi;2\pi) = \frac{1}{\pi}\int_0^{2\pi}\int_0^{\pi/2}\rho(\theta_i,\phi_i;2\pi)\cos\theta_i \sin\theta_i d\theta_i d\phi_i \tag{5.25}$$

Under natural illumination conditions, the actual albedo is commonly influenced by a combination of diffuse and direct irradiance. For the special case of pure diffuse isotropic irradiance, a situation that may be most closely approximated in the field only by a thick cloud or aerosol layer, the resulting bihemispherical reflectance is referred to as white-sky albedo.

To obtain actual albedo values for a certain day, it is suggested to linearly combine the DHR and white-sky BHR (see Equation 5.24), corresponding to the actual ratio of diffuse/direct illumination [Zhou, 2003]. The underlying assumption of an isotropic diffuse illumination may lead to significant uncertainties due to the actual distribution of the incoming diffuse radiation given anisotropy in the sky irradiance and the terrain reflected irradiance. All above mentioned albedo values, with the exception of the BHR under pure diffuse illumination conditions, depend on the actual illumination angle. Thus it is highly recommended to include the corresponding solar geometry for any further studies applying albedo values.

5.3 Case studies comparing different reflectance quantities

The following case studies highlight differences of the above described reflectance quantities using MISR data products for several scenes, as well as model simulations for a vegetation canopy, snow cover, and an artificial target. The differences of hemispherical versus directional reflectance and reflectance factors (i.e., BHR (Case 9) versus DHR (Case 3) and HDRF (Case 7) versus BRF (Case1)) are computed for different wavelengths regions and various ratios of direct to diffuse illumination conditions.

We concentrate in these case studies on the reflectance and reflectance factor quantities. Deriving the bidirectional reflectance distribution function from HDRF measurements without correcting for the diffuse illumination component, leads to severe distortions of the resulting function [Lyapustin, 1999].

5.3.1 Analysis of MISR surface reflectance data products

a) Methods and selected datasets

Various land surface reflectance products are available from the MISR sensor, launched in 1999 [Diner, 1999]. MISR has nine cameras with centre view directions of 26.1°, 45.6°, 60.0°, and 70.5° in forward and afterward direction, as well as one looking in nadir direction. All cameras cover four spectral bands with a centre wavelength at 446, 558, 672, and 867 nm. The crosstrack IFOV and sample spacing of each pixel is 275 m for all of the off-nadir cameras, and 250 m for the nadir camera. Downtrack IFOVs depend on view angle, ranging from 214 m in the nadir to 707 m at the most oblique angle. However, sample spacing in the downtrack direction is 275 m in all cameras [Diner, 1999].

We briefly describe the retrieval of the land surface products HDRF, BHR, BRF, and DHR. The mathematical conversion is discussed in Martonchik [1998]. The top-of-atmosphere MISR radiances are first atmospherically corrected to produce the HDRF and the BHR, surface reflectance properties as would be measured at ground level but at the MISR spatial resolution. The MISR surface retrievals do not explicitly incorporate tilt or slope effects [Diner, 1999]. The HDRF and BHR then are further atmospherically corrected to remove all diffuse illumination effects, resulting in the BRF and DHR. The determination of these surface products obviously requires that the atmosphere be sufficiently characterized in order for the correction process to occur. This characterization is accomplished by means of an aerosol retrieval. After a BRF is determined, it is fitted to a three parameter empirical BRF model, which provides a convenient representation of the surface scattering characteristics.

We statistically analyzed the differences of directional and hemispherical MISR reflectance data products, namely DHR versus BHR and BRF versus HDRF. These data products are compared to each other by their respective mean values, mean absolute and relative difference. Additionally, the correlation between

HDRF and BRF, and between BHR and DHR were derived. For further analysis of the products and their differences, the mean value of the absolute HDRF uncertainty and relative BHR uncertainty product was calculated, as well as the mean aerosol optical depth value in the green spectral band of all analyzed pixels.

The ratio of diffuse to direct illumination increases with increasing atmospheric optical depth. Therefore we expect the largest difference between HDRFs and BRFs in shorter wavelength ranges, wherein the blue band should show the largest difference. This wavelength dependence is due to the decreasing influences of Rayleigh scattering and aerosols with the increase in wavelength. For example, under at 1000 hP, Rayleigh scattering contributes 0.236, 0.094, 0.044, and 0.016 to the atmospheric optical depth in the blue, green, red, and near-infrared bands respectively.

We selected ten datasets, acquired in 2001 that correspond to MISR data product version 12 [Lewicki, 2003]. For all analyzed blocks, a comparison of MISR optical depths with those from an included ground based AERONET site showed good correlation in all four MISR spectral bands. Nevertheless, all surface parameters of data product version 12 do have the provisional status, i.e., a limited comparison with independent sources has been made and obvious artifacts fixed. The reliability of the land surface reflectance values depends upon the aerosol optical depth (AOD) magnitude. Therefore, pixels with a MISR optical depth greater than 0.5 at 558 nm (green spectral band) have been excluded from the MISR scenes. In the following, all quantities called 'scene-averaged' rely on this exclusion. Additionally, the two MISR data products, 'HDRF uncertainty averaged over all cameras' and the 'relative BHR uncertainty', were analyzed in parallel with the reflectance data. We assumed that these uncertainty products also apply to the BRF and DHR surface products, respectively (http://eosweb.larc.nasa.gov/PRODOCS/misr/Quality_Summaries/L2_AS_Products_20030125.html).

In addition to the AOD validation, the sites were selected to represent different biome types, following the MODIS IGBP land cover map. Three sites are covered twice, under different atmospheric conditions and sun zenith angles (see Table 5.3).

Site	Date 2001	SZ [°] AOD	IGBP Biome	
Howland, Maine, US	07/21	27.7 0.10	Mixed forest, deciduous broadleaf forest	
Railroad Valley, Nevada, US	08/17	28.4 0.99	Barren or sparsely vegetated	

Site	Date 2001	SZ [°] AOD	IGBP Biome	
Mongu, Zambia	07/11	44.6 0.05	Savannas, croplands	
Banizoumbou, Niger	10/04	24.1 0.31	Savannas	
	12/23	41.4 0.11		
Hombori, Mali	07/05	19.6 0.36	Savannas	
Avignon, France	07/12	25.2 0.07		
	08/29	36.9 0.19		
Bordeaux, France	05/30	24.5 0.24	Evergreen needleleaf forest, croplands, mixed forest	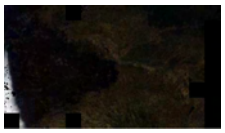
	07/01	24.0 0.12		

Table 5.3: Overview of MISR data selected for the analysis of the land surface products. SZ corresponds to the scene-averaged solar zenith angle, whereas AOD is the scene-averaged aerosol optical depth at 558 nm over all valid pixels. Images show the corresponding red-green-blue band composite of HDRF data acquired by the nadir looking camera (An) of the MISR sensor.

b) Results

Differences between BHR (Case 9) and DHR (Case 3)

In general, BHR and DHR product values derived from the MISR sensor are highly correlated (Figure 5.2), with r^2 values between 0.98 and 1.0 throughout all spectral bands and analyzed scenes (with the exception of the Hombori scene blue band, where r^2 reaches 0.84 only).

For all analyzed MISR images, the relative scene-averaged difference between BHR and DHR reaches a maximum of 2.7% of the BHR value (with the exception of the difference in the blue band of the Hombori scene reaching 5.1%) for all four spectral bands (Table 5.4). Numerically, this is a small difference, compared to the data uncertainties. The lowest scene-averaged relative BHR uncertainty is 5.6% for the NIR spectral band of the Avignon (07/12) scene, whereas relative BHR uncertainty can easily reach values around 20% and much higher, with a maximum of 88% for the blue spectral band of the Banizoumbou (10/04) scene. As DHR uncertainties are comparable to BHR uncertainties, it must be stated that the differences between BHR and DHR are very small compared to the actual product uncertainties

.

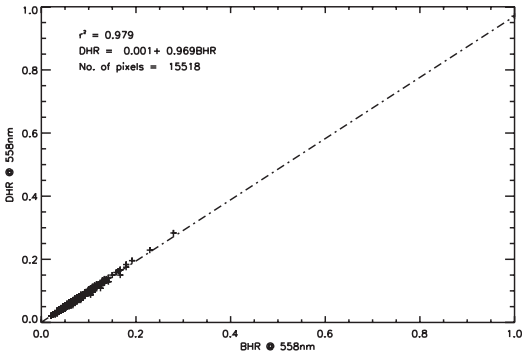

Figure 5.2: Relation between BHR and DHR exemplified by the green spectral band of the Howland scene.

As detailed above, we expect a trend of decreasing differences between BHR and DHR with increasing wavelength, thus the blue band reflectances should show the largest relative differences. Results show that the relative reflectance difference of five scenes is biggest in the blue band, whereas for the other 5 cases, differences reach the same or even higher values in at least one of the other bands.

Differences between the BHR and DHR product can be related to the actual aerosol optical depth in the green spectral band (Figure 5.3). This relation is weak for the BHR-DHR differences in the blue band ($r^2 = 0.29$) and gets much stronger with increasing wavelengths, with a maximum for the NIR region ($r^2 = 0.79$). It remains unclear, why increasing AOD values do not systematically lead to larger differences of the reflectance products in the blue spectral band. One explana-

tion for this unexpected result may be found in the biome specific directional properties, which are not accounted for in this analysis. Nevertheless, even the comparison between two images of the same site (and thus same biome type) reveals inconsistent results (Table 5.4). Whereas for the Banizoumbou scene reflectances, the relative difference between BHR and DHR are generally larger for the larger AOD, as expected, for Avignon, the scene with smaller AOD values shows larger differences of the reflectance products.

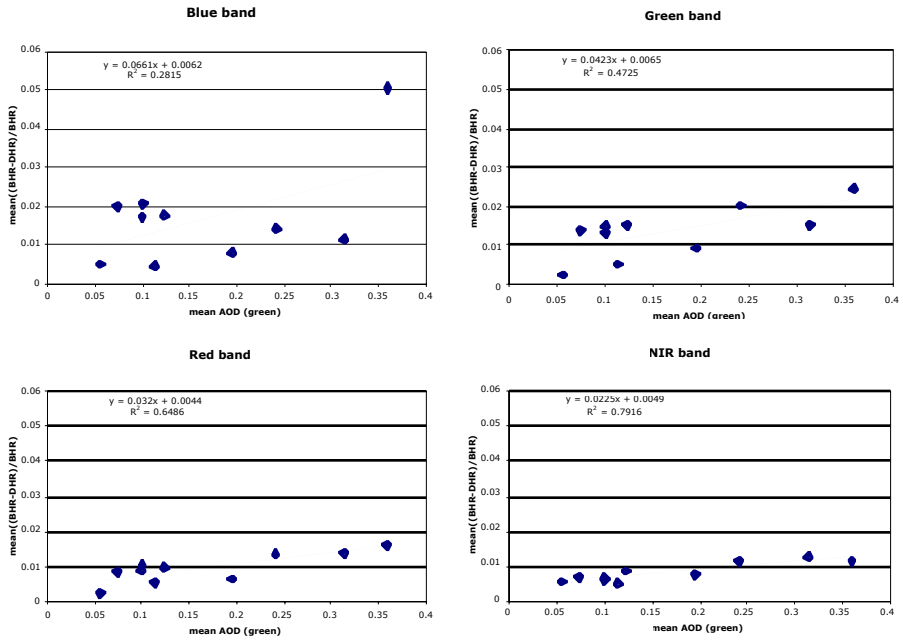

Figure 5.3: Relation of relative BHR-DHR differences in all four MISR spectral bands with mean aerosol optical depth in the green spectral band.

A high correlation of the relative BHR to DHR difference is found in the solar zenith angle (Figure 5.4). The bigger the solar zenith, the smaller are the differences between the two quantities. This correlation is again wavelength dependent, with an r^2 of 0.51, 0.88, 0.82, 0.51 for the blue, green, red and NIR band, respectively.

Site	SZ [°]	AOD	Mean BHR Mean ((BHR-DHR)/BHR) [%]			
			446 nm	558 nm	672 nm	867 nm
Howland	27.7	0.10	0.031 2.1	0.053 1.5	0.028 1.1	0.318 0.7
Railroad Valley	28.4	0.99	0.095 1.7	0.137 1.3	0.170 0.9	0.238 0.7
Mongu	44.6	0.05	0.046 0.5	0.078 0.3	0.094 0.3	0.246 0.6
Banizoumbou	24.1	0.31	0.060 1.2	0.126 1.5	0.176 1.4	0.357 1.3
	41.4	0.11	0.084 0.5	0.160 0.5	0.261 0.6	0.376 0.6
Hombori	19.6	0.36	0.108 5.1	0.232 2.5	0.349 1.6	0.412 1.2
Avignon	25.2	0.07	0.045 2.0	0.075 1.4	0.069 0.9	0.307 0.8
	36.9	0.19	0.050 0.9	0.081 0.9	0.079 0.7	0.286 0.8
Bordeaux	24.5	0.24	0.059 1.5	0.097 2.0	0.087 1.4	0.320 1.2
	24.0	0.12	0.048 1.8	0.078 1.5	0.073 1.0	0.304 0.9

Table 5.4: Comparison of BHR and DHR values for the selected MISR scenes. Aerosol optical depth at 558 nm, averaged over all analyzed pixels, are indicated, as well as BHR mean values and BHR to DHR differences, in relation to the BHR for all four spectral bands.

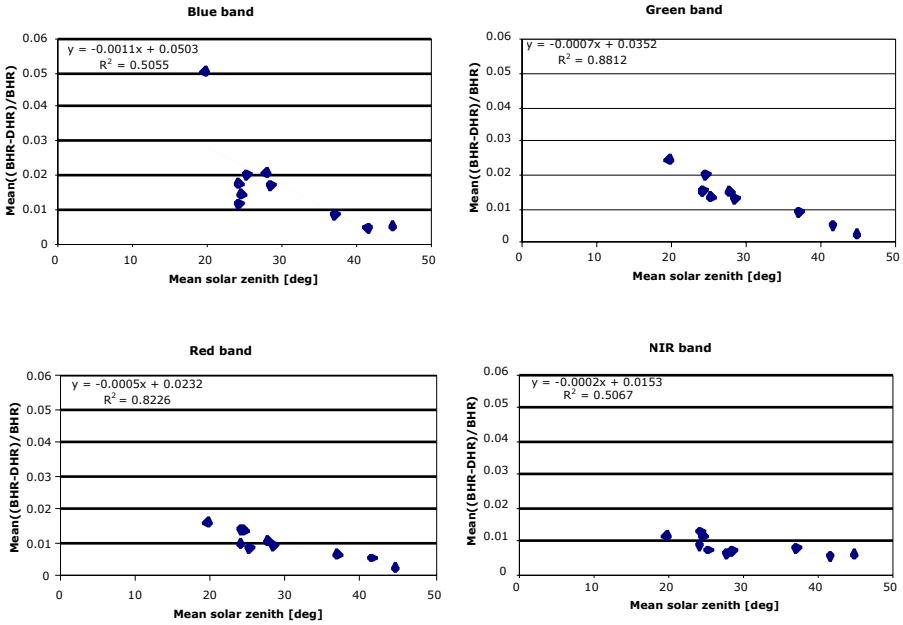

Figure 5.4: Relation of relative BHR-DHR differences in all four spectral bands with mean solar zenith angle.

Differences between HDRF (Case 7) and BRF (Case 1)

As with the results for the hemispherical reflectances, the relationship between HDRF and BRF values show a high correlation, with r^2 values above 0.98 (Figure 5.5) throughout all spectral bands and view angles of all scenes (with the exception of the Hombori scene blue band reaching an r^2 of 0.67 only).

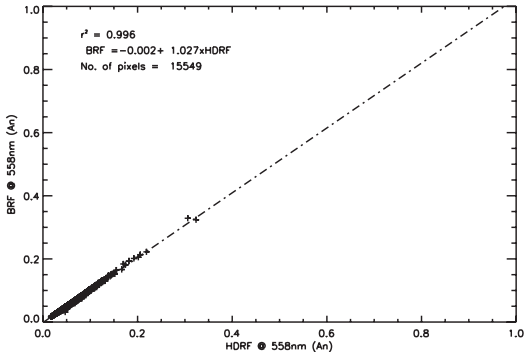

Figure 5.5: Relation between HDRF and BRF exemplified by the green spectral band of the nadir looking camera (An) of the Howland scene.

Compared to the quantities integrated over an extrapolation of the view hemisphere, the relative differences of the reflectances of the single view angles are larger and reach up to 10% of the HDRF value (with the exception of the Hombori scene blue band reflectance difference of 14.2%).

The trend of decreasing differences with increasing wavelength is much stronger for the directional quantities than for the hemispherically integrated quantities. Thus, the largest differences were found in the blue spectral band, with very few exeptions.

Comparing the relative HDRF-BRF differences with regard to the viewing direction, there is a clear trend of higher differences for the forward looking camera, with the exception of single bands for the A cameras (view zenith of 26.1°), where sometimes the differences for the afterward looking camera do exceed the differences of the forward looking camera.

Further, we investigated the relative differences of the HDRF-BRF values with regard to the nine cameras. For most scenes and spectral bands, the Ba camera (view zenith of 45.6°, afterward looking) shows the smallest differences between HDRF and BRF values. This indicates, that whenever the hemispherical irradiance component is neglected and HDRF data are equated with BRF data, the introduced uncertainties can be reduced by applying off-nadir data in the backward scattering direction, instead of nadir data.

Maximum relative HDRF-BRF differences can be related to high green spectral band AOD values. Averaging the relative difference over all spectral bands and cameras over a scene, a linear correlation with an r^2 of 0.27 can be found (Figure 5.6).

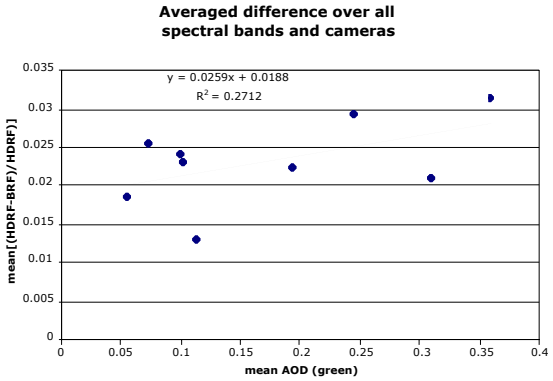

Figure 5.6: Correlation between mean aerosol optical depth in the green spectral band and the relative difference of the HDRF – BRF data to the HDRF, averaged over each scene, all spectral bands and cameras.

Comparing two scenes of the same site (thus for the same biome type), but with different mean aerosol optical depth values, the Banizoumbou and Bordeaux scenes with larger AOD show higher relative differences between HDRF and BRF data, except for some blue band data. This does not hold true for the Avignon site, where the scene corresponding to the smaller AOD generally shows larger relative differences of the reflectance products.

5.3.2 Vegetation canopy reflectance simulations using the RPV model

a) Methods and data

Using the PARABOLA instrument [Deering, 1986], black spruce forest HDRF data were observed at eight solar zenith angles (35.1°, 40.2°, 45.2°, 50.2°, 55.0°, 59.5°, 65.0°, 70.0°) [Deering, 1995]. After applying a simple HDRF to BRF atmospheric correction scheme [Tanre, 1983], data of the red band (650 to 670 nm wavelength range) were fitted to the parametric RPV model [Engelsen, 1996]. Resulting fit parameters and the RPV model are used to simulate different reflectance quantities of a black spruce canopy under various illumination conditions. The model was run for a solar zenith angel of 30° and increments of direct (d) and diffuse irradiance of d=1.0, d=0.6, d=0.4, d=0.2, d=0.0. These irradiance scenarios correspond to BRF and DHR for d=1.0, and HDRF and BHR for the rest, including the special case of white-sky HDRF (see Equation 5.13), i.e. purely diffuse irradiance (d=0.0).

b) Results

Figure 5.7 reports the HDRF of black spruce for a variety of direct-diffuse ratios, assuming the incident diffuse radiation is isotropic. The wavelength range is 650 to 670 nm. The direct illumination is from the left and was chosen to be at a zenith angle of 30°. As is expected for a vegetation canopy, there is a large amount of backscattering, and a hot spot at view zenith 30° due to the lack of shadowing. For d approaching 0, the anisotropy is smoothed and the hot spot becomes invisible.

The same data, reduced to the principal plane, are shown in Figure 5.8 (top). Again, the hot spot, clearly visible in the BRF, disappears for lower values of d.

Figure 5.8 (center) reports the DHR of black spruce as a function of the illumination zenith angle. As expected for vegetation, the DHR increases with increasing illumination zenith [Kimes, 1983]. For comparison, the white-sky BHR (although not a function of any angle) is also plotted. According to Equation 5.24, the actual albedo can be expressed as a combination of DHR and white-sky BHR if the diffuse incident radiation is assumed to be isotropic. The actual albedo for a given illumination zenith angle then lies on a vertical line between the DHR and white-sky BHR as shown in the graph for an example of 20° solar zenith.

Finally, Figure 5.8 (bottom) reports the BRF at nadir view as a function of the illumination zenith angle, along with the white-sky HDRF at nadir view (al-

though not a function of any illumination angle). According to Equation 5.13, the actual HDRF can be expressed as a combination of BRF and white-sky HDRF if the diffuse incident radiation is assumed to be isotropic. For any given illumination zenith, it then lies on a vertical line between the BRF and white-sky HDRF, as shown in the graph for an example of 20° solar zenith.

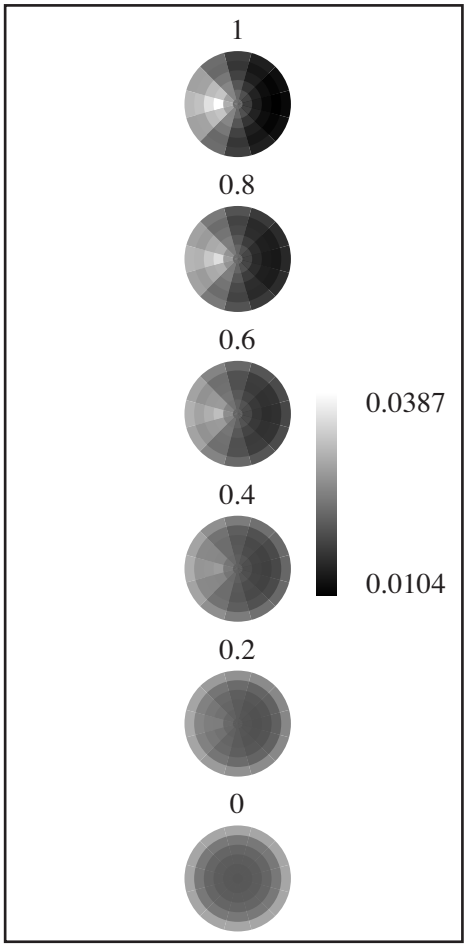

Figure 5.7: HDRF of a black spruce forest canopy at 650 to 670 nm as a function of the relative direct illumination (between 1 and 0). The direct illumination, at 30° zenith, is from the left. The top image corresponds to the BRF, while the bottom image corresponds to the white-sky HDRF.

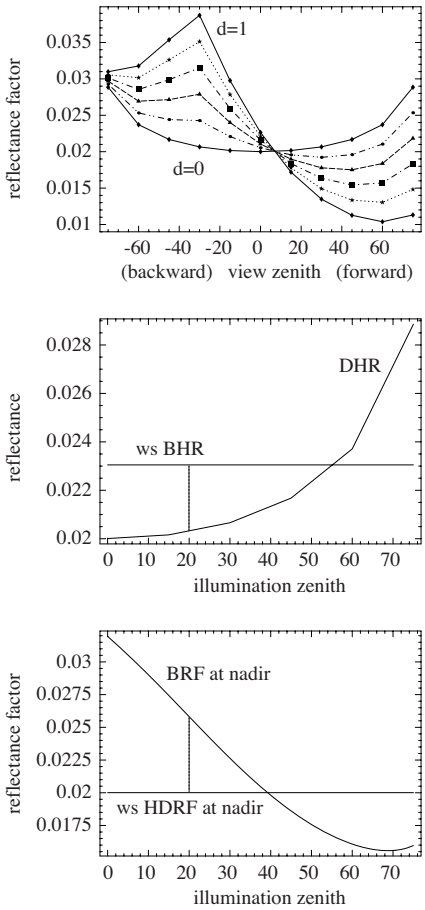

Figure 5.8: Simulated BRF (d=1.0) data for a black spruce canopy in the solar principal plane, and corresponding HDRF for varying direct to diffuse irradince conditions (d=0.8 to d=0.0) (top); DHR, and BHR for pure diffuse illumination as a reference (centre); BRF at nadir, and HDRF at nadir for pure diffuse illumination (bottom).

5.3.3 Snow reflectance simulations

a) Methods and data

This case study presents model results from a snow directional reflectance model. The model is the coupling of single-scattering parameters and a discrete-ordinates multiple scattering model. Single-scattering parameters were determined with a ray-tracing model for spheroidal particles [Macke, 1996] and the multiple scattering calculations were performed with the DISORT model [Stamnes, 1988].

The single-scattering parameters used in the model were the single-scattering albedo, extinction efficiency, and the single-scattering phase function. Model results shown here are for a spheroid of minimum and maximum radii of 208 μm and 520 μm, respectively. This spheroid has the same surface area to volume ratio (SVR) as a sphere of radius 250 μm. We then determined 20 Legendre moments of the single-scattering phase function for input to the multiple scattering model.

The multiple scattering model was run for a solar zenith angle of 30° and increments of direct and diffuse irradiance of d =1.0, d = 0.8, d = 0.6, d = 0.4, d = 0.2, and d = 0.0. These irradiance scenarios corresponded to BRF (d = 1.0) and HDRF for the rest. We ran a complete wavelength span of 0.4 to 2.5 μm at a spectral resolution of 0.01 μm.

b) Results

In Figure 5.9, we show the angular distributions of the irradiance scenarios for wavelength 0.55 μm.

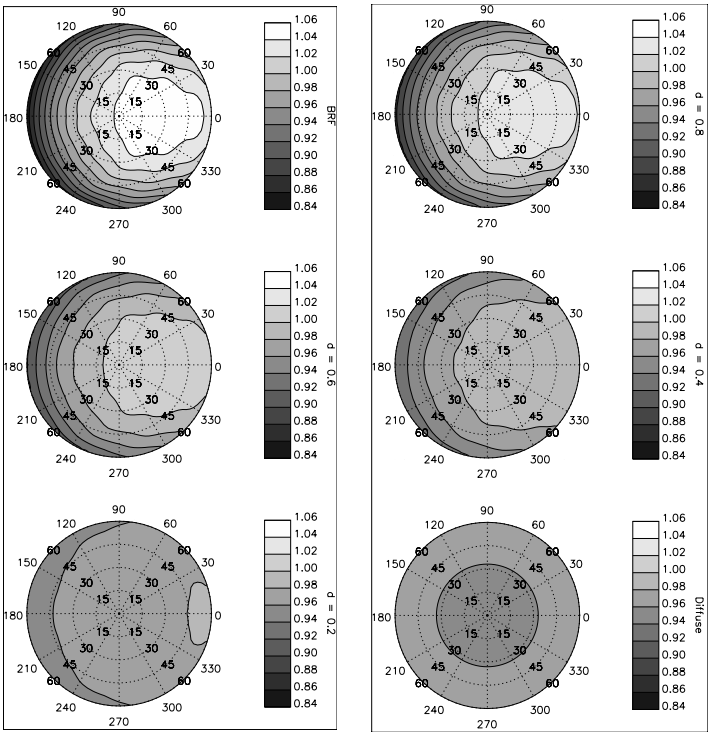

Figure 5.9: Angular distributions of reflectance for the range of irradiance cases at 0.55 μm and solar zenith angle = 30°. The target center represents the view geometry θ_r, ϕ_r= (0°, 0°), radial distance from center represents the view zenith angle, and the angle about the center represents the view azimuth angle. The forward reflectance direction is ϕ_r = 0°.

The models for d = 1.0 through d = 0.2 irradiance exhibit a forward reflectance distribution that decreases in magnitude with increasing diffuse component. For the totally diffuse irradiance scenario, the distribution has a shallow bowl shape. This minimum at nadir results from the angular intersection of the strong forward scattering phase function with the surface. Off-zenith irradiance has a greater chance than zenith irradiance of surviving multiple scatterings due to the orders of magnitude greater single scattering in the forward direction. In other words, zenith irradiance requires far more scattering events to produce reflected radiance than off-zenith. Therefore, the distribution will have greater reflectance at the larger view zenith angles. The principal plane for these scenarios is given in Figure 5.10 (top).

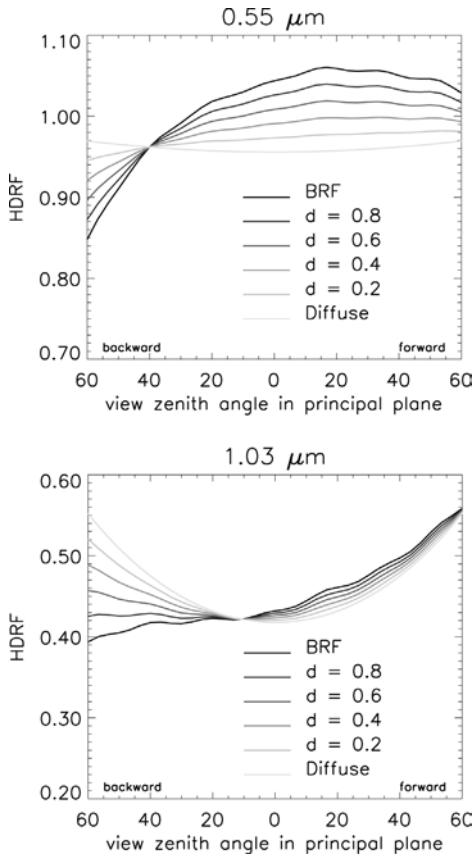

Figure 5.10: Directional reflectance in the principal plane for the range of irradiance scenarios at wavelengths 0.55 μm (top) and 1.03 μm (bottom).

The bowl-shaped distribution for diffuse irradiance becomes relatively deeper at longer wavelengths (Figure 5.10 (bottom)), such as 1.03 μm. We show the 1.03 μm model because this is the wavelength range in which snow reflectance is

most sensitive to grain size and thus is used in imaging spectroscopy models for inference of grain size and albedo [Nolin, 2000; Green, 2002]. The enhancement of the bowl shape at greater diffuse irradiance is explained as above coupled with a decrease in the single-scattering albedo at the longer wavelengths. This in turn is due to the increase in the imaginary part k of the complex refractive index at these wavelengths [Warren, 1982]. Only for the BRF and $d = 0.8$ irradiance cases is the distribution properly forward reflecting.

The spectral ratio of direct BRF to diffuse HDRF becomes increasingly anisotropic with increasing wavelength (Figure 5.11). In particular, a ratio peak becomes more prominent near $\theta_r = 30°$ in the forward reflectance direction as wavelength increases. In the side-reflected to backward azimuths for $\theta_r = 30°$, the ratio drops from ~1.0 at 0.55 μm to ~0.4 at 2.25 μm indicating a significant drop in reflectance in these angles for the direct beam case relative to the diffuse irradiance case. Moreover, the distribution changes from prominently convex about the forward direction at 0.55 μm to concave at 1.8 μm and longer.

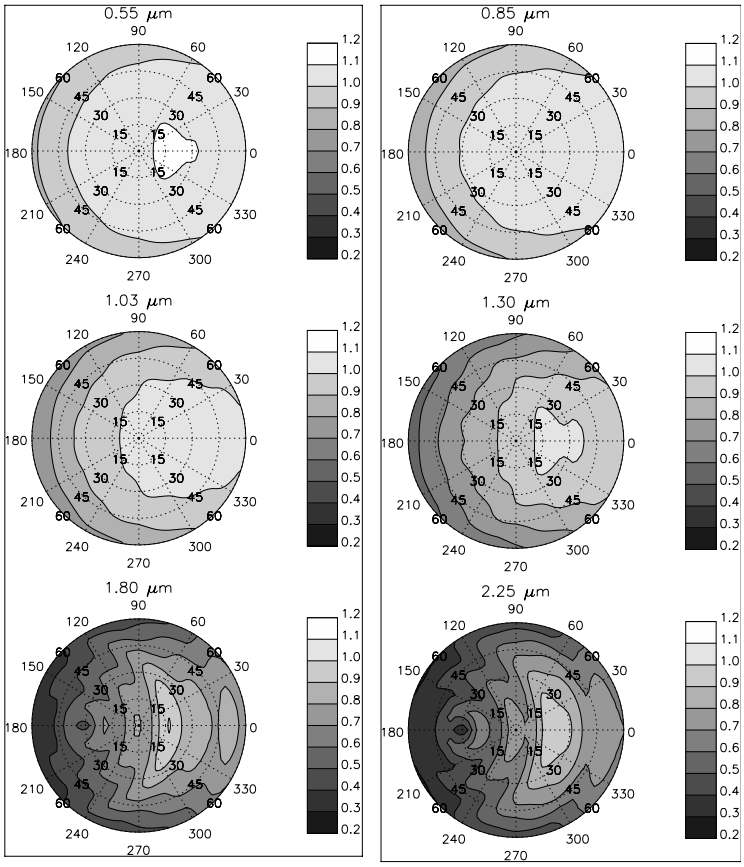

Figure 5.11: Angular distributions of the ratios between the direct and diffuse irradiance cases for various wavelengths.

The angularly integrated spectral albedo of snow under diffuse irradiance is approximately the same as under direct irradiance of $\theta_i \approx 45\text{-}50°$ being greater for $\theta_i > 45\text{-}50°$. Therefore, in this case of $\theta_0 = 30°$, the angularly integrated spectral albedo decreases as the proportion of diffuse irradiance increases (Figure 5.12).

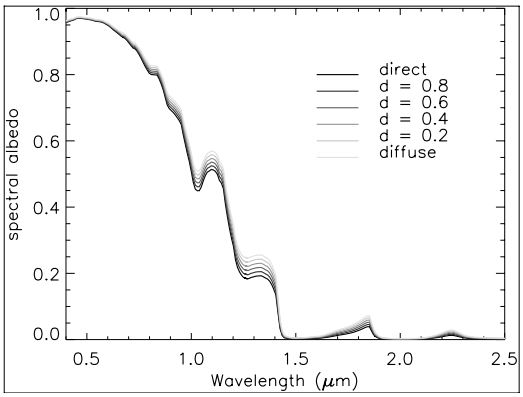

Figure 5.12: Spectral albedo for indicated irradiance scenarios.

Figure 5.13 shows DHR of snow relative to the illumination zenith angle at wavelengths 0.55 μm and 1.03 μm with the associated white-sky BHR included for reference. For both wavelengths, the DHR increases with increasing zenith angle but the increase is far greater in absolute and relative reflectance for the 1.03 μm case. The increase in both cases is due to the change in the angle of the intersection of the single scattering phase function with the surface. The single scattering phase function of ice particles in the forward angles is several orders of magnitude greater than in the rest of the scattering domain. Therefore, as the illumination zenith angle increases, the forward scattered photons have a higher probability of escaping the snowpack. This in turn increases the albedo of snow.

Because the single scattering albedo of ice particles (in this case a spheroid of radii 208 μm and 520 μm) is 0.9999817 at 0.55 μm versus 0.9930210 at 1.03 μm, multiply scattered photons are more likely to be absorbed at 1.03 μm. The greater increase in albedo at 1.03 μm results then from the increase in the contribution of singly scattered photons to albedo due to the increase in illumination zenith angle. At both wavelengths, the effective illumination zenith angle for the white-sky BHR is 49-50°, as discussed above.

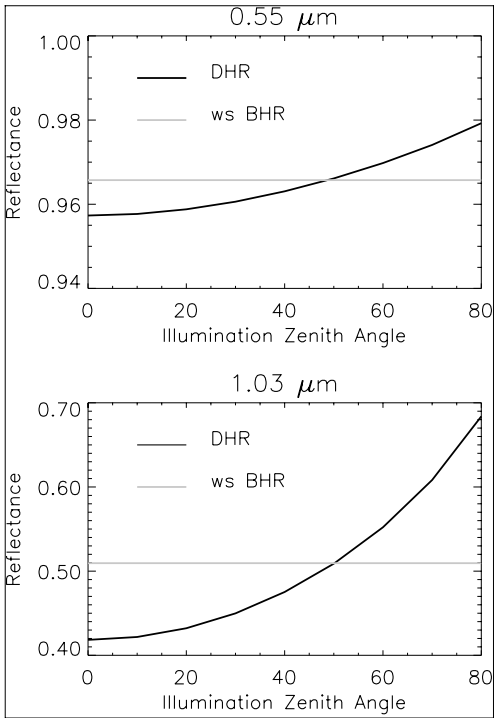

Figure 5.13: Directional-hemispherical reflectance versus illumination zenith angle for snow at wavelengths 0.55 μm and 1.03 μm. The bihemispherical reflectance for purely diffuse illumination is included for comparison.

5.3.4 Artificial panel reflectance simulations using a geometric-optical model

a) Methods and data

Here we consider the reflectance properties of an artificial target, which was initially used for a comparison of laboratory goniometric measurements with a radiative transfer model [Govaerts, 1997]. The design focused on large anisotropy, inertness and simplicity of construction. The artificial target consists of a matrix of cubes, carved out of a plate of duraluminium (Figure 5.14).

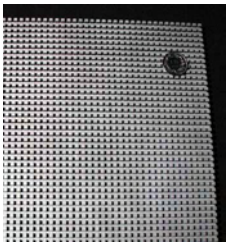

Figure 5.14: The artificial JRC reflection panel with sanded aluminum surface. The size of the cubes is 3.3 mm, the distance between the cubes 2 mm.

The sides of the cubes are 3.3 mm long, the distance between the cubes is 2 mm. All surfaces have been sanded to avoid specular reflection. The target can be seen as a simple model of a city with blocks and streets.

For the following calculations, we used a simple BRDF model of this artificial target, based on geometrical optics. For given view and illumination directions, the model calculates the sum of observed areas that are not shadowed. Only single scattering is considered. The surface itself was modeled using the parametric Modified Rahman-Pinty-Verstraete (MRPV) model [Engelsen, 1996] and the model parameters were fitted to target measurements collected using the Laboratory Goniometer System (LAGOS) [Dangel, 2003]. The wavelength for all calculations was chosen to be 496 nm. Note that the BRF of this artificial target is not rotational symmetric since an illumination/ view parallel to the streets clearly subtends a different collection of surfaces than e.g. an illumination / view at an azimuth of 45°. Whereas rotational symmetry is often assumed for natural targets and in many BRF models, the aluminum target provides an example for asymmetry. In the following, the illumination was chosen to be parallel to the streets.

b) Results

Figure 5.15 shows the HDRF of the JRC target at 496 nm for a variety of direct-diffuse ratios, assuming the incident diffuse radiation is isotropic. The direct illumination is from the left, parallel to the streets, and at a zenith angle of 30°. Unlike the case of vegetation, this target is mostly forward scattering. Note that due to the rotational asymmetry of the BRF, also the white-sky HDRF is rotational asymmetric. The target appears brighter if viewed parallel to the streets since, compared to off-parallel viewing, a large part of the streets remains visible even for large view zenith angles.

The same data, reduced to the principal plane, are shown in Figure 5.16 (top). The strong forward scattering, clearly visible in the BRF, disappears for lower values of d.

Figure 5.16 (centre) shows the DHR of the JRC target as a function of the illumination zenith angle. Unlike the cases of vegetation and snow, the DHR decreases with increasing illumination zenith angle. A simple explanation for this is that for increasing illumination zenith, more and more of the side areas of the cubes become shadowed by their neighbours. For comparison, the white-sky BHR (although not a function of any angle) is also plotted. According to Equation 5.24, the actual albedo can be expressed as a combination of DHR and white-sky BHR if the diffuse incident radiation is assumed to be isotropic. The actual albedo for a given illumination zenith angle then lies on a vertical line between the DHR and white-sky BHR as shown in the graph for an example of 20° solar zenith.

Finally, Figure 5.16 (bottom) reports the BRF at nadir view as a function of the illumination zenith angle, along with the white-sky HDRF at nadir view (although not a function of any illumination angle). Note the kink at about 31° in

the BRF. It is due to the fact that for illumination parallel to the streets, the sides of the cubes begin to become shadowed by their neighbours at illumination zenith arctan(distance/sides) = arctan(2 mm/3.3 mm) ≈ 31.22°.

According to Equation 5.13, the actual HDRF can be expressed as a combination of BRF and white-sky HDRF if the diffuse incident radiation is assumed to be isotropic. For any given illumination zenith, it then lies on a vertical line between the BRF and white-sky HDRF, as shown in the graph for an example of 20° solar zenith.

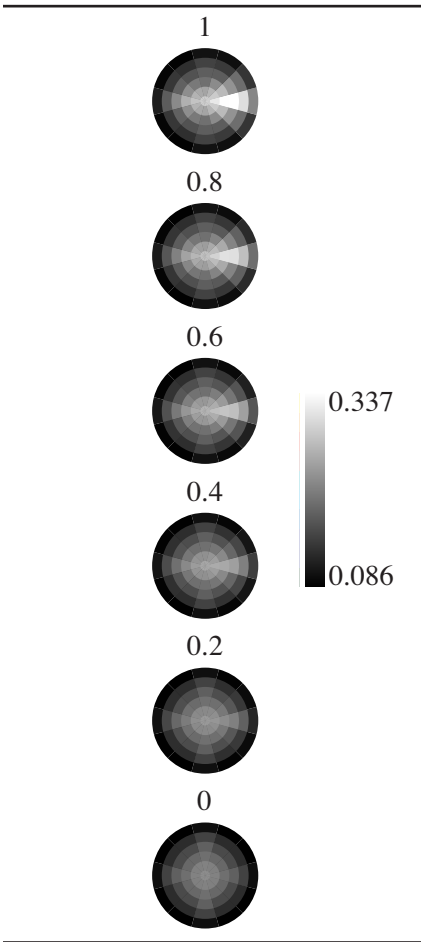

Figure 5.15: HDRF of the artificial JRC target as a function of the relative direct illumination (between 1 and 0, in steps of 0.2). The direct illumination, at 30° zenith, is from the left and parallel to the rows of cubes. The top image corresponds to the BRF. The bottom image corresponds to the white-sky HDRF, which is rotational asymmetric due to the rotational asymmetry of the BRDF.

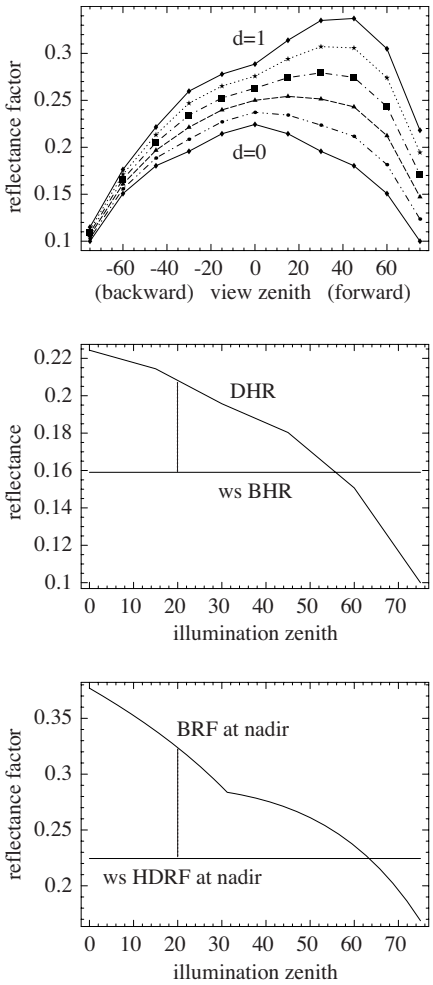

Figure 5.16: Simulated BRF (d = 1.0) data for the JRC panel in the solar principal plane, and corresponding HDRF for varying direct to diffuse irradiance conditions (d = 0.8 to d = 0.0) (top); DHR, and BHR for pure diffuse illumination as a reference (centre); BRF at nadir, and HDRF at nadir for pure diffuse illumination (bottom).

5.4 Discussion of case studies

If multiangular HDRF data are only collected under a single illumination angle, under the condition $d \neq 1$ (i.e., diffuse illumination is present, true for any field measurement), no information on the BRF can be derived without further assumptions or additional measurements. If we only have measured one view hemisphere (for a given value of d and solar zenith), no reasonable assumption can be made in which direction the HDRF would have to be corrected in order to better

approximate the BRF. This fact inherently stresses the fact that diurnal or even seasonal measurements of terrestrial targets must be aimed at, in order to minimize the interpolation uncertainties. Further on, if we can assume L_i^{diff} to be isotropic and have at least two measurements for different values of d (at the same solar zenith) at hand, we can use the differences between the HDRFs to derive the BRF according to Equation 5.13. However, such a setup of measurements is very impractical for obvious reasons.

The only practical solution is a full BRDF retrieval [Martonchik, 1994; Lyapustin, 1999] which requires the measurement of several hemispheres at different solar zenith angles and, in addition, the measurement of L_i^{diff}, the incoming diffuse radiation, as a function of the angles and wavelength.

5.5 Conclusions and outlook

All remotely sensed information - and therefore also the derived products - depends on the illumination and view geometry of the sensor, as well as on it's opening angle (FOV and IFOV). Different reflectance quantities have been defined to describe the corresponding conditions of the measurements. The basis for the proper use of these reflectance quantities is a standardized nomenclature, well known throughout the remote sensing community. This study summarizes the nomenclature articles of Nicodemus [1977] and Martonchik [2000], finally allowing for a unified access to the concept of spectrodirectional data treatment.

Further the importance of choosing an adequate reflectance product is demonstrated. All reflectance measurements performed under natural conditions include a diffuse fraction. Its amount is a function of the atmospheric conditions, the topography, the surroundings of the observed surface, and the wavelength. It thus introduces spectral effects to spectrometer data. The presented case studies are concentrating on the opening angle of the illumination, restricting it to directional irradiance only, or allowing for a diffuse irradiance component. The effect of varying direct to diffuse irradiance ratio is significant in modelled data, as well as in analysed MISR reflectance data.

As it is the nature of the BRDF to be dependent on many factors (e.g., Schoenermark, 2004), the quantification of directional effects of the illumination and view angle on the reflectance always remains exemplary, be it in the case of real or simulated data.

This paper is addressing different remote sensing communities. It shows that the use of any remote sensing data has to include the analysis of the corresponding illumination and view geometry, as well as the FOV, as a prerequisite for further analysis with quantifiable accuracy. State of the art models today allow users to account for the anisotropy of the target and the illumination conditions. This will further reduce unexpected results and significantly reduce uncertainties. Some satellite products (e.g., MODIS, MISR) already account for the above issues.

Nevertheless it remains a significant task of the users to identify and choose an adequate product, possibly guided a common reflectance nomenclature and a quality indication by the product's provider.

We shall motivate the spectro-directional data users to take this reflectance nomenclature into account and use the presented common basis in the evaluation of product quality and consistency.

5.6 Acknowledgement

This work was supported by the Swiss National Science Foundation, under contract 200020-101517. The authors would like to thank Brian Hosgood of the EC Joint Research Centre, Ispra, Italy, for lending the duraluminum target for measurements using the LAGOS goniometric facilities at the Remote Sensing Laboratories, Univ. Zurich, Switzerland. The MISR data were obtained from the NASA Langley Research Center Atmospheric Sciences Data Center.

5.7 References

Asrar, G., and R. Myneni, Atmospheric Effects in the Remote Sensing of Surface Albedo and Radiation Absorption by Vegetation Canopies, Remote Sensing Reviews, 7, 197-222, 1993.

Barnsley, M.J., P.D. Hobson, A.H. Hyman, W. Lucht, J.P. Muller, and A.H. Strahler, Characterizing the spatial variability of broadband albedo in a semidesert environment for MODIS validation, Remote Sensing of Environment, 74 (1), 58-68, 2000.

Breuer, L., K. Eckhardt, and H.G. Frede, Plant parameter values for models in temperate climates, Ecological Modelling, 169 (2-3), 237-293, 2003.

Dangel, S., M. Kneubühler, R. Kohler, M. Schaepman, J. Schopfer, G. Schaepman-Strub, and K. Itten, Combined Field and Laboratory Goniometer System – FIGOS and LAGOS, in IGARSS, Toulouse, France, 2003.

Deering, D.W., S.P. Ahmad, T.F. Eck, and B.P. Banerjee, Temporal Attributes of the Bidirectional Reflectance for three Boreal forest canopies, in IGARSS, pp. 1239-1241, Florence, Italy, 1995.

Deering, D.W., and T.F. Eck, Atmospheric Optical Depth Effects on Angular Anisotropy of Plant Canopy Reflectance, International Journal of Remote Sensing, 8 (6), 893-916, 1987.

Deering, D.W., and P. Leone, A Sphere-Scanning Radiometer for Rapid Directional Measurements of Sky and Ground Radiance, Remote Sensing of Environment, 19 (1), 1-24, 1986.

Di Girolamo, L., Generalizing the definition of the bi-directional reflectance distribution function, Remote Sensing of Environment, 88 (4), 479-482, 2003.

Diner, D.J., J.V. Martonchik, C. Borel, S.A.W. Gerstl, H.R. Gordon, Y. Knyazikhin, R. Myneni, B. Pinty, and M. Verstraete, Multi-angle Imaging Spectro-Radiometer Level 2 Surface Retrieval Algorithm Theoretical Basis, JPL D-11401, Rev. D, December 2, 1999, JPL, (http://www-misr.jpl.nasa.gov), Jet Propulsion Laboratory, California Institute of Technology, 1999.

Dozier, J., A Clear-Sky Spectral Solar-Radiation Model for Snow-Covered Mountainous Terrain, Water Resources Research, 16 (4), 709-718, 1980.

Engelsen, O., B. Pinty, M. Verstraete, and J.V. Martonchik, Parametric bidirectional reflectance factor models: evaluation, improvements and applications, pp. 114, EC Joint Research Centre, Ispra, Italy, 1996.

Govaerts, Y., M. Verstraete, and B. Hosgood, Evaluation of a 3-D Radiative Transfer Model Against Goniometer Measurements on an Artificial Target, International Journal of Remote Sensing, 1, 131-136, 1997.

Green, R.O., J. Dozier, D. Roberts, and T. Painter, Spectral snow-reflectance models for grain-size and liquid-water fraction in melting snow for the solar-reflected spectrum, Annals of Glaciology, Vol 34, 2002, 34, 71-73, 2002.

Kimes, D.S., Dynamics of Directional Reflectance Factor Distributions for Vegetation Canopies, Applied Optics, 22 (9), 1364-1372, 1983.

Kimes, D.S., and D.W. Deering, Remote-Sensing of Surface Hemispherical Reflectance (Albedo) Using Pointable Multispectral Imaging Spectroradiometers, Remote Sensing of Environment, 39 (2), 85-94, 1992.

Kimes, D.S., P.J. Sellers, and D.J. Diner, Extraction of Spectral Hemispherical Reflectance (Albedo) of Surfaces from Nadir and Directional Reflectance Data, International Journal of Remote Sensing, 8 (12), 1727-1746, 1987.

Kipp and Zonen, Instruction Manual CM11 Pyranometer/ CM14 Albedometer, pp. 65, Kipp and Zonen, Delft, The Netherlands, 2000.

Koechler, C., B. Hosgood, G. Andreoli, G. Schmuck, J. Verdebout, A. Pegoraro, J. Hill, W. Mehl, D. Roberts, and M. Smith, The European optical goniometeric facility: technical description and first experiments on spectral unmixing, in IGARRSS'94, pp. 2375-2377, Pasadena, USA, 1994.

Kriebel, K.T., On the Variability of the Reflected Radiation Field Due to Differing Distributions of the Irradiation, Remote Sensing of Environment, 4, 257-264, 1976.

Lewicki, S., C. Moroney, K. Crean, S. Gluck, K. Miller, M. Smyth, and S. Paradise, MISR Data Products Specifications -- Incorporating the Science Data Processing Interface Control Document, aka the MISR DPS, JPL D-13963, Revision I, July, 2003. (http://eosweb.larc.nasa.gov/PRODOCS/misr/Version/pge9.html), 2003.

Lewis, P., and M.J. Barnsley, Influence of the sky radiance distribution on various formulations of the earth surface albedo, in 6th International Symposium on Physical Measurements and Signatures in Remote Sensing, ISPRS, pp. 707-715, Val d'Isere, France, 1994.

Liu, C.H., A.J. Chen, and G.R. Liu, Variability of the Bare Soil Albedo Due to Different Solar Zenith Angles and Atmospheric Haziness, International Journal of Remote Sensing, 15 (13), 2531-2542, 1994.

Lucht, W., A.H. Hyman, A.H. Strahler, M.J. Barnsley, P. Hobson, and J.P. Muller, A comparison of satellite-derived spectral albedos to ground-based broadband albedo measurements modeled to satellite spatial scale for a semidesert landscape, Remote Sensing of Environment, 74 (1), 85-98, 2000.

Lyapustin, A.I., and J.L. Privette, A new method of retrieving surface bidirectional reflectance from ground measurements: Atmospheric sensitivity study, Journal of Geophysical Research-Atmospheres, 104 (D6), 6257-6268, 1999.

Macke, A., and M.I. Mishchenko, Applicability of regular particle shapes in light scattering calculations for atmospheric ice particles, Applied Optics, 35 (21), 4291-4296, 1996.

Martonchik, J.V., Retrieval of Surface Directional Reflectance Properties Using Ground-Level Multiangle Measurements, Remote Sensing of Environment, 50 (3), 303-316, 1994.

Martonchik, J.V., C.J. Bruegge, and A. Strahler, A review of reflectance nomenclature used in remote sensing, Remote Sensing Reviews, 19, 9-20, 2000.

Martonchik, J.V., D.J. Diner, B. Pinty, M.M. Verstraete, R.B. Myneni, Y. Knyazikhin, and H.R. Gordon, Determination of land and ocean reflective, radiative, and biophysical properties using multiangle imaging, Ieee Transactions on Geoscience and Remote Sensing, 36 (4), 1266-1281, 1998.

Middleton, E.M., Quantifying Reflectance Anisotropy of Photosynthetically Active Radiation in Grasslands, Journal of Geophysical Research-Atmospheres, 97 (D17), 18935-18946, 1992.

Nicodemus, F.E., Directional Reflectance and Emissivity of an Opaque Surface, Applied Optics, 4 (7), 767-&, 1965.

Nicodemus, F.E., J.C. Richmond, J.J. Hsia, I.W. Ginsberg, and T. Limperis, Geometrical Considerations and Nomenclature for Reflectance, National Bureau of Standards, US Department of Commerce, Washington, D.C., 1977.

Nolin, A.W., and J. Dozier, A hyperspectral method for remotely sensing the grain size of snow, Remote Sensing of Environment, 74 (2), 207-216, 2000.

Painter, T.H., and J. Dozier, Measurements of the hemispherical-directional reflectance of snow at fine spectral and angular resolution, Journal of Geophysical Research-Atmospheres, 2004, in press.

Ranson, K.J., L.L. Biehl, and M.E. Bauer, Variation in spectral response of soybeans with respect to illumination, view and canopy geometry, International Journal of Remote Sensing, 6, 1827-1842, 1985.

Russell, C.A., J.R. Irons, and P.W. Dabney, Bidirectional reflectance of selected BOREAS sites from multiangle airborne data, Journal of Geophysical Research-Atmospheres, 102 (D24), 29505-29516, 1997a.

Russell, M.J., M. Nunez, M.A. Chladil, J.A. Valiente, and E. LopezBaeza, Conversion of nadir, narrowband reflectance in red and near-infrared channels to hemispherical surface albedo, Remote Sensing of Environment, 61 (1), 16-23, 1997b.

Sandmeier, S., and D.W. Deering, Structure analysis and classification of boreal forests using airborne hyperspectral BRDF data from ASAS, Remote Sensing of Environment, 69 (3), 281-295, 1999.

Schoenermark, M., B. Geiger, and H.P. Roeser (eds.), Reflection Properties of Vegetation and Soil, Wissenschaft und Technik Verlag, Berlin, 2004.

Sellers, P.J., B.W. Meeson, F.G. Hall, G. Asrar, R.E. Murphy, R.A. Schiffer, F.P. Bretherton, R.E. Dickinson, R.G. Ellingson, C.B. Field, K.F. Huemmrich, C.O. Justice, J.M. Melack, N.T. Roulet, D.S. Schimel, and P.D. Try, Remote-Sensing of the Land-Surface for Studies of Global Change - Models, Algorithms, Experiments, Remote Sensing of Environment, 51 (1), 3-26, 1995.

Snyder, W.C., Definition and invariance properties of structured surface BRDF, Ieee Transactions on Geoscience and Remote Sensing, 40 (5), 1032-1037, 2002.

Stamnes, K., S.C. Tsay, W. Wiscombe, and K. Jayaweera, Numerically Stable Algorithm for Discrete-Ordinate-Method Radiative-Transfer in Multiple-Scattering and Emitting Layered Media, Applied Optics, 27 (12), 2502-2509, 1988.

Strub, G., M.E. Schaepman, Y. Knyazikhin, and K.I. Itten, Evaluation of spectrodirectional Alfalfa canopy data acquired during DAISEX '99, Ieee Transactions on Geoscience and Remote Sensing, 41 (5), 1034-1042, 2003.

Tanre, D., M. Herman, and P.Y. Deschamps, Influence of the Atmosphere on Space Measurements of Directional Properties, Applied Optics, 22 (5), 733-741, 1983.

Vermote, E.F., and A. Vermeulen, Atmospheric correction algorithm: Spectral reflectances (MOD09), MODIS ATBD, pp. 107, University of Maryland, Dept. of Geography, 1999.

Warren, S.G., Optical-Properties of Snow, Reviews of Geophysics, 20 (1), 67-89, 1982.

Zhou, L., R.E. Dickinson, Y. Tian, X. Zeng, Y. Dai, Z.L. Yang, C.B. Schaaf, F. Gao, Y. Jin, A. Strahler, R.B. Myneni, H. Yu, W. Wu, and M. Shaikh, Comparison of seasonal and spatial variations of albedos from Moderate-Resolution Imaging Spectroradiometer (MODIS) and Common Land Model, Journal of Geophysical Research-Atmospheres, 108 (D15), -, 2003.

Chapter 6

Spectrodirectional Reflectance Analysis and Definition for the Estimation of Vegetation Variables - a Synthesis

6.1 Introduction

The estimation of vegetation variables using spectroscopy and multiangular remote sensing data will further be advanced by recent and upcoming sensor systems. As currently the availability of spectrodirectional data is still limited by the design of existing sensors and data transmission requirements, studies on the estimation of vegetation variables focus mainly on spectroscopy or multiangular analysis, whereas combined approaches are still rare.

Chapter 1 to 5 of this thesis have outlined different aspects of spectrodirectional reflectance data. The analysis and quantification of the variations of observed and modelled quantities at the reflectance level substantiate the initial research questions, which are recalled in the following:

- What is the range of uncertainty in the analysis of measured and modelled spectrodirectional reflectance data introduced by neglecting sun and view angle effects, at the reflectance level?
- What spectral effects are present in measured and simulated spectrodirectional reflectance data?
- What is the range of uncertainty in the analysis of reflectance data introduced by improper usage of existing reflectance nomenclature, at the reflectance level?
- Can a common terminology of reflectance be derived to minimize these uncertainties in the future?

The following section presents answers to the above questions and a synthesis of the results.

6.2 Variation of spectrodirectional reflectance

A typical range of variation in diurnal spectrodirectional reflectance data has been assessed in this thesis to quantify uncertainties in reflectance data when view and illumination angle effects are neglected. It is important to assign these uncertainties to reflectance data, because they are further propagated into the estimation of vegetation variables.

The goniometer experiments performed on soil and Alfalfa (as described in Chapter 2, and analyzed in Chapter 3 and 4) show typical ranges of variation in terms of sun angles, as field measurements are often performed throughout the day. The variation caused by different view angles highlights a potential additional information content introduced by off-nadir looking sensors (Berger, 2001, Strub, 2002).

The total variation of the reflectance data throughout a day is not only limited to the effect of the Sun and view zenith and azimuth angle changes, but includes as well changes of the atmospheric composition and the vegetation status. The overall variation of measured HDRF data for the whole viewing sphere throughout the day reaches a maximum of 25% of the mean HDRF in the visible wavelength range, and a minimum variation in the NIR spectral range of about 10% (Strub, 2003).

The variation of nadir-looking HDRF data only, acquired throughout the day, and corresponding simulated data were analysed as well. The results show also significant errors introduced, when nadir measurements during field campaigns are performed without taking into account the changes of the solar angle and atmospheric composition.

Nadir HDRF measurements throughout the day, deviate up to 40% of the solar noon nadir HDRF in the visible domain. Corresponding modelled nadir data show a smaller, but still significant deviation of 20%.

Albedo values resulting from the radiative transfer model do not reflect diurnal variations as observed in measured field data (Strub, 2003). Thus it is essential that field measurements are performed at the exact time they are needed (e.g., in calibration experiments), rather than simulated or extrapolated from data acquired under a different sun angle constellation.

6.3 Spectral effects in directional reflectance data

Spectral effects in the radiance reflected by vegetation canopies are the function of a coupled soil-vegetation-atmosphere radiative transfer, dominated by the reflectance, transmittance, and absorptance of leaves and other elements of the canopy, in a multiple scattering environment.

Thus, measurements performed throughout a day are not only subject to changing sun angles, but also depend on the variation of the aerosol optical depth throughout the day. It is often assumed that the division of the target reflected radiance by the Spectralon reflected radiance is eliminating the influence of the atmospheric effects in field measurements. Never the less, the absorption in vegetation canopies is not a linear process with respect to the wavelength, whereas for the Spectralon panel this is approximately true. As the amount of diffuse and direct irradiance changes throughout the day and thus influences the spectral character of the incoming radiance, the division of the vegetation reflected radiance by the one reflected by the Spectralon panel only corrects for the total amount of incoming radiance. Thus, the effects of changing irradiance are propagated wavelength specifically into the reflectance factors of the observed canopies. Therefore it is difficult to separate the effects of changes of the sun angle and the atmosphere represented in hemispherical-directional reflectance factors (for a constant view angle), as they are acquired during field campaigns.

The WDVI, a vegetation index commonly used for the estimation of the leaf area, was derived from nadir measurements throughout a day and proved to differ significantly, resulting in a variation of the LAI that is actually constant within this short time. Thus it is recommended to use vegetation variable estimation methods based on indices with caution (Strub, 2002).

Further on, spectral effects present in canopy anisotropy are even more pronounced in field measured data and show features not represented in modelling results at all. We can conclude that radiative transfer models cannot fully explain - and thus substitute - observed canopy directional reflectances. Therefore, regular and frequent observations are needed for calibration and validation experiments as well as for the generation of a priori BRDF knowledge databases. The dense Alfalfa canopy used in this thesis is a very homogeneous canopy compared to other crops or ecosystem types. Thus, it can be expected that much higher variations of the HDRF data measured over heterogeneous canopies are seen.

6.4 Importance of consistent use of reflectance nomenclature

As it has been shown in Chapters 3, 4 and 5, spectrodirectional reflectance data show high variations, partly caused by the sun and view angle, but also by the amount and distribution of the diffuse irradiance. Many directional field measurements performed in the framework of international campaigns do exist. Unfortunately there is a lack of consistency not only in applied field instruments, but especially in the data acquisition and preprocessing. A recent example of misunderstanding the importance of reflectance quantities is a collection of so called albedo values, recommended as reference parameters for models in temperate climate (Breuer, 2003). These data collected from very different sources range from leaf albedo to nadir observations of canopies and thus should not be used without

further consulting the original reference, even though the species-specific values are tempting.

The desirable quantity for the estimation of structural and biochemical vegetation variables is the bidirectional reflectance factor. Nevertheless, all outdoor measurements are influenced by the atmospheric composition. Further, it is of major importance to know the actual irradiance conditions for the calculation of energy fluxes between the atmosphere and the biosphere. Therefore, all reflectance quantities are relevant, but have to be named and applied appropriately. Numerically, these quantities may differ only slightly from each other, as has been shown in this thesis through the analysis of MISR data products, but the differences reach or exceed data uncertainties. In the framework of this thesis, these differences have been quantified the first time for MISR reflectance products of single scenes (Schaepman-Strub, 2004, in print; Schaepman-Strub, 2004, in preparation). The high sensitivity of climate models to the albedo input, sometimes requesting an uncertainty as low as 2% (Sellers, 1995), indicates the need for a clear discrimination of different albedo quantities and corresponding satellite remote sensing products.

This demonstrates, that an adequate use of the existing reflectance nomenclature is not only a theoretical exercise, but is a prerequisite for the reliable estimation of vegetation variables, and investigations of other surfaces, such as snow. It further will be helping to set the baseline for future spectrodirectional field measurements and research.

Consequently, a consistent reflectance nomenclature throughout the remote sensing community ensures higher data quality standards, allows the intercomparison of results of various studies and products, and increases the awareness of the user of a potential problem.

6.5 Conclusion

While many studies on the estimation of vegetation variables discuss the performance of inversion methodologies on resulting product quality, this thesis emphasizes on the variations at the reflectance level. These are primarily caused by the changing sun and view direction, as well as the definition of the reflectance quantity itself (Schaepman-Strub, 2004, in preparation). As long as the variations are neglected, they are introduced as uncertainties in the process of vegetation variable estimation.

This thesis for the first time shows the comparison of extensive diurnal spectrodirectional field measurements of an Alfalfa canopy, with corresponding modelling results. Further, an in-depth analysis of spectrodirectional effects of these data was performed. This allows for an uncertainty assessment of the reflectance data with respect to the wavelength, when the illumination and viewing geometry are neglected. After having recognized the importance of the diffuse component

of the irradiance for the measured reflectance, with respect to direct illumination only, this effect was extensively quantified on MISR data products. In the framework of this thesis, the comparison of different MISR reflectance data products was published for the first time (Schaepman-Strub, 2004, in print).

Several studies specified the benefit of continuous, narrowband spectrometer data and multiangular data for the characterisation of the atmosphere and the vegetation (e.g., Barnsley, 1997; Bicheron, 1997; Gobron, 2002; White, 2002; Zhang, 2002; ESA, 2004). Some of them emphasize the optimal combination of spectral bands and observation angles for the estimation of selected variables (e.g., Weiss, 2000). Driven by the planned application and a given variable it is therefore possible to define the optimal configuration of spectral bands (Schlapfer, 2002), view and sun angles. The estimation of e.g. vegetation variables is a problem including different aspects of the coupled soil-vegetation-atmosphere radiative transfer. It is therefore based on different subsets of the spectrodirectional data space at the pixel level, due to the heterogeneity given by each pixel. Therefore it is suggested to include all available information, but assign and reduce data uncertainties, and include them in the analysis. For future remote sensing systems, majour emphasize should be put on the characterization of the atmosphere. Uncertainties in the characterization of the atmosphere lead to high uncertainties of the derived reflectance products in the blue and green spectral band. Even though a full retrieval of the atmospheric properties is performed for MISR spaceborne data, uncertainties assigned to the reflectance products in the blue and green spectral band are so large, that the LAI retrieval algorithm was limited to the red and NIR spectral bands (Hu, 2003). Thus, all the factors and their weights influencing the radiometric signal of the vegetation canopy, as specified in Chapter 1.2, determine the optimal set of view and illumination angles for the most accurate estimation of a given variable. This thesis does not define an optimal spectral and angular configuration of measurements for a given application, but is more generally quantifying variations of several measured and modelled reflectance products, with respect to the wavelength. It therefore gives an estimate on uncertainties at the reflectance level, as it is summarized in the following.

It was shown, that on the side of measurements, neglectance of sun and view angles, as well as the fuzzy use of reflectance definition have a majour influence on the observed reflectance quantity. On the other hand it was demonstrated, that measured and forward modelled hemispherical-directional reflectance factor data did not describe the same spectrodirectional space. This implies high uncertainties introduced in the inversion of vegetation models, which cannot fully be assigned to measurement errors.

The estimation of vegetation variables using measured spectrodirectional reflectance data needs a better understanding of the observed quantity, and an improved interface of vegetation models to account for the spectral variation of measured reflectance quantities. As it has been shown, the introduction of the direct to diffuse ratio of the irradiance did not fully account for the observed wave-

length dependent effects, even though state of the art measurement equipment and modelling was used. Therefore, a combination of leaf, soil and atmospheric optical properties has to be investigated.

The true combination of spectral and directional reflectance information of vegetation canopies in variable estimation still is very sobering. Thus there is a need for high quality data in both, the spectral and directional dimension. Vegetation studies often neglect phenological aspects. In agricultural as well as climate research applications, phenological processes are of great importance. Thus it will be necessary to integrate this aspect in the planning of spectrodirectional observations. This is a strong argument for the continuation of outdoor measurements, despite all advantages laboratory observations might have.

The thesis clearly highlights the challenges when BRDF a priori knowledge databases shall be generated from HDRF measurements. The acquisition of HDRF data, reflecting actual atmospheric conditions, is recommended for infield calibration and validation experiments of multiangular air- and spaceborne sensor data. In addition to the directional measurements covering the full ground sphere, it is suggested to observe the corresponding sky sphere as well, determining the angular diffuse and direct irradiance component. This is a prerequisite for the retrieval of BRFs and a reliable BRDF. Any modelling approach for the derivation of the BRDF, based on HDRF data without atmospheric correction for the incoming diffuse component, is influenced by the actual atmospheric conditions and does lead to a distortion of the resulting function. Thus it is recommended to characterize the physical and chemical surface, as well as atmospheric properties for a joint storage with reflectance characteristics in the database (Bojinski, 2003; 2004). For any measurement, the solid angle of the irradiance and reflected radiance has to be included, to reduce uncertainties and misunderstandings. This will enable the users to employ radiative transfer models in forward and inverse mode for the analysis of spectrodirectional reflectance data.

Apart from the conception of BRDF a priori knowledge databases it is of major importance to proceed with investigations in spectrodirectional reflectance data. Spectral features in observed canopy directional reflectance data have to be investigated with regard to existing radiative transfer models, to enhance their inversion. Research on spectrodirectional canopy data is not only needed for the estimation of the vegetation structure, but is important for the analysis of angular effects influencing biochemical variable mapping from spectral data and for the reliable correction of undesired angular effects in imaging spectrometer data, without manipulating the spectral information. In further analysis of measured spectrodirectional data it is of major importance to correct for atmospheric effects and thus separate spectral effects introduced by atmospheric conditions from contributions by the soil and leaf optical properties.

It is obvious, that all performed work has to take directional effects into account, by using one out of three main strategies: (1) Evaluate the effect of view and sun

angle on the data - which may lead to the conclusion that it can or has to be neglected in certain cases, (2) correct for the directional effects to reduce uncertainties of the results, or (3) include the available directional information in further analysis. The prerequisite for the third strategy is an adequate atmospheric correction of reflectance data acquired under ambient sky conditions to reduce spectral effects in multiangular vegetation data which are introduced by the atmosphere.

As of today, the true combination of spectral and directional information for the estimation of vegetation variables is still primarily fundamental research driven, rather than available in operational environments.

6.6 Outlook

The estimation of vegetation variables for applications in climate change, agricultural, landscape as well as ecosystem research is directing towards a more integrated approach applying combined ecological and radiative transfer models. For the scaling of the corresponding radiative transfer models and their validation it is important to adapt data acquisition schemes. Thus not only canopy reflectances have to be observed for the infield calibration of air- or spaceborne sensors data, but quantities such as the canopy transmittance, reflectance of the soil and understory, and leaf optical properties have to be measured as well. Instead of only validating the final variables at the local/regional scale, comparative validation tests can be performed, analysing radiative transfer modelled quantities with respect to radiometric measurements (i.e., reflectance, transmittance) at the leaf as well as canopy level. This will enable to assign the final product quality and thus enhance the algorithm's performance and resulting product's reliability.

Once the data uncertainties are determined with respect to their wavelength dependence, they have to be accounted for in existing algorithms estimating vegetation variables. These variables with the assigned product quality are a baseline for the assimilation of remote sensing derived products into climate and ecosystem models. As a last step, products and their uncertainties have to be adapted to requirements indicated by the identified user community.

Apart from the albedo, LAI and FPAR estimation using directional data, more studies are needed to demonstrate the usefulness of this new approach and generate ecologically relevant products from directional remote sensing data. As of today, there is a continuous sampling of large scale directional reflectance properties of the surface by diverse satellite systems. For their calibration and validation as well as for regional scale applications and algorithm development with extended spectral range, there is a need for small-scale multiangular measurements with corresponding documentation and storage facilities as a basis for an extensive analysis of spectrodirectional data.

Data acquisitions with major emphasis on both, the spectral and directional component, will help to overcome the difficulties in dealing with the enhanced information content which is often regarded as data uncertainties today or excluded from the analysis. Solid field campaigns with strong emphasis on both dimensions will deliver data for a in-depth analysis of advantages of spectrodirectional data for the estimation of vegetation variables, and thus resolve the promises made over the years of which spectroscopy and multiangular remote sensing still suffer today.

It is recommended to reduce and include reflectance data uncertainties in future applications by following a consistent reflectance nomenclature, and further investigate the representation of spectral effects in spectrodirectional measurements and modelling results, with respect to the single scattering components of the coupled soil-vegetation-atmosphere radiative transfer.

Planned missions (e.g., SPECTRA) will help to acquire the required data, but the remote sensing community conceptualizing and providing data product algorithms has to agree on a joint concept for the definition of spectrodirectional reflectance quantities. This will help the users to appropriately apply the data. More experience with measured data and modelling studies are needed for a reliable estimation of vegetation variables which then will prove their importance in many applications, such as in ecology (e.g., Schaepman, 2004).

6.7 References

Barnsley, M.J., D. Allison, and P. Lewis, On the information content of multiple view angle (MVA) images, International Journal of Remote Sensing, 18 (9), 1937-1960, 1997.

Berger, M., M. Rast, P. Wursteisen, E. Attema, J. Moreno, A. Muller, U. Beisl, R. Richter, M. Schaepman, G. Strub, M.P. Stoll, F. Nerry, and M. Leroy, The DAISEX campaigns in support of a future land-surface-processes mission, Esa Bulletin-European Space Agency (105), 101-111, 2001.

Bicheron, P., M. Leroy, O. Hautecoeur, and F.M. Breon, Enhanced discrimination of boreal forest covers with directional reflectances from the airborne polarization and directionality of Earth reflectances (POLDER) instrument, Journal of Geophysical Research-Atmospheres, 102 (D24), 29517-29528, 1997.

Bojinski, S., M. Schaepman, D. Schlapfer, and K. Itten, SPECCHIO: a spectrum database for remote sensing applications, Computers & Geosciences, 29 (1), 27-38, 2003.

Bojinski, S., D. Schlapfer, M. Schaepman, J. Keller, and K. Itten, Aerosol Mapping over Land with Imaging Spectroscopy Using Spectral Autocorrelation, International Journal of Remote Sensing, 2004, in print.

Breuer, L., K. Eckhardt, and H.G. Frede, Plant parameter values for models in temperate climates, Ecological Modelling, 169 (2-3), 237-293, 2003.

ESA, SPECTRA - Surface Processes and Ecosystem Changes Through Response Analysis, Reports for Mission Selection, The Six Candidate Earth Explorer Missions, pp. 74, European Space Agency, Mission Experts Division, Noordwijk, The Netherlands, 2004.

Gobron, N., B. Pinty, M.M. Verstraete, J.L. Widlowski, and D.J. Diner, Uniqueness of multiangular measurements - Part II: Joint retrieval of vegetation structure and photosynthetic activity from MISR, Ieee Transactions on Geoscience and Remote Sensing, 40 (7), 1574-

1592, 2002.

Hu, J., B. Tan, N. Shabanov, K.A. Crean, J.V. Martonchik, D.J. Diner, Y. Knyazikhin, and R. Myneni, Performance of the MISR LAI and FPAR algorithm: a case study in Africa, Remote Sensing of Environment, 2003.

Schaepman, M., B. Koetz, G. Schaepman-Strub, N.E. Zimmermann, and K.I. Itten, Quantitative retrieval of biogeophysical characteristics using imaging spectroscopy - a mountain forest case study, Community Ecology, 5 (1), 93-104, 2004.

Schaepman-Strub, G., T. Painter, S. Huber, S. Dangel, M. Schaepman, J.V. Martonchik, and F. Berendse, About the Importance of the Definition of Reflectance Quantities - Results of Case Studies, in Proc. of XX. ISPRS Congress, Istanbul, Turkey, 2004, in print.

Schaepman-Strub, G., M. Schaepman, T. Painter, S. Dangel, J.V. Martonchik, and M. Verstraete, Review of Reflectance Nomenclature Used in Optical Remote Sensing with Quantitative Comparisons, 2004, in preparation.

Schlapfer, D., and M. Schaepman, Modeling the noise equivalent radiance requirements of imaging spectrometers based on scientific applications, Applied Optics, 41 (27), 5691-5701, 2002.

Sellers, P.J., B.W. Meeson, F.G. Hall, G. Asrar, R.E. Murphy, R.A. Schiffer, F.P. Bretherton, R.E. Dickinson, R.G. Ellingson, C.B. Field, K.F. Huemmrich, C.O. Justice, J.M. Melack, N.T. Roulet, D.S. Schimel, and P.D. Try, Remote-Sensing of the Land-Surface for Studies of Global Change - Models, Algorithms, Experiments, Remote Sensing of Environment, 51 (1), 3-26, 1995.

Strub, G., U. Beisl, M. Schaepman, D. Schlaepfer, C. Dickerhof, and K. Itten, Evaluation of diurnal hyperspectral HDRF data acquired with the RSL field goniometer during the DAISEX'99 campaign, Isprs Journal of Photogrammetry and Remote Sensing, 57 (3), 184-193, 2002.

Strub, G., M.E. Schaepman, Y. Knyazikhin, and K.I. Itten, Evaluation of spectrodirectional Alfalfa canopy data acquired during DAISEX '99, Ieee Transactions on Geoscience and Remote Sensing, 41 (5), 1034-1042, 2003.

Weiss, M., F. Baret, R.B. Myneni, A. Pragnere, and Y. Knyazikhin, Investigation of a model inversion technique to estimate canopy biophysical variables from spectral and directional reflectance data, Agronomie, 20 (1), 3-22, 2000.

White, H.P., J.R. Miller, and J.M. Chen, Four-Scale Linear Model for Anisotropic Reflectance (FLAIR) for plant canopies - Part II: Validation and inversion with CASI, POLDER, and PARABOLA data at BOREAS, Ieee Transactions on Geoscience and Remote Sensing, 40 (5), 1038-1046, 2002.

Zhang, Y., Y. Tian, R.B. Myneni, Y. Knyazikhin, and C.E. Woodcock, Assessing the information content of multiangle satellite data for mapping biomes I. Statistical analysis, Remote Sensing of Environment, 80 (3), 418-434, 2002.

Acknowledgement

This thesis was supported by the Swiss National Science Foundation projects 2000-061431.0 and 200020-101517, a research grant from Astrium GmbH, Friedrichshafen, Germany, and a research grant from Paul Scherrer Institute, Villigen, Switzerland.

I appreciate the commitment of John Miller to review this thesis and perform an expertise.

My whole PhD was a real journey..... and I mostly enjoyed it thanks to the company and support of precious persons.

Fortunately my supervisor Klaus Itten always kept a stable and reliable position in Zürich. He raised my interest in remote sensing during the Master studies in Geography with nice satellite images from all over the world. After I got the opportunity to perform a PhD in his group, he supported my adventure throughout the last years in a very generous way.

It was a pleasure to accomplish this thesis in the inspiring ambiance of the SpectroLab team. With Stefan Bojinski, Ben Kötz, Silvia Huber, Mathias Kneubühler, Daniel Schläpfer, Johannes Kaiser, Peter Keller, Stefan Dangel, Uli Beisl, Jason Brazile, Anko Börner, Jens Nieke, and Jürg Schopfer I spent many hours discussing life during coffee breaks, sitting in meetings, calibrating instruments, and performing field campaigns. Sometimes we even found the time to meet with their partners and talk about real life instead of science. During the whole journey I got continuous scientific advice and networking support, by the former team leader, Michael Schaepman.

Now and then, 'pixel counting' was becoming too much. In these moments, many people of the Department of Geography at the University of Zurich did an excellent job in entrapping me in distracting discussions. Further, I could always count on Othmar Wigger for solving IT problems, even from a long distance.

Throughout the first one an a half years of my PhD, I was partly commuting to Villigen to learn more about atmospheric processes. Johannes Keller and Urs Baltensperger from the Paul Scherrer Institut gave me this excellent opportunity.

I had the pleasure to take twice the ferry over the Lake of Constance to Friedrichshafen to present our achieved scientific results to Manfred Langemann and his team at Astrium GmbH.

I will never forget the travel to Valencia in an old brownish VW Caravan, with the FIGOS in the trailer. Jose Moreno and his staff (especially Luis Alonso) did an excellent job by convincing many different scientific groups to contribute to the DAISEX campaigns, such as the POLDER team led by Marc Leroy. The

team work was definitively enhanced through the nice tapas and paella dinners, organized by Jose Moreno and Jose Antonio Sobrino.

I had the opportunity to participate in Weisswurst and Weissbier campaigns in and around Oberpfaffenhofen on a regular basis, thanks to Andreas Mueller, Rolf Richter, and Andrea Haushold.

Unfortunately I never made it to home towns of the French 'mafia' dealing with spectrodirectional data of vegetation canopies. This includes especially Frederic Baret and his team, as well as Stephane Jacquemoud and Cedric Bacour.

After reading many publications about radiative transfer, and meeting Ranga Myneni and Yuri Knyazikhin in Aussois, I was determined to apply for a research visit at Boston University. These two excellent researchers generously gave me an insight into important scientific topics and beyond, including radiative transfer, the American research culture, and publishing strategies. It was a pleasure to work in the inspiring environment of the whole Department of Geography at BU, and discuss with the PhD students, as well as enjoying Boston and surroundings with them and their partners. I am especially thankful to Nikolay Shabanov, Sveta Kotchenova, Jiannan Hu, Wolfgang Buermann, Alex Lotsch, Chung Yi Lung, Hideki Kanamaru, Alessandro Baccini, Asuka Imai, Liming Zhou, and Yuhong Tian. Without the people outside BU, including Paula Hurley, Dirk Riehle and Julie Burba, I would have missed most important real life experiences, such as the preparation of a thanks giving turkey ;-) .

Being back to Zürich in December 2001, I took a rest from moving around in PhD life for more personal journeys - cut ;-)

Tom Painter and Tanja Unatin gave an excellent opportunity to come to Boulder, Colorado in summer 2002. This allowed me to finally get to know the famous ASD company and 'their' Nate Bloomingdale. After this short break I got ready for the next move towards *the* last year of the PhD, including the destination of Wageningen, the Netherlands.

Thanks to the advice of Bernhard Schmid and Arnold Bregt, and especially thanks to the generosity of Frank Berendse, I was able to integrate into the Nature Conservation and Plant Ecology group at Wageningen University. This whole team, together with the members of the Resource Ecology Group and their head Herbert Prins, welcomed and hosted me in a excellent way during this last year in Wageningen. They were never tired of switching to English during coffee break, introducing me to Dutch habits, and giving daily live advice. I promise herewith to improve my Dutch within the next few months!

All the first and co-authors of the mentioned publications are responsible for many invaluable comments and contributions. In addition to above-mentioned scientists, these include Michael Berger, Carol Bruegge, John Martonchik, Michael Rast, Maria von Schönermark, and Michel Verstraete.

Dear all, many thanks for your support throughout these past years. Many of you have not only become good colleagues and reliable project partners, but personal friends. I wish you all the best in your private and scientific life and hope to cross your way soon again!

Event though there were many movements during my PhD, some people always remained in their position, having an open ear in difficult times, and contributing to enjoy life while I was back in Zurich. These are especially Patrick Laube, Daniel Isenegger, Jonas Witzig, Gaby Noser, and Wolfgang Schweitzer.

Women have different ways of travelling- be it in science or in private life. Exchanging experiences made during this journey with female buddies kept me moving many times. I especially appreciate the long lasting company of Pascale Herzig, Anna Jablonkay, Tabitha Walther, Corina Aeppli, and Nicole Salamin.

One of the last destinations of this long journey was to have written down all majour results in a booklet. Without the invaluable input of Rashunda Tramble, many more breakdowns in the English language would be represented in this thesis.

Even though the Netherlands seem to be the final destination in my PhD journey, I do not forget my roots in Switzerland. To my parents, Antoinette and Ruedi Strub, I wish many travels to further discover the world. I hope to have many opportunities to welcome my brother, my sisters and their partners, Nicole and Adrian, Michael's parents and siblings where ever we will move to. A special thank to Werner and Agnes Röllin, who gave me convincing reasons to decide to go for the big adventure of a PhD.

During journeys you sometimes meet a person with whom travelling around the world gets a real adventure, including the discovery of yet undiscovered grounds. I enjoy the 'tourist party' with Michael Schaepman and Linus beyond the current journey and look forward to many common destinations of our dreams.

Curriculum Vitae

Name	Schaepman
Maiden name	Strub
First name	Gabriela
Date of birth	31.10.1973
Place of birth	Olten, Switzerland
Citizenship	Zürich, ZH, and Läufelfingen, BL
Education	
1992	Gymnasium Liestal, Switzerland 21 December 1992, Matriculation ('Matura') Type D.
1993 – 1999	University of Zurich, Switzerland. Studies in Geography (major subject), Biology (minor subject), European Ethnology (minor subject). 4 February 1999, Diploma in Geography (dipl. geogr.)
1997 – 1998	MSc thesis 'Spectroradiometric Measurements in Grassland Communities' (in German). Supervision by Prof. Dr. K. I. Itten.
1999 – 2004	University of Zurich, Switzerland PhD thesis 'Spectrodirectional Reflectance Analysis and Definition for the Estimation of Vegetation Variables'. Supervision by Prof. Dr. K. I. Itten.

Bibliography

The following list summarizes all communications by Gabriela Schaepman-Strub published in the framework of this thesis.

Peer Reviewed Journals

Berger, M., M. Rast, P. Wursteisen, E. Attema, J. Moreno, A. Muller, U. Beisl, R. Richter, M. Schaepman, **G. Strub**, M.P. Stoll, F. Nerry, and M. Leroy, The DAISEX campaigns in support of a future land-surface-processes mission, Esa Bulletin-European Space Agency (105), 101-111, 2001.

Strub, G., U. Beisl, M. Schaepman, D. Schlaepfer, C. Dickerhof, and K. Itten, Evaluation of diurnal hyperspectral HDRF data acquired with the RSL field goniometer during the DAISEX'99 campaign, Isprs Journal of Photogrammetry and Remote Sensing, 57 (3), 184-193, 2002.

Strub, G., M.E. Schaepman, Y. Knyazikhin, and K.I. Itten, Evaluation of spectrodirectional Alfalfa canopy data acquired during DAISEX '99, Ieee Transactions on Geoscience and Remote Sensing, 41 (5), 1034-1042, 2003.

Schaepman, M., B. Koetz, **G. Schaepman-Strub**, N.E. Zimmermann, and K.I. Itten, Quantitative retrieval of biogeophysical characteristics using imaging spectroscopy - a mountain forest case study, Community Ecology, 5 (1), 93-104, 2004.

Schaepman, M., B. Koetz, **G. Schaepman**, K. Itten, Quantitative Imaging Spectroscopy for the Improved Estimation of Biogeophysical and -chemical Variables: Platform Strategies and Two Case Studies, Intl. J. Applied Earth Observation and Geoinformation, 2004, submitted.

Schaepman-Strub, G., M. Schaepman, T. Painter, S. Dangel, J. Martonchik, M. Verstraete, Review of Reflectance Nomenclature Used in Optical Remote Sensing with Quantitative Comparisons, 2004, in preparation.

Book Chapter

Bruegge, C.J., M. Schaepman, G. Strub, U. Beisl, A. Demircan, B. Geiger, T. Painter, B. Paden, and J. Dozier, Field measurements of bi-directional reflectance, in Reflection Properties of Vegetation and Soil - with a BRDF Data Base, edited by M. Von Schönermark, B. Geiger, and H.P. Röser, Wissenschaft und Technik Verlag, Berlin, 2004.

Conference Contributions

Beisl, U., G. Strub and C. Dickerhof, Validation of Hyperspectral Imaging Data from the Barrax Test Site with BRDF Ground Measurements in the Reflective Wavelength Range, 2nd EARSeL Workshop on Imaging Spectroscopy, Enschede, CD-ROM, 2000.

Strub, G., U. Beisl, M. Schaepman, D. Schlaepfer, C. Dickerhof and K. Itten, Evaluation of Diurnal Hyperspectral BRF Data Acquired with the RSL Field Goniometer during the DAISEX'99 Campaign, 2nd EARSeL Workshop on Imaging Spectroscopy, Enschede, CD-Rom, 2000.

Strub, G., J. Keller, M. Schaepman, U. Beisl and K. Itten, Comparison of Modeled and Measured Directional Reflectance Data of an Alfalfa Canopy, Proc. of 8th International Symposium on Physical Measurements and Signatures in Remote Sensing, Aussois, France, pp. 285-290, 2001.

Schaepman, M., Dangel, S., Kneubühler, M., Schläpfer, D., Bojinski, S., Brazile, J., Kötz, B., **Strub, G.**, Kohler, R., Popp, Ch., Schopfer, J. and Itten, K. Quantitative Field Spectroscopic Measurement Instrumentation and Techniques. Proceedings 1st EPFS Workshop on Field Spectrometry. NERC, Southampton, UK, 13 pp., CD-ROM, 2002.

Strub, G., B.Koetz, M. Schaepman, K.I. Itten, Evaluation of Spectro-Directional Alfalfa Field Measurements Acquired During DAISEX'99, Poster Presentation, IWMMM-3, Steamboat Springs, USA, 2002.

Dangel, S., M. Kneubühler, R. Kohler, M. Schaepman, J. Schopfer, **G. Schaepman-Strub**, K. Itten, Combined Field and Laboratory Goniometer System – FIGOS and LAGOS, Proc. of IGARSS, Toulouse, France, 2003.

Dangel, S., Kneubühler, M., Schaepman, M., **Schaepman-Strub, G.**, Schopfer, J. & K. I. Itten, Combined Field and Laboratory Goniometer System - FIGOS and LAGOS, Proc. of 2nd SPECTRA Workshop, M. Rast (ed.), WPP-255, CD-ROM, ESA/ESTEC, Nordwjik, The Netherlands, 2004.

Schaepman-Strub, G., Schaepman, M., Moreno, J., Knyazikhin, Y., and K. Itten, Diurnal Spectro-Directional Characterization of Alfalfa with FIGOS. Geophys. Res. Abstracts, EGU, Vol. 5, p. 12311, 2003.

Schaepman-Strub, G., M. Schaepman, Y. Knyazikhin, K. I. Itten, Towards Spectro-Directional Prior Information – Case Study on an Alfalfa Canopy Observed During DAISEX'99, Proc. of 2nd SPECTRA Workshop, M. Rast (ed.), WPP-255, CD-ROM, ESA/ESTEC, Nordwjik, The Netherlands, 2004.

Schaepman-Strub, G., T. Painter, S. Huber, S. Dangel, M. Schaepman, J. Martonchik, F. Berendse, About the Importance of the Definition of Reflectance Quantities - Results of Case Studies, Proc. of XX. ISPRS Congress Istanbul, Turkey, 2004, in print.

Reports

Strub, G., M. Schaepman, K. Itten, Retrieval of Vegetation Parameters from Hyperspectral Imaging Sensor Data. Report Phase I, Astrium GmbH, 35 p., 2000.

Strub, G., M. Schaepman, K. Itten, Retrieval of Vegetation Parameters from Hyperspectral Imaging Sensor Data. Report Phase II, Astrium GmbH, 68 p., 2001.

Schaepman-Strub, G., M. Schaepman, S. Huber, and K. Itten, Retrieval of Vegetation Parameters from Hyperspectral Imaging Sensor Data, Final Report, Astrium GmbH, 75 p., 2003.

Schaepman-Strub, G., M. Schaepman, and K. Itten, Ground BRDF Data Analysis, Normalization and Modelling, in Scientific Analysis of the ESA Airborne Multi-Annual Imaging Spectrometer Campaign, Final Report, ESA Contract-No. 15343/01/NL/MM, edited by J. Moreno, 2004, submitted.

Itten, K.I., Schaepman, M., **Schaepman-Strub, G.**, Bojinski, S., and M. Kneubühler, Investigation of Imaging Spectrometry as an Earth Observation Method for Environmental Analysis, Final Report, Swiss National Science Foundation, No. 2000-061431.0, 6 p., 2003.

Key

Submitted
: Papers submitted to a journal or to proceedings, in the review process.

In print
: Papers accepted for publication and awaiting print.

In preparation
: Papers written by the authors and ready to be submitted to a journal.